MINERAL DISSOLUTION IN SOIL AS A FUNCTION OF LANDSCAPE POSITION, VEGETATION AND FUNGI AT THE HUBBARD BROOK EXPERIMENTAL FOREST, NEW HAMPSHIRE

by

Carmen Ann Nezat

A dissertation submitted in partial fulfillment
of the requirements for the degree of
Doctor of Philosophy
(Geology)
in The University of Michigan
2006

Doctoral Committee:

Professor Joel D. Blum, Chair
Professor Philip A. Meyers
Professor Lynn M. Walter
Professor Donald R. Zak

DEDICATION

....

ACKNOWLEDGEMENTS

TABLE OF CONTENTS

LIST OF FIGURES

LIST OF TABLES

LIST OF APPENDICES

CHAPTER 1

INTRODUCTION

Chemical weathering, the partial or complete dissolution of minerals, provides nutrients to vegetation, neutralizes acid deposition, and controls soil, groundwater and streamwater compositions – functions that are vital to the health of forest and stream ecosystems. In recent decades, forest health in the northeast USA has been threatened by a loss of plant-available nutrients from the soil. In particular, essential plant nutrients such as Ca, Mg, and K have been leached from the soil cation exchange pool, the pool of cations from which vegetation obtains most of their nutrients (Likens et al., 1996; Huntington et al., 2000; Driscoll et al., 2001). It has been hypothesized that continued calcium depletion from the soil exchange pool will result in calcium-related stress, and subsequently a decline in forest productivity (Likens et al., 1998). Understanding the controls on mineral dissolution and the method by which certain trees obtain their nutrients is important for predicting the health of forest ecosystems in response to anthropogenic disturbances such as acid deposition.

Most of my research was focused at the Hubbard Brook Experimental Forest (HBEF) in the White Mountains, New Hampshire. The geology, soils and vegetation of HBEF are characteristic of northern hardwood forests in the northeastern USA. Atmospheric deposition, stream water, soil, and vegetation have been monitored at HBEF since 1963. Therefore, this is an ideal location to study the role of mineral weathering as a nutrient source in an ecosystem affected by Ca loss.

Mineral weathering

In order to understand Ca biogeochemical cycling in a forest ecosystem, contributions from mineral weathering must be characterized. In Chapter 2, the interaction between vegetation and mineral dissolution at HBEF was examined. The goals were to determine 1) the influence of vegetation and landscape position (e.g., slope, elevation) on mineral weathering rates, 2) the long-term mineral weathering rates relative to present-day cation losses from the soil, and 3) the presence of apatite in the soils. In order to accomplish this, I analyzed the chemical composition of soils collected from several depths from ~50 soil pits across a small watershed.

Identification and quantification of apatite in soil

Plagioclase, one of the dominant minerals in crystalline silicate (i.e., igneous and metamorphic) rocks, typically contains most of the total calcium content in these rocks. Another ubiquitous Ca-bearing mineral in these rocks is apatite, $Ca_5(PO_4)_3(F,Cl,OH)$, an accessory mineral that generally occurs in low abundance (<1 wt %) as minute inclusions in larger silicate minerals. Due to its rapid dissolution rate (orders of magnitude faster than plagioclase), apatite may supply a significant amount of Ca to terrestrial and aquatic ecosystems despite its relatively low abundance (Blum et al., 2002; Nezat et al., 2004; Yanai et al., 2005). Apatite is also the dominant P-bearing primary mineral in soils developed on crystalline rocks and thus an important soil nutrient reservoir (Crews et al., 1995; Schlesinger et al., 1998).

Because apatite is present as inclusions in silicate minerals and usually occurs in trace amounts, quantifying the amount of apatite that may be exposed to soil solution is

difficult. Chapter 3 discusses the development and application of a sequential extraction procedure that can isolate the dissolution of apatite from other Ca-bearing minerals in the soil so that it can be quantified. This procedure was first tested on individual minerals separated from glacial till in order to identify which minerals were dissolved during each step. Next, the influence of acid strength and temperature on the isolation of apatite was determined. Finally, to interpret the chemical composition of sequential extracts of weathered soils and demonstrate the usefulness of the technique, the procedure was applied to soils from HBEF where the weathering of primary minerals and accumulation of secondary minerals in soil profiles had previously been characterized (Chapter 2).

In Chapter 2, it was established that apatite was present in HBEF soils and may be an important source of Ca. Chapter 3 explores the regional distribution and availability of apatite in soils across the northeastern United States. Soil parent material derived from crystalline silicate and sedimentary rock were collected and sequentially leached. The Ca and P concentrations in the 1M HNO_3 extract were used to quantify the amount of apatite in soil.

Mineral dissolution by microbes

Most trees in northern hardwood forests have a symbiotic association with fungi called mycorrhizae. Mycorrhizae form a sheath of hyphae (threadlike filaments) around the tree roots and extend hyphae into the soil (Lakhanpal, 2000). The hyphal tips exude organic acids that weather minerals such as biotite, apatite and microcline (Jongmans et al., 1997; Landeweert et al., 2001; Wallander, 2000). The mycorrhizae then transport these nutrients back to the tree roots.

The focus of Chapter 5 is on microbial response to the presence of Ca-bearing minerals. To test this, mesh bags containing quartz (as a control), apatite, or wollastonite ($CaSiO_3$) were buried in the rooting zone in soils at HBEF. The mesh size allowed fungi and bacteria to enter the bags, but not roots. The mesh bags were buried in stands of spurce-fir, beech and sugar maple. Microbial community composition and biomass were estimated using phospholipid fatty acid analysis. The results of this experiment help to determine the role that both fungi and bacteria play in mineral dissolution, the nutrients that are available to fungi, and the importance of mineral sources of calcium and phosphorous to vegetation in the northeast United States.

References

Blum, J.D., Klaue, A., Nezat, C.A., Driscoll, C.T., Johnson, C.E., Siccama, T.G., Eagar, C., Fahey, T.J., Likens, G.E., 2002. Mycorrhizal weathering of apatite as an important calcium source in base-poor forest ecosystems. Nature 417, 729-731.

Crews, T.E., Kitayama, K., Fownes, J.H., Riley, R.H., Herbert, D.A., Mueller-Dombois, D., Vitousek, P.M., 1995. Changes in soil phosphorous fractions and ecosystem dynamics across a long chronosequence in Hawaii. Ecology 76 (5), 1407-1424.

Driscoll, C.T., Lawrence, G.B., Bulger, A.J., Butler, T.J., Cronan, C.S., Eagar, C., Lambert, K.F., Likens, G.E., Stoddard, J.L., Weathers, K.C., 2001. Acidic deposition in the northeastern United States: Sources and inputs, ecosystem effects, and management strategies. BioScience 51 (3), 180-198.

Huntington, T.G., Hooper, R.P., Johnson, C.E., Aulenbach, B.T., Cappellato, R., Blum, A.E., 2000. Calcium depletion in a southeastern United States forest ecosystem. Soil Science Society of America Journal 64, 1845-1858.

Likens, G.E., Driscoll, C.T., Buso, D.C., 1996. Long-term effects of acid rain: Response and recovery of a forest ecosystem. Science 272, 244-246.

Likens, G.E., Driscoll, C.T., Buso, D.C., Siccama, T.G., Johnson, C.E., Lovett, G.M., Fahey, T.J., Reiners, W.A., Ryan, D.F., Martin, C.W., Bailey, S.W., 1998. The biogeochemistry of calcium at Hubbard Brook. Biogeochemistry 41, 89-173.

Schlesinger, W.H., Bruijnzeel, L.A., Bush, M.B., Klein, E.M., Mace, K.A., Raikes, J.A., Whittaker, R.J., 1998. The biogeochemistry of phosphorous after the first century of soil development on Rakata Island, Krakatau, Indonesia. Biogeochemistry 40, 37-55.

CHAPTER 2

INFLUENCE OF LANDSCAPE POSITION AND VEGETATION ON LONG-TERM WEATHERING RATES AT THE HUBBARD BROOK EXPERIMENTAL FOREST, NEW HAMPSHIRE, USA

Abstract

The spatial variability of long-term chemical weathering in a small watershed was examined to determine the effect of landscape position and vegetation. We sampled soils from forty-five soil pits within an 11.8-hectare watershed at the Hubbard Brook Experimental Forest, New Hampshire. The soil parent material is a relatively homogeneous glacial till deposited ~14,000 years ago and is derived predominantly from granodiorite and pelitic schist. Conifers are abundant in the upper third of the watershed while the remaining portion is dominated by hardwoods. The average long-term chemical weathering rate in the watershed, calculated by the loss of elements integrated over the soil profile, is 35 meq m^{-2} yr^{-1} — similar to rates in other ~10 to 15 ka old soils developed on granitic till in temperate climates. The present-day loss of base cations from the watershed, calculated by watershed mass balance, exceeds the long-term weathering rate, suggesting that the pool of exchangeable base cations in the soil is being diminished. Despite the homogeneity of the soil parent material in the watershed, long-term weathering rates decrease by a factor of two over a 260 m decrease in elevation.

Estimated weathering rates of plagioclase, potassium feldspar and apatite are greater in the upper part of the watershed where conifers are abundant and glacial till is thin. The intra-watershed variability across this small area demonstrates the need for extensive sampling to obtain accurate watershed-wide estimates of long-term weathering rates.

Introduction

Silicate mineral weathering consumes atmospheric CO_2, and is thus an important process for regulation of global climate over geologic time scales (e.g., Berner et al., 1983). Over shorter periods of time, mineral weathering in soils provides nutrients to vegetation, neutralizes acid deposition, and controls soil water compositions – functions that are vital to the growth and maintenance of forest ecosystems. In the eastern U.S. and Europe, where acid deposition has decreased exchangeable base cation (Ca, Mg, K, Na) pools (Kirchner and Lydersen, 1995; Wesselink et al., 1995; Likens et al., 1996; Huntington et al., 2000; Driscoll et al., 2001), it has been hypothesized that continued calcium depletion from soils will result in calcium-related stress, and subsequently a decline in forest productivity (Likens et al., 1998). Despite a reduction in atmospheric emissions of acid-forming compounds since 1970, the exchangeable base cation concentrations of most forest soils have not yet recovered from the effects of acid deposition (Likens et al., 1996; Driscoll et al., 2001).

The two dominant sources of plant-available base cations in unmanaged forested watersheds are atmospheric deposition and mineral weathering. Unlike atmospheric contributions, the flux of base cations released from mineral weathering cannot be

measured directly on a watershed scale. Assuming that forest growth is at steady-state (i.e., cation uptake by vegetation equals cation loss via mortality), the inputs from atmospheric deposition (P) and mineral weathering (W) are balanced by stream export (S) and any changes in the exchangeable pool (?X) (Likens et al., 1998):

$$P + W = S + ?X. \qquad (1)$$

By measuring atmospheric input and stream fluxes of base cations, the net loss of base cations from a watershed (? X – W) can be calculated. Partitioning these present-day cation fluxes into cations released from mineral weathering and changes in the soil cation exchange pool is more challenging.

Long-term chemical weathering rates can be estimated by computing the depletion of cations in the soil, relative to parent material. This approach has been successfully applied in post-glacial environments where the time of soil development and the soil parent material can be reliably identified (April et al., 1986a; Taylor and Blum, 1995). Interestingly, these long-term weathering rates can vary significantly within single watersheds (April et al., 1986a; Kirkwood and Nesbitt, 1991; Bain et al., 1994). The spatial heterogeneity of soils within watersheds is the result of many factors, including differences in parent material, topography, vegetation type, soil mixing by windthrows and animal burrowing, and other processes. Despite the variability, long-term weathering rates are frequently estimated from relatively few soil profiles within a watershed. Although many studies have observed systematic changes in weathering across soil chronosequences (Merritts et al., 1992; Bain et al., 1993; Taylor and Blum, 1995), intra-watershed variability in long-term weathering rates has not been thoroughly examined for

patterns with forest type and landscape position features such as topography, glacial till thickness, and hydrologic flowpaths.

In this study, we examined 1) the variability of soil composition across a small watershed; 2) mineral weathering rates along an elevational and forest-composition gradient; and 3) long-term chemical weathering rates relative to present-day cation losses. To examine the inherent heterogeneity of soil development and weathering in an individual watershed, we sampled forty-five soil pits across an 11.8-hectare watershed.

Setting

The Hubbard Brook Experimental Forest (HBEF) is located in the White Mountains of central New Hampshire. There are six adjacent, south-facing experimental watersheds having similar glacial till composition, vegetation zones, slope, elevation range, and watershed size at the HBEF. Watershed 1 (W-1), the focus of this study, is 11.8 ha (0.118 km^2) in area and ranges in elevation from 488 to 747 m above sea level (Figure 2-1). Watershed 6 (W-6), which lies ~1.5 km to the west of W-1, is a biogeochemical reference watershed; that is, it functions as an undisturbed control for manipulated watersheds at HBEF. At the time of soil sampling for this study, neither Watershed 1 nor 6 had been disturbed since logging in the early 1900's. The Silurian-aged Rangeley Formation, a pelitic schist and meta-sandstone, underlies the eastern half of the Hubbard Brook Experimental Forest, including W-1 (Barton et al., 1997). The bedrock of the western portion of the HBEF is Devonian Kinsman granodiorite, a foliated granitoid rock with megacrysts of potassium feldspar (Barton et al., 1997). Continental ice sheets, which receded from the area ~14,000 years ago (Davis et al., 1985), deposited

glacial till derived mostly from local bedrock. Pebbles in W-1 glacial till are predominantly porphyritic granodiorite and mica schist derived from the Kinsman granodiorite to the northwest and from the underlying bedrock, respectively (Bailey et al., 2003). The glacial till is thinner on ridges, is often absent in streambeds, and thickens towards the base of the watershed. The till has an average thickness of ~2 m. Well-drained Spodosols (haplorthods), about 60 cm deep, are the dominant soils in the watershed (Johnson et al., 1991a).

The HBEF is predominantly northern hardwood forest, dominated by American beech (*Fagus grandifolia* Ehrh.), sugar maple (*Acer saccharum* Marsh), and yellow birch (*Betula alleghaniensis* Britton). White birch (*Betula papyrifera* Marsh.), red spruce (*Picea rubens* Sarg.), and balsam fir (*Abies balsamea* L.) are dominant at higher elevations (Figure 2-1). The uppermost part of the watershed is poorly drained and has relatively flat topography, while well-drained steeper slopes are present in the rest of the watershed. For the purpose of this study, W-1 was divided into six regions based on elevation and vegetation (Figure 2-1, Table 2-1).

Sampling and Analytical Methods

During the summer of 1997, soil samples were collected from forty-five randomly located sites within W-1 (Figure 2-1). Samples were collected by horizon from the Oie (abbreviation for the combined Oi and Oe horizons), Oa, E, Bh, Bs1, Bs2, and C horizons, and sieved through a 5-mm (O horizon) or 2-mm (mineral soil) screen. To minimize the effects of heterogeneity within the six regions of W-1, a composite soil sample was created for each horizon in each region by combining 1% of the total mass of

10

the respective horizon from each soil pit within that region. The data reported in this study were generated by the analysis of these composite horizon samples.

A variety of soil parameters were either directly measured or estimated to calculate cation pools in the soil profiles. The masses of the Oie and Oa horizons were measured on samples collected in 1996 and 1998 and averaged for the two years. For the mineral horizons, the mass of soil per unit area (m_{soil}, Mg ha^{-1}) was calculated as

$$m_{soil} = 100 * ? * z * (1-?) \tag{2}$$

where 100 is the conversion factor between measured and calculated units, ? is the bulk density (g cm^{-3}), z is the horizon thickness (cm), and ? is the fraction (by volume) of coarse fragments (i.e., >2 mm) in the horizon. We considered weathering of the >2 mm fraction to be negligible due to its relatively low surface area-to-volume ratio. Dry bulk density was estimated from total carbon versus bulk density relationships established for HBEF soils (Huntington et al., 1989). Total carbon was measured by combustion/gas chromatography on a Carlo Erba EA1108 elemental analyzer. The thickness of each horizon was measured at the time of field collection, and the fraction of coarse fragments (>2 mm) was estimated from earlier field measurements in Watershed 5, a watershed of similar glacial till composition, vegetation, slope, and elevation that is located ~1 km west of W-1 (Huntington et al., 1989). The volume fractions of coarse fragments in the E, Bh, Bs1, and Bs2 horizons were estimated to be 0.105, 0.105, 0.112, and 0.198, respectively.

The chemical compositions of the composite soil samples were determined by analysis of LiBO$_2$ fused-samples. Prior to fusion, dried soils were pulverized for 60 seconds in a tungsten carbide ring mill. About 1 g of technical grade LiBO$_2$ and ~0.1 g of

soil were mixed in a graphite crucible and heated for 20 minutes at 1100 °C. The molten

bead was dissolved in ~60 mL of trace metal grade 5% HNO_3 on a magnetic stir plate.

The solution was filtered with cellulose fiber paper (25 µm pore size) to remove any

graphite. Four USGS Geochemical Reference Standards and a procedural blank ($LiBO_2$

only) were also digested. Solutions were analyzed on a Perkin Elmer Optima 3300DV

Inductively Coupled Plasma-Optical Emission Spectrometer (ICP-OES) using a five- to

eight-point calibration curve. $LiBO_2$ was added to the calibration and quality control

standards to obtain the same matrix as the digested soil solutions. Quality control

standards (USGS and High-Purity® CRM Soil Solution A) were analyzed to within ±7%

for Ca, Mg, Na, Sr and Ti; and 12% for K. Recovery of P was within 3% for

concentrations near 900 mg kg^{-1} solution, but less accurate for lower P concentrations

(±25% below 700 mg kg^{-1} solution).

Depletion factors, which represent the fraction of an element lost (or gained) from

a horizon during soil development, were calculated for each base cation in each soil

horizon. The depletion factor ($d_{x,h}$) for an element X in horizon h is:

$$d_{x,h} = (X_h/Ti_h)/(X_C/Ti_C) \qquad (3)$$

where X_h and X_C (mmol g^{-1}) are concentrations of element X in the <2 mm fraction of

horizon h and the C horizon, respectively; Ti_h and Ti_C (mmol g^{-1}) are concentrations of Ti

in horizon h and the C horizon. Following previous studies, we made several common

assumptions: 1) the >2 mm fraction and the C horizons have not been appreciably

weathered; 2) the initial composition of a weathered horizon was similar to the

corresponding C horizon; and 3) Ti was essentially immobile in young soils (e.g., April et

al., 1986a; Taylor and Blum, 1995; Hodson, 2002). Although some studies have

normalized base cations to Zr (e.g., Kirkwood and Nesbitt, 1991; Bain et al., 1993), we chose Ti instead as our conservative element for several reasons: 1) our analytical accuracy was better for Ti (4% instead of 12%), 2) several C horizons had lower Zr concentrations than their overlying horizons, and 3) Ti is a major element in common rock-forming minerals and is less likely to suffer from heterogeneity in the distribution of a trace phase such as zircon.

The base cation loss from the <2 mm fraction in each soil profile was determined as the difference between the initial and the current composition of the entire profile (Taylor and Blum, 1995). The original number of moles of element X per unit area ($M_{x,initial}$, mol m^{-2}) in the weathered soil profile was estimated as

$$M_{x,initial} = 10 * X_C * \rho_C * z_{Total} * (1-\phi) \qquad (4)$$

where 10 is the conversion factor between measured and calculated units, ρ_C is the bulk density (g cm^{-3}) of the C horizon and z_{Total} (cm) is the thickness of the weathered soil profile (i.e., from the top of the E horizon to the top of the C horizon). The current number of moles of an element per unit area ($M_{x,current}$, mol m^{-2}) in each weathered horizon was calculated as

$$M_{x,current} = 10 * X_h * Ti_C/Ti_h * \rho_h * z_h * (1-\phi) \qquad (5)$$

where 10 is the conversion factor between measured and calculated units, ρ_h and z_h are the bulk density and thickness of horizon h, respectively (units are the same as in Equation 4). The current number of moles of cations per unit area in the individual weathered horizons were summed over the entire soil profile and subtracted from the original number of moles to estimate a total loss of each element x from each soil profile ($M_{x,loss}$, mol m^{-2}):

$$M_{x,loss} = M_{x,initial} - M_{x,current}. \tag{6}$$

The long-term chemical weathering rate (W_{LT}, meq m^{-2} yr^{-1}) of a soil is the total loss of base cationic charge (BC_{loss}, eq m^{-2}) from the soil profile divided by the age of the soil (t, years):

$$W_{LT} = 1000 * BC_{loss}/t, \tag{7}$$

where $\qquad\qquad BC_{loss} = 2 * M_{Ca,loss} + 2 * M_{Mg,loss} + M_{Na,loss} + M_{K,loss}, \qquad$ (8)

1000 is the conversion factor between measured and calculated units, and the constants preceding the number of moles in Equation 8 are the equivalents per mole for each cation. Due to the retention of much of the Al and Si in soils in the form of secondary minerals (e.g., kaolinite), Al and Si are typically not included in this type of weathering calculation.

The Oa horizons of forest soils have a significant amount of organic matter that contains base cations previously weathered from minerals. Thus, the concentration of only the mineral fraction of the Oa horizon was estimated for soil budget calculations. The composition of the organic fraction of the Oa horizon was assumed to be similar to the chemical composition of the Oie horizon. Hence, the concentration of element X in the mineral fraction of the Oa horizon (X_{Oa-min}) is:

$$X_{Oa-min} = (X_{Oa} - f_{LOI} * X_{Oie})/(1 - f_{LOI}) \tag{9}$$

where X_{Oa} and X_{Oie} are the total concentrations of element X in the Oa and Oie horizons, respectively. The term f_{LOI} is the fraction of mass lost on ignition — an estimate of the organic matter content —measured by ashing ~1 g of soil at 1000 ºC for 10 min. When normalized to Ti, the concentrations in the mineral fraction of the Oa horizon (X_{Oa-min}) were similar to those in the underlying E horizon (X_E). The composition of the mineral

fraction of the Oa horizon was used when calculating depletion factors and elemental losses from the soil profile.

For each C horizon, a polished thin section was made from an epoxy-impregnated subsample of the <2 mm fraction. Individual minerals were identified by an energy dispersive spectrometer (EDS) on a Hitachi S3200N Scanning Electron Microscope (SEM), and mineral abundances were determined on a 100-point grid. Apatite and trace calcite were identified by cathodoluminescence on a Technosyn Luminescence 8200 Mk II. Mineral composition was analyzed on a Cameca MBX electron microprobe (EMP) using mineral standards and the PAP correction procedure (Pouchou and Pichoir, 1984). The mean chemical composition of each mineral was determined from analysis of multiple grains.

Results

Physical and Chemical Properties of Soils

Vegetation changes across W-1 and four vegetation zones have been designated: spruce-fir, high hardwoods, middle hardwoods and lower hardwoods. Region 1 and a part of Region 2 are located in the spruce-fir zone (Figure 2-1). All of the soil pits in Region 1 were located in the spruce-fir zone while half of the soil pits in Region 2 were located in this zone. The area outside of the spruce-fir zone in Region 2 is in the high-hardwoods zone. Regions 3 and 4 are located in the middle hardwoods, and Regions 5 and 6 are located in the low hardwoods.

The soil depth to the top of the C horizon ranged from ~30 cm (in Region 1, at the top of the watershed where the glacial till is thinnest) to 50-70 cm (Regions 5 and 6 at

lower elevations) (Table 2-2; Figure 2-1). Not all horizons were present in each soil pit; for example, only three of the nine soil pits in Region 3 contained an identifiable E horizon (Table 2-2).

Quartz, plagioclase, potassium feldspar, muscovite and biotite were the dominant minerals in the C horizon; hornblende, epidote, chlorite, garnet, ilmenite, zircon, monazite, apatite and calcite were present in trace (<1%) abundances (Table 2-3). The mean Ca/Na ratio (0.22 ± 0.12, mean ± sd) measured in plagioclase, an important parameter for estimating plagioclase weathering rates from watershed fluxes, agreed with data from other HBEF studies (e.g., Likens et al., 1998; Bailey et al., 2003).

The chemical composition of the soils is shown in Table 2-4. There were no statistically significant relationships between elevation and elemental concentrations in the C horizon (p > 0.2; Figure 2-2). The coefficient of variation of the major oxides in the C horizons across the watershed ranged from 12 to 24%. Relative to the C horizons, the chemical variability was much greater in the upper horizons and within each profile due to differential rates of chemical weathering. The loss on ignition varied from a mean of 54% in the Oa horizons to 3% in the C horizons.

Estimates of Chemical Weathering

Titanium Variability

The Ti concentration in each soil horizon was normalized to the Ti concentration in the corresponding C horizon (the till, or parent material of the soil profile) in order to estimate weathering intensity within and between soil profiles. Titanium concentrations in the mineral soil decreased with depth in all of the composite profiles (Figure 2-3). The

16

Ti enrichment at any given depth in Region 1 (highest elevation) was greater than in all other regions (Figure 2-1); however, the weathering in the other regions extended to a greater depth. Overall, the Ti enrichment in the soil profiles decreased towards the bottom of the watershed. At the lower elevations, the E horizon can be clearly identified by the high Ti concentrations (Figure 2-3).

Elemental Depletion Factors

Elemental depletion factors (Equation 3) were determined for the six composite soil profiles (Figure 2-4). In general, the base cations in soils at higher elevations were intensely depleted throughout the profile. At lower elevations, base cation concentrations decreased more gradually with depth in the composite soil profiles. Calcium depletion profiles fell into two distinct groups: Regions 1–2, and Regions 3-6. In the E, Bh, Bs1 and Bs2 horizons, Ca was highly depleted in Regions 1 and 2 where ~75-83% of the Ca had been lost. In the four lower regions (3-6), Ca was less depleted and the loss decreased from ~ 60% in the E horizon to an average of 34% in the Bs2 horizon. Overall, Na depletion decreased with decreasing elevation and was correlated with Ca depletion ($r^2 =$ 0.95; $p < 0.001$). Approximately 80% of the Na has been lost from each horizon in Region 1 compared to a loss of 22-60% in the regions at lower elevations. Potassium loss generally decreased with depth and with a decrease in elevation, an indicator that weathering of K-bearing minerals occurs to a greater extent at shallower depths in the soil and at higher elevations. Magnesium depletion was similar among profiles and showed only a small decreasing trend with decreasing elevation. Magnesium was depleted in the E horizon and less depleted with increasing depth.

Long-term Weathering Rates

Calculated long-term weathering rates in W-1 (Equations 4-8) range from 21 to 47 meq m^{-2} yr^{-1} (Table 2-5, Figure 2-5) assuming that the present soil profiles began developing ~14,000 years ago following the last glacial retreat from this area (Davis et al., 1985). The long-term weathering rate at the highest elevation, Region 1, was 33 meq m^{-2} yr^{-1}. Although a large percentage of the base cations was lost from Region 1, soil development has been limited by the shallower glacial till depth (i.e., weathering rate is a function of soil depth; see Equation 4). The greater weathering intensity and base cation depletion (Figs. 3 and 4) in Region 1 suggest that if the glacial till in Region 1 had been thicker, its weathering rate might have been higher than Region 2. From the next highest elevation (Region 2) to the lowest elevation (Regions 5 and 6), the rates decreased from 47 to 21 meq m^{-2} yr^{-1}. The watershed average, weighted by the area of each region, was 35 meq m^{-2} yr^{-1}.

Discussion

Weathering Variability with Depth and Landscape Position

We made the common assumption that the mineral and chemical composition of the C horizon was representative of the parent material of the overlying soil (e.g., April et al., 1986a; Bain et al., 1994; Taylor and Blum, 1995). Because concentrations of Ti and other immobile elements (e.g., Zr, Nb) increase in soils as more mobile elements are removed during weathering, the Ti concentration in a soil horizon relative to its parent material is an indicator of the weathering intensity of that horizon. The overall decrease

of Ti with depth in the W-1 soil profiles is consistent with expected decreases in weathering intensity with depth (Figure 2-3). The soil profile with the shallowest depth to the C horizon (Region 1), is the most intensely weathered (i.e., it has lost the largest fraction of base cations), but has a low long-term weathering rate due to its comparatively shallow soil profile. In general, the soils at any given depth are more highly weathered in the upper part of the watershed. Because there is no trend between cation concentrations in the parent material and elevation (Figure 2-2), the pattern of cation loss in the weathered horizons of the soil profiles can be attributed to differences in weathering rather than variability of the parent material.

If Ti concentrations in the soil are primarily controlled by chemical weathering, then the C horizon should have the lowest Ti concentration. This pattern is observed for Regions 1-5 (Table 2-4). However, in Region 6, the Bs1 and Bs2 horizons have lower Ti concentrations than the C horizon, (Table 2-4, Figure 2-3) suggesting that either the C horizon is more weathered than the Bs1 and Bs2 horizons, or the analyzed C horizon sample is not representative of the parent material of the upper horizons in that region. It seems unlikely that the C horizon composite sample could have been more highly weathered than the B horizon samples during soil development. The most likely explanation for the high Ti concentration in the C horizon of the Region 6 sample is compositional heterogeneity of the till. The Ti concentration in the C horizon sample in Region 6 is considerably higher than in the other five C horizon samples (Table 2-4). Although there is certainly heterogeneity among the individual samples used to create composites for the other five regions, the composite samples appear to subdue this heterogeneity and result in Ti patterns in the soil profile that are consistent with expected

weathering patterns. Since the C horizon sample of Region 6 is a composite of only four samples (range of pits per region is 4 to 11), it may have been more easily skewed by one or more particularly Ti-rich till samples. To retain information from the rest of the Region 6 profile, we have used the mean composition of the C horizons in Regions 1-5 in place of the composition of the C horizon in Region 6. The "corrected" cation depletion profiles for Region 6 (represented by "Region 6*") look similar to those in Region 5, which has a similar slope, forest composition and elevation, and suggests that this substitution is reasonable. Although the results from Region 6 must be interpreted with some caution, deletion of these results do not change the overall conclusions presented in this study.

Long-Term Weathering Rates

There are several factors that affect weathering rates, including climate (White and Blum, 1995), composition of soil parent material (Meybeck, 1987), and age of soil (Bain et al., 1993; Taylor and Blum, 1995). Investigations of soil chronosequences developed on granitoid parent materials indicate that weathering rates decrease rapidly as weathering surfaces age (Bain et al., 1993; Taylor and Blum, 1995). This decrease in weathering rate is due to the removal of more easily dissolved minerals during the early stages of weathering, as well as the decrease in the reactive surface areas of soil minerals (Taylor and Blum, 1995). Bain et al. (1993) found that long-term weathering rates exponentially declined with age for a series of soils developed on river terraces. Taylor and Blum (1995) calculated a power-law equation for the empirical relationship between the long-term weathering rate and the age of granitoid soil profiles developed on glacial

20

moraines (0.4 to = 300 ka old) in the Wind River Mountains, Wyoming (Figure 2-5).

Taylor and Blum (1995) noted that soils developed on granitoid parent materials in other

regions with similar climates also had weathering rates consistent with this trend. The

range of long-term weathering rate that we have estimated at the HBEF (21–47 meq m^{-2}

yr^{-1}) is consistent with rates predicted by Taylor and Blum (1995) for 10–15 ka soils

formed on granitoid glacial till (Table 2-5, Figure 2-5).

Present-day Weathering Rates and Cation Losses

Present-day rates of cation loss, based on watershed mass balance, are a measure

of base cation loss from mineral weathering, cation exchange, and vegetation pools (see

Equation 1). Because a loss of base cations from the exchange pool cannot be measured

directly, we would like to be able to estimate the present-day mineral weathering rates in

order to determine the change in the cation exchange pool. Laboratory mineral

weathering rates have not been successfully extrapolated to rates at a watershed scale, so

instead we estimated present-day weathering rates from long-term weathering rates.

Based on a power-law equation describing the decrease in long-term weathering rates

with soil age, Taylor and Blum (1995) derived a mathematical expression which suggests

that at any point in soil development, present-day mineral weathering rates should be

about one third of long-term weathering rates. Thus W-1, which has an average long-term

weathering rate of 35 meq m^{-2} yr^{-1}, is expected to have a present-day mineral weathering

rate of 10 meq m^{-2} yr^{-1}. In the absence of natural or anthropogenic disturbance, the

present-day mineral weathering rate should be equal to the present-day cation loss, a

value calculated by watershed mass balance from annual measurements of base cations in

streamflow, atmospheric inputs, and change in biomass storage (Equation 1). The cation

loss from the reference watershed (W-6) at Hubbard Brook Experimental Forest averaged

91 meq m^{-2} yr^{-1} during 1982-92 (Johnson et al., 2000), nine times the estimated present-

day weathering rate, and more than twice the long-term weathering rate that we

measured. Cation losses were as high as 200 meq m^{-2} yr^{-1} during the late 1960s, when

strong acid concentrations in atmospheric deposition peaked (Likens et al., 1998).

The relationship between present-day cation losses and long-term mineral

weathering rates differed among the six regions in W-1. Johnson et al. (2000) calculated

present-day cation losses in three vegetation zones (spruce-fir, high hardwood and low

hardwood) in W-6 at the HBEF that correspond to Regions 1-2, 3-4, and 5-6 in this study,

respectively. The lithology, aspect, elevation, hydrology, and slope are similar between

each W-6 vegetation zone and its paired region in W-1. Present-day cation losses from

individual vegetation zones in W-6 ranged from 25 to 141 meq m^{-2} yr^{-1} during 1982-92

(Johnson et al., 2000). In the spruce-fir zone, the present-day cation loss (25 meq m^{-2} yr^{-1})

was less than half the long-term weathering rate (33 to 47 meq m^{-2} yr^{-1}), but twice the

present-day weathering rate (10 meq m^{-2} yr^{-1}) based on the relationship between long-

term and present-day mineral weathering rates (Taylor and Blum, 1995; Figure 2-6). In

this vegetation zone, Johnson et al. (2000) estimated from Na mass balance that

plagioclase weathering could account for 87% of the base cation loss. Similarly, the

watershed of Cone Pond, located 10 km southeast of the HBEF, and containing glacial till

of similar composition, had an average cation loss rate of 35 meq m^{-2} yr^{-1} for the period

from 1989-1994 (Hyman et al., 1998). The authors argued that plagioclase dissolution

could account for most of the Ca and total base cation loss from the soils at Cone Pond

(61 and 68%, respectively). In contrast, only 26-37% of the Ca lost from the soils in the

hardwood zones of W-6 could be attributed to plagioclase dissolution and the remaining

63-74% was due to removal from soil exchange sites and organic matter (Johnson et al.,

2000). These high present-day cation losses in the high and low hardwoods far exceed the

long-term mineral weathering rates (Figure 2-6). According to Taylor and Blum (1995),

the expected present-day mineral weathering rates should be ~11 and 7 meq m^{-2} yr^{-1},

respectively, values which are significantly lower than the soil cation losses from these

vegetation zones (52 and 141 meq m^{-2} yr^{-1}, respectively). Thus the difference between

present-day cation losses and present-day mineral weathering rates increases downslope

at the HBEF.

Of the three vegetation zones, the spruce-fir zone in W-1 lost the least amount of

base cations from the soil exchange pool during 1982-92 (Figure 2-6; Johnson et al.,

2000). Johnson et al. (2000) suggested the relatively small loss was due to the thinner

glacial till at the top of the watershed. That is, contact between soil water and glacial till

increased downslope which allowed for more acid neutralization, greater base cation

fluxes from the soil, and an increased pH downstream (Johnson et al., 2000). The effect

of glacial till depth in neutralizing incoming acidity has also been proposed for

watersheds surrounding Woods Lake and Panther Lake in the Adirondack Mountains.

Long-term weathering rates were similar for these two watersheds but Woods Lake soils

were developed on thinner glacial till, had a lower present-day base cation loss, and had

more acidic soil water (April et al., 1986a). The authors suggested that Panther Lake was

able to neutralize incoming acidity due to its thick glacial till; as a result, more base

cations but less acid waters were released from its soils.

From the 1950s until emissions were reduced by the Clean Air Act in 1970, acid deposition in the northeast U.S. accelerated base cation loss from the exchange pool (Likens et al., 1996) by mobilizing aluminum, which displaces cations (especially Ca) on soil exchange sites (Lawrence et al., 1995). The difference between cation losses and expected present-day mineral weathering rates suggests that acid deposition has accelerated base cation loss in the high and low hardwoods at the HBEF by a factor of four to eighteen. If acid deposition has decreased soil pH, it may have also enhanced mineral weathering rates to a small degree because laboratory experiments indicate that feldspar dissolution rates increase as pH decreases below 5 (e.g., Blum and Stillings, 1995). However, it appears that the pH of the soils in eastern North America and Europe has not changed significantly (Wright, 1988). Also, the base cations released from mineral dissolution appear to be a small fraction of annual watershed losses and have not balanced the loss from cation exchange sites due to acid deposition (Likens et al., 1998).

Mineral Weathering Rates

In addition to calculating an overall loss of elements from the composite soil profiles, we estimated the long-term weathering rates of individual minerals using a geochemical mass balance approach. Most of the base cations released by chemical weathering at the HBEF are derived from a small number of minerals, which include plagioclase, potassium feldspar, biotite, and apatite (Table 2-3).

Plagioclase

First, we assumed that all of the Na lost from the W-1 soil profiles (Table 2-5) was due to weathering of the average plagioclase composition in W-1 ($Na_{0.83}Ca_{0.17}Al_{1.2}Si_{2.8}O_8$), which is an oligoclase. In temperate climates such as at the HBEF, plagioclase generally weathers to kaolinite resulting in the loss of Ca and Na and the retention of Al and Si as secondary weathering products in the soil. Using the stoichiometry of oligoclase, we estimated that plagioclase has weathered from the soil profile at an average rate of 15 mmol m^{-2} yr^{-1}, and — depending on the region in W-1 — accounts for 64-78% of the Ca lost from the soils over the last 14,000 years (Table 2-6). Thus, plagioclase weathering has been the dominant weathering source of Ca to the watershed over the age of the soil (Figure 2-7), as well as during the last few decades (Likens et al., 1998).

Our analysis of plagioclase from W-1 soil parent materials revealed only plagioclase with low Ca contents (i.e., oligoclase). However, more anorthite-rich plagioclase (up to An_{95}) has been reported in the local bedrock at the HBEF (Likens et al., 1998). For example, plagioclase with a high anorthite content (An_{95}) is present in the calc-silicates of the Rangeley Formation, although it is not very abundant in the experimental watersheds (Bailey et al., 2003). Because Ca-rich plagioclase weathers much faster than its sodic counterpart, especially above ~80% anorthite content (Blum and Stillings, 1995), its dissolution could account for some of the Ca lost from the soils in excess of what is expected from the weathering of oligoclase.

Hornblende, another Ca- and Na-bearing mineral, is also present in HBEF soils. Because hornblende is much less abundant than plagioclase and laboratory dissolution rates of these two minerals are similar at a pH of ~4 (Blum and Stillings, 1995; Brantley

25

and Chen, 1995), we assumed that hornblende weathering did not account for a significant loss of Ca or Na from the soil profiles. April et al. (1986) calculated long-term hornblende weathering rates in soil profiles in Adirondack watersheds underlain by granitoid-derived glacial till. Normalizing their long-term weathering rate (~1 mmol hornblende $m^{-2} yr^{-1}$) by the volume percent of hornblende in the Adirondack soils, and using the hornblende stoichiometry measured in HBEF soils (1.8 mol Ca and 0.4 mol Na per mol hornblende), we estimated that hornblende weathering could account for a maximum of ~8% of Ca and ~1% of Na lost from the soils.

Present-day rates of plagioclase weathering at the HBEF have been estimated from net Na fluxes (i.e., the difference between atmospheric input and stream fluxes). Unlike other base cations, only negligible amounts of Na are stored in exchangeable pools, secondary minerals or organic matter and, hence, net Na fluxes from the watershed have been used to estimate plagioclase weathering rates (Johnson et al., 1991b; Likens et al., 1998; Bailey et al., 2003). At a watershed level, present-day Na net fluxes have been relatively constant over the last 40 years (Likens et al., 1998; Johnson et al., 2000). The current rate of plagioclase weathering estimated from these fluxes (~30 mmol plagioclase $m^{-2} yr^{-1}$) is greater than the mean long-term weathering rate of plagioclase in W-1 (15 mmol $m^{-2} yr^{-1}$, Table 2-6). For comparison, the present-day weathering rate of plagioclase in nearby Cone Pond watershed, estimated from net Na fluxes during 1989-1994, was 17 mmol plagioclase $m^{-2} yr^{-1}$ (Hyman et al., 1998).

Long-term weathering rates of plagioclase decrease downslope, whereas present-day weathering rates (as well as the flux of each of the base cations) increase downslope. Using net Na losses, Johnson et al. (2000) calculated present-day weathering rates of

plagioclase in the three vegetation zones in W-6 at the HBEF. Present-day rates of plagioclase weathering in the spruce-fir and high hardwood vegetation zones in W-6 (18.5 and 18.9 mmol m^{-2} yr^{-1} respectively) are similar to the long-term weathering rates we calculated (19 and 15 mmol m^{-2} yr^{-1}). In the lower hardwoods, however, the current rate of plagioclase weathering (43.5 mmol m^{-2} yr^{-1}) is almost three times higher than the long-term weathering rate (9 to 13 mmol m^{-2} yr^{-1}). Only 12 and 24% of the Na remains in the soil profiles in Regions 1 and 2, respectively, whereas 40 to 72% of the initial Na is still present in soil minerals in Regions 3-6. The high long-term weathering rates and small pool of remaining Na in Regions 1 and 2 suggest that plagioclase is more depleted at the high-elevation sites. In addition, the Na depletion profiles (Figure 2-4), which represent the fraction of Na lost from the profile at different depths, suggest that, in general, a higher proportion of plagioclase has been weathered from the upper soil horizons.

Apatite

Although the Ca content of the soils is dominated by plagioclase, there are other Ca-bearing minerals present in the soil parent material. We found abundant, small crystals of apatite, $Ca_5(PO_4)_3(F,Cl,OH)$, which were completely or partially included in feldspars and quartz in the soil parent material. Apatite dissolves much more rapidly than oligoclase (Welch and Ullman, 1993; Valsami-Jones et al., 1998; Welch et al., 2002) and is the dominant P-bearing phase in almost all crystalline rocks, followed by the much less abundant mineral, monazite (Ce-phosphate). Assuming that all of the mineral P in the C horizon is hosted in apatite, we estimated from apatite stoichiometry that ~20% of the Ca

in the C horizon is in apatite. Next, we estimated the minimum amount of Ca loss due to apatite weathering by assuming that the P depletion in the upper horizons was due to apatite dissolution. Since P is retained in organic matter and Fe- and Al-oxides in soils (e.g., Crews et al., 1995), some of the P that is released from apatite remains in the soil in non-mineral form making our estimates of apatite weathering minimum values. Estimated rates of apatite weathering in W-1 ranged from 0.08 to 0.22 mmol m^{-2} yr^{-1}, with the highest rates in Region 2. This long-term pattern in apatite dissolution in W-1 is similar to the present-day pattern of apatite loss suggested by Blum et al. (2002). Also, the Ca/Sr and ^{87}Sr/^{86}Sr ratios of spruce and fir foliage were more similar to that of apatite than other tree species, and it was proposed that ectomycorrhizal trees such as spruce and fir may be capable of enhancing the dissolution of apatite (Blum et al., 2002).

The Ca associated with P that has been weathered from apatite accounts for 12-22% of the total Ca lost from the profile (Figure 2-7). This study as well as others (Likens et al., 1998; Blum et al., 2002; Bailey et al., 2003) found small amounts of other Ca-bearing minerals in the soil parent material that weather more rapidly than oligoclase including hornblende, augite, diopside, actinolite, epidote, and trace amounts of calcite. The dissolution of these minerals appears to release only a small fraction of calcium. It should be emphasized that our apatite weathering rates are based on the amount of P loss from the soils; hence, the weathering of hornblende or other Ca-bearing (but non-P bearing) minerals would not change our estimates of apatite dissolution. According to our estimates, plagioclase and apatite weathering are responsible for 89% of the Ca loss from the soils; as mentioned in Section 5.4.1, ~8% can be attributed to weathering of hornblende.

Blum et al. (2002) estimated that apatite contains at least 12% of the Ca in the soil parent material based on Ca and P contents of sequential leaches of the C horizon, and that apatite is largely depleted from the upper horizons in the W-1 soils, but not from the Bs2 and C horizons. The percent of Ca associated with apatite in the C horizon estimated by Blum et al. (2002) is also a conservative estimate because many apatite inclusions in feldspar and quartz are not dissolved by acid leaches unless their host minerals are digested.

Biotite

Because biotite is the dominant Mg-bearing mineral in the soil, we made the assumption that most of the Mg lost from the soil was released by the weathering of biotite to vermiculite. We further assumed that the stoichiometry of vermiculite in W-1 is similar to that found in the Adirondacks (April et al., 1986b) and Cone Pond (Hyman et al., 1998); that is, that each mole of vermiculite contains ~0.03 moles of Mg. Since biotite in W-1 averaged 0.63 moles of Mg per mole of biotite (Table 2-3), we estimated that 0.60 moles of Mg were lost for every mole of weathered biotite. Based on this stoichiometry and the loss of Mg from the soils, biotite is estimated to have weathered at an average rate of 2.2 to 5.1 mmol m^{-2} yr^{-1} (Table 2-6) and accounts for 17-25% of the total K lost from the soils at the HBEF. This long-term weathering rate of biotite at the HBEF is faster than the present-day weathering rate (1.1 mmol biotite m^{-2} yr^{-1}) estimated for the nearby Cone Pond watershed (Hyman et al., 1998).

Potassium Feldspar

We assumed that the K loss in excess of that lost from biotite weathering was due to weathering of potassium feldspar, which constitutes ~20% of the soil parent material by volume. Potassium feldspar, which is more stable in soils than oligoclase, releases K as it dissolves congruently and/or transforms to kaolinite. Muscovite, another K-bearing mineral, is more weathering-resistant than potassium feldspar and biotite (Nagy, 1995) and less abundant; thus we assumed that weathering of muscovite was not a significant source of base cations in these soils. Long-term weathering rates of potassium feldspar ranged from 5 to 11 mmol m^{-2} yr^{-1} with a weighted watershed mean of ~8 mmol m^{-2} yr^{-1} (Table 2-6). The rates of potassium feldspar and plagioclase weathering at higher elevations were twice the rates at lower elevations in the watershed. High Ba/Sr ratios in the cation exchange pool and soil water in the spruce-fir zone of W-1 are consistent with our finding that the present-day weathering rate of potassium feldspar (which has a high Ba/Sr ratio) is greatest at the top of the watershed (Hogan and Blum, 2003).

Spatial Variation of Weathering

Mineral weathering rates are highest at the higher elevations in W-1. Regions at the top of the watershed are completely (Region 1) or partially (Region 2) located within the spruce-fir zone. Conifers enhance mineral weathering in a number of ways. First, conifers produce more acidic soils than deciduous trees (e.g., Augusto et al., 2000). The spruce-fir soil waters at the HBEF are highly acidic and contain elevated dissolved organic carbon concentrations, indicating high production of organic acids (Johnson et al., 2000). These conditions promote mineral weathering and may be responsible for the intense weathering of potassium feldspar and plagioclase at the top of the watershed

(Hogan and Blum, 2003). Secondly, spruce and fir trees have ectomycorrhizae that exude low molecular weight organic acids which have been shown to enhance the weathering of minerals, including microcline, hornblende, biotite and apatite (Jongmans et al., 1997; Wallander and Wickman, 1999; van Breemen et al., 2000; Wallander, 2000; Welch et al., 2002). Some hardwoods in the lower part of W-1 also have ectomycorrhizal associations, but overall, trees with ectomycorrhizal associations are more abundant at higher elevations. In addition, conifers more effectively intercept atmospheric deposition, including sulphate ions, due to the frequency of cloud immersion and the year-round presence of foliage (Lovett et al., 1999). As a result, total acid deposition may be higher in conifer forests compared to deciduous forests.

Despite the evidence that conifers are capable of enhancing mineral weathering rates in soils, it is difficult to indisputably establish that conifers are responsible for the high long-term weathering rates at higher elevations in W-1 due to the fact that the current forest composition may have been changed by logging over the past 200 years (Hamburg and Cogbill, 1988). However, pollen and plant microfossils in lake sediments in the White Mountains indicate that mixed hardwood forests below 700 m were established ~7000 years ago and conifers have been predominant above 750 m for the last ~10,000 years (Spear et al., 1994). Thus, it appears that over most of the age of the soil, the distribution of hardwoods and conifers at the HBEF has probably been similar to its present-day composition.

Present-day net Na fluxes from W-6 indicate that present-day plagioclase weathering rates increase downslope (Johnson et al., 2000). The authors suggest that this pattern is due to increased mineral/water contact time downhill. While hydrologic

flowpaths should influence weathering rates in the soil, the trend that we observe in long-term weathering rates is opposite with bulk soil and plagioclase weathering rates decreasing downslope. The reason for this discrepancy is unclear.

Temperature, which typically decreases with elevation in a watershed, may also affect weathering rates. Present-day plagioclase weathering rates, calculated from solute fluxes of Na, were compared in two small catchments of similar parent rock, hydrology, and vegetation located in the Blue Ridge Mountains, North Carolina (Velbel, 1993). A catchment at the lower mean elevation (849 m) had a higher weathering rate than the second catchment at a higher elevation (1019 m). This difference in weathering rates was attributed to a 1.1 °C difference in mean annual temperature (Velbel, 1993). Although the relief in W-1 (~260 m) is similar to the watershed in the Blue Ridge Mountains, the pattern of long-term plagioclase weathering rates in W-1 exhibits the opposite trend with elevation. Thus, variables other than temperature have had a greater influence on mineral weathering rates in the Hubbard Brook watersheds over the last 14,000 years.

We have made the assumption that soil profiles in W-1 at the HBEF were not significantly affected by downslope movement. Soil profiles generally appear to be undisturbed, and we observed sharp boundaries between soil horizons, thin and well-defined E horizons, and very few repeated soil horizons. Thus it appears that physical transport of soil does not lead to a great deal of soil mixing or variability in observed weathering rates across the watershed. Redistribution of weathered soil material downslope would tend to yield more highly weathered soil profiles at lower elevations, contrary to the long-term pattern we observe in W-1.

The variability of weathering rates that we calculated for the six regions of W-1 (HBEF) is as great as the variability among several 10 to 15 ka-old watersheds across the U.S. and Canada (April et al., 1986a; Kirkwood and Nesbitt, 1991; Bain et al., 1993; Taylor and Blum, 1995). Although long-term weathering rates in soils of similar parent material in similar climates are primarily dependent on soil age, other factors within a watershed such as parent material heterogeneity, landscape position and vegetation appear to cause about the same amount of variability in weathering rates as would an approximately 5 ka difference in the duration of soil development (Figure 2-5).

Intra-watershed variability in long-term weathering rates has been observed in several previous studies. Measurements of long-term weathering rates in two watersheds in the Adirondack Mountains, New York varied by 34 and 50% (coefficient of variation) (April et al., 1986a). Bain et al. (1994) found that long-term weathering rates calculated from seven soil profiles in a 10-km^2 watershed (Cairngorn Mountains, Scotland) ranged by almost an order of magnitude (7-64 meq m^{-2} yr^{-1}) and that long-term loss of K and Na (110 and 82% coefficient of variation, respectively) varied significantly. Long-term weathering rates have been typically calculated from one soil profile per age in soil chronosequences studies (e.g., Bain et al., 1993; Taylor and Blum, 1995) because the difference in rates among soils of different ages is presumed to be higher than the variability among multiple profiles on a single-age surface. Because W-1 has homogeneous soil parent material and uniform precipitation, the variability in long-term chemical weathering rates can be attributed to the effects of till depth, vegetation, and hydrology. The wide range of weathering rates that we observed in this small watershed suggests that our composite sampling strategy is necessary, and that even with our

composite sampling, the analysis of multiple composite soil profiles may be needed to provide a reliable estimate of long-term weathering rates in a watershed.

Conclusions

The average long-term chemical weathering rate in W-1 at the Hubbard Brook Experimental Forest (35 meq m^{-2} yr^{-1}) is similar to rates in other ~10 to 15 ka-old soils developed on granitic till in temperate climates, but is less than half of the present-day cation loss from the watershed (Johnson et al., 2000). Because long-term weathering rates are an integration of mineral weathering rates over the last 14 ka and typically decrease rapidly over time (e.g., Bain et al., 1993; Taylor and Blum, 1995), the current mineral weathering rates are expected to be about one-third of the long-term weathering rates in the absence of disturbance (Taylor and Blum, 1995). Therefore, relatively high present-day cation losses from the watershed, which represent the amount of base cations released from both cation exchange pools and minerals, support the hypothesis that the pool of exchangeable base cations is decreasing in HBEF soils (Likens et al., 1996; Likens et al., 1998).

Despite a relatively homogeneous soil parent material and uniform precipitation over a small area, long-term weathering rates in W-1 at the Hubbard Brook Experimental Forest are highly variable. Long-term weathering rates in the bulk soil, as well as plagioclase, potassium feldspar and apatite weathering rates, are greater at the top of the watershed. Because the soils are developed on relatively homogeneous glacial till, the variations in soil chemistry and weathering patterns are most likely due to the effects of landscape position and vegetation on chemical weathering. The long-term weathering

rates are higher where conifers are abundant and soils have developed on thin glacial till. This variability over a small area suggests that extensive soil sampling is needed to estimate a representative long-term weathering rate for a watershed.

In the soil parent material at the Hubbard Brook Experimental Forest, we found ubiquitous small inclusions of apatite in major minerals. Our data suggest that apatite may be a significant source of calcium to vegetation due to the high solubility of this mineral. A geochemical mass balance of the soil chemistry suggests that plagioclase weathering is responsible for most of the Ca lost from the soils (64-78%) but that apatite dissolution may account for a significant amount (12-22%) of the Ca lost from the soils.

Acknowledgements

Table 2-1. Characteristics of the six regions in Watershed 1

Region	Elevation (m)	Slope (%)	Predominant Forest Type
1	723-742	11	spruce-fir
2	689-740	25	spruce-fir
3	576-683	21	hardwood
4	571-677	23	hardwood
5	489-571	13	hardwood
6	496-563	13	hardwood

Table 2-2. Properties of W-1 soil horizons

Horizon	n[a]	Thickness (cm) Mean[b]	Thickness (cm) s.d.[c]	Bulk ? (g cm^{-3})	Mass (Mg ha^{-1})
		Region 1			
Oie	4 of 4	2.6	1.2	nd[d]	34
Oa	3 of 4	4.0	5.5	nd	78
E	4 of 4	3.2	3.4	0.88	254
Bh	2 of 4	1.9	2.1	0.52	90
Bs1	4 of 4	4.3	2.5	0.62	236
Bs2	3 of 4	19.1	8.1	0.72	1098
Total above C		39.0	13.5		
		Region 2			
Oie	8 of 8	3.3	0.8	nd	38
Oa	7 of 8	2.9	0.9	nd	164
E	6 of 8	3.5	5.1	0.87	273
Bh	6 of 8	1.8	0.7	0.51	84
Bs1	8 of 8	4.7	1.1	0.59	246
Bs2	8 of 8	51.8	17.9	0.78	3253
Total above C		68.3	16.7		
		Region 3			
Oie	11 of 11	3.0	0.8	nd	40
Oa	11 of 11	4.8	3.2	nd	166
E	10 of 11	2.6	1.7	1.10	251
Bh	11 of 11	3.6	1.8	0.72	232
Bs1	11 of 11	5.9	2.6	0.78	408
Bs2	11 of 11	55.7	17.0	0.92	4116
Total above C		76.3	18.2		
		Region 4			
Oie	9 of 9	3.91	0.76	nd	40
Oa	9 of 9	3.84	1.39	nd	123
E	3 of 9	0.43	1.74	1.09	42
Bh	8 of 9	4.90	4.34	0.44	192
Bs1	9 of 9	7.13	4.24	0.63	396
Bs2	9 of 9	38.97	23.83	0.96	2990
Total above C		61.7	20.9		
		Region 5			
Oie	9 of 9	3.8	0.8	nd	35
Oa	9 of 9	5.1	2.5	nd	74
E	7 of 9	2.3	1.4	1.28	259
Bh	9 of 9	3.0	1.5	0.88	238
Bs1	9 of 9	5.1	1.5	0.88	396
Bs2	9 of 9	52.4	9.1	1.03	4311
Total above C		72.6	8.8		
		Region 6			
Oie	4 of 4	2.8	0. 8	nd	32
Oa	4 of 4	3.0	1.0	nd	72

E	4 of 4	2.1	0.6	1.15	221
Bh	4 of 4	2.0	1.8	1.15	208
Bs1	4 of 4	5.0	1.2	0.98	436
Bs2	4 of 4	49.3	17.0	1.17	4635
Total above C		65.2	19.4		

(a) The number of pits with the specified horizon per total number of pits in that region.

(b) Mean thickness was calculated by assigning missing horizons a thickness of zero.

(c) Standard deviation.

(d) Not determined for Oie and Oa horizons.

Table 2-3. Abundance and mean chemical composition of major elements in minerals from Watershed 1

Mineral	Abundance[a] volume %	n	CaO	Fe_2O_3[b]	Al_2O_3	SiO_2	K_2O	MgO	Na_2O	TiO_2
					weight %					
Plagioclase	27	19	3.68	<0.1	23.4	62.8	0.12	<0.02	9.65	<0.05
Alkali feldspar	18	5	<0.03	<0.1	19.3	64.3	15.4	<0.02	0.94	<0.05
Biotite	3	6	0.04	27.6	20.3	37.0	8.0	6.41	0.10	3.28
Hornblende	1	4	12.05	22.4	13.0	43.2	0.65	8.64	1.61	0.61
Muscovite	4	5	<0.03	1.9	37.5	48.7	9.67	0.85	0.62	0.85

(a) Estimated from point counts of C horizon soils collected across the watershed. The remaining 47% is quartz.

(b) Total Fe as Fe_2O_3.

Table 2-4. Chemical composition of Watershed 1 soil horizon composites

Region	Horizon	CaO	K$_2$O	MgO	Na$_2$O	P$_2$O$_5$	TiO$_2$	Sr	LOI
					wt %			mg g^{-1}	%
1	Oa	0.44	1.44	0.23	0.88	0.32	0.67	0.048	49.2
2	Oa	0.47	1.46	0.23	0.89	0.27	0.44	0.053	40.6
3	Oa	0.43	1.13	0.16	0.75	0.19	0.29	0.043	53.9
4	Oa	0.28	0.81	0.14	0.49	0.33	0.29	0.033	60.0
5	Oa	0.51	0.88	0.12	0.56	0.19	0.17	0.044	76.6
6	Oa	0.43	0.94	0.11	0.60	0.22	0.20	0.042	46.5
1	E	0.61	2.44	0.33	1.32	0.12	1.12	0.066	12.7
2	E	0.54	2.29	0.25	1.23	0.10	0.85	0.068	8.7
3	E	0.56	2.58	0.14	1.42	0.04	0.48	0.066	4.6
4	E	0.63	2.15	0.20	1.26	0.04	0.75	0.072	8.0
5	E	0.61	2.28	0.15	1.49	0.04	0.47	0.067	3.7
6	E	0.66	2.35	0.17	1.53	0.04	0.48	0.071	5.1
1	Bh	0.41	2.07	0.19	0.97	0.28	0.69	0.053	32.5
2	Bh	0.51	1.97	0.27	1.06	0.23	0.63	0.061	28.0
3	Bh	0.55	1.95	0.21	1.21	0.12	0.43	0.061	17.7
4	Bh	0.46	1.42	0.23	0.88	0.23	0.53	0.055	36.7
5	Bh	0.62	1.94	0.25	1.36	0.12	0.45	0.064	14.3
6	Bh	0.61	1.83	0.22	1.38	0.05	0.40	0.062	13.8
1	Bs1	0.53	1.64	0.39	0.99	0.27	1.00	0.053	25.0
2	Bs1	0.52	1.81	0.31	1.04	0.20	0.59	0.061	23.5
3	Bs1	0.56	1.88	0.25	1.16	0.12	0.40	0.059	16.3
4	Bs1	0.51	1.61	0.30	1.05	0.18	0.59	0.060	29.1
5	Bs1	0.65	1.84	0.31	1.34	0.14	0.41	0.064	15.6
6	Bs1	0.64	1.87	0.27	1.38	0.10	0.44	0.066	12.7
1	Bs2	0.93	1.77	0.87	1.43	0.32	1.24	0.075	24.6
2	Bs2	0.72	2.06	0.48	1.41	0.19	0.60	0.074	15.9
3	Bs2	0.70	2.04	0.34	1.49	0.15	0.37	0.070	11.5
4	Bs2	0.57	1.90	0.41	1.18	0.14	0.56	0.067	14.0
5	Bs2	0.76	2.01	0.34	1.51	0.14	0.31	0.069	8.3
6	Bs2	0.75	1.86	0.34	1.47	0.13	0.33	0.070	6.1
1	C	1.09	2.87	0.51	2.17	0.18	0.37	0.098	1.8
2	C	0.93	2.13	0.33	1.73	0.16	0.30	0.073	2.3
3	C	1.00	2.99	0.52	2.13	0.15	0.35	0.090	3.7
4	C	0.82	2.60	0.51	1.67	0.14	0.38	0.076	5.3
5	C	1.04	2.34	0.38	1.96	0.17	0.30	0.086	2.5
6	C	1.55	3.03	0.67	2.65	0.20	0.47	0.117	2.3

Table 2-5. Cumulative loss of individual elements from composite soil profiles, loss of base cations (BC_{loss}), long-term weathering rates (W_{LT}), and estimated present-day weathering rates (W_{PD}) for the six regions in W-1. Present-day cation losses ($?X_{PD}$) from the HBEF reference watershed, W-6, during the period from 1982-1992 are listed for comparison (Johnson et al., 2000). The values for Region 6* were calculated by substituting the mean C horizon chemical composition (see Section 5.1 for more detail).

Region	Ca	K	Mg	Na	P	BC_{loss}	W_{LT}	W_{PD}	$?X_{PD}$
	mol m^{-2}					eq m^{-2}	meq m^{-2} yr^{-1}		
1	47	149	26	173	4.8	468	33	10	25
2	77	192	29	255	9.1	659	47	14	
3	54	191	43	208	4.0	594	42	12	52
4	39	144	32	143	3.3	428	31	9	
5	49	97	18	153	5.3	384	27	8	141
6*	28	98	20	99	3.8	294	21	6	

Table 2-6. Long-term rates of major minerals in W-1, HBEF compared to present-day weathering rates calculated by mass balance in W-6 and nearby Cone Pond watershed, New Hampshire

Region	Forest Type	Plagioclase Long-term	Plagioclase Present-day[b]	Apatite Long-term	Biotite Long-term	K feldspar Long-term
				$mmol\ m^{-2}\ yr^{-1}$		
1	spruce-fir	15	19[c]	0.11	3.1	9
2	spruce-fir	22		0.22	3.5	11
3	hardwood	18	19[c]	0.09	5.1	10
4	hardwood	12		0.08	3.8	8
5	hardwood	13	44[c]	0.13	2.2	5
6*	hardwood	9		0.09	2.4	5
Mean HBEF values[a]		15	31[c] (27-30)	0.12	3.5	8
Cone Pond, NH			17[d]		1.1[d]	

(a) Weighted by area of each region.

(b) Calculated by watershed mass balance.

(c) W-6, 1982-92 (Johnson et al., 2000); values in parentheses are range of rates for 1965-92 (Likens et al., 1998).

(d) Present-day weathering rates for 1989-94 (Hyman et al., 1998).
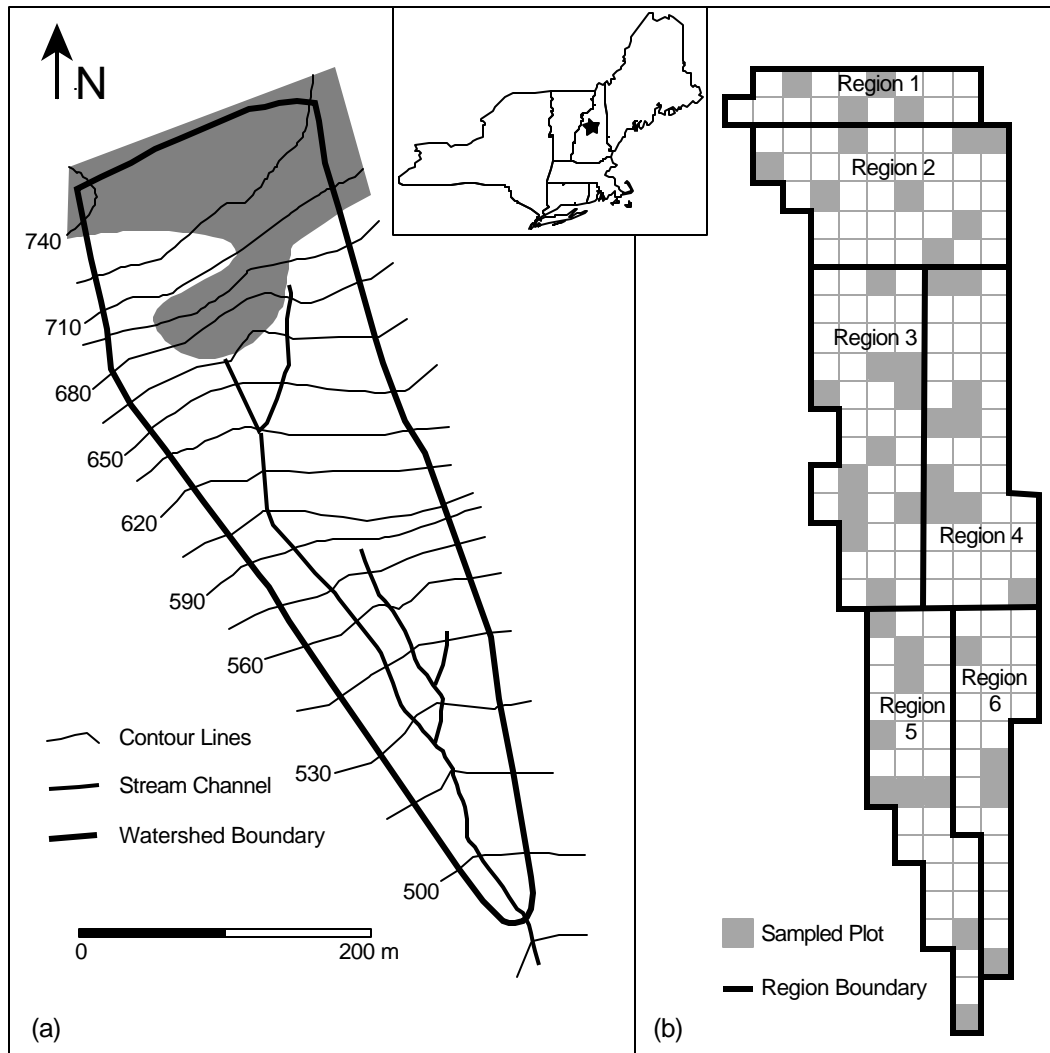
Figure 2-1. Map of study location. (a) Topographic map of Watershed-1, Hubbard Brook Experimental Forest, New Hampshire (modified from Hogan and Blum, 2003). The shaded area represents the spruce-fir zone. (b) Grid map of the same watershed. The shaded squares indicate the location of randomly-located soil pits.
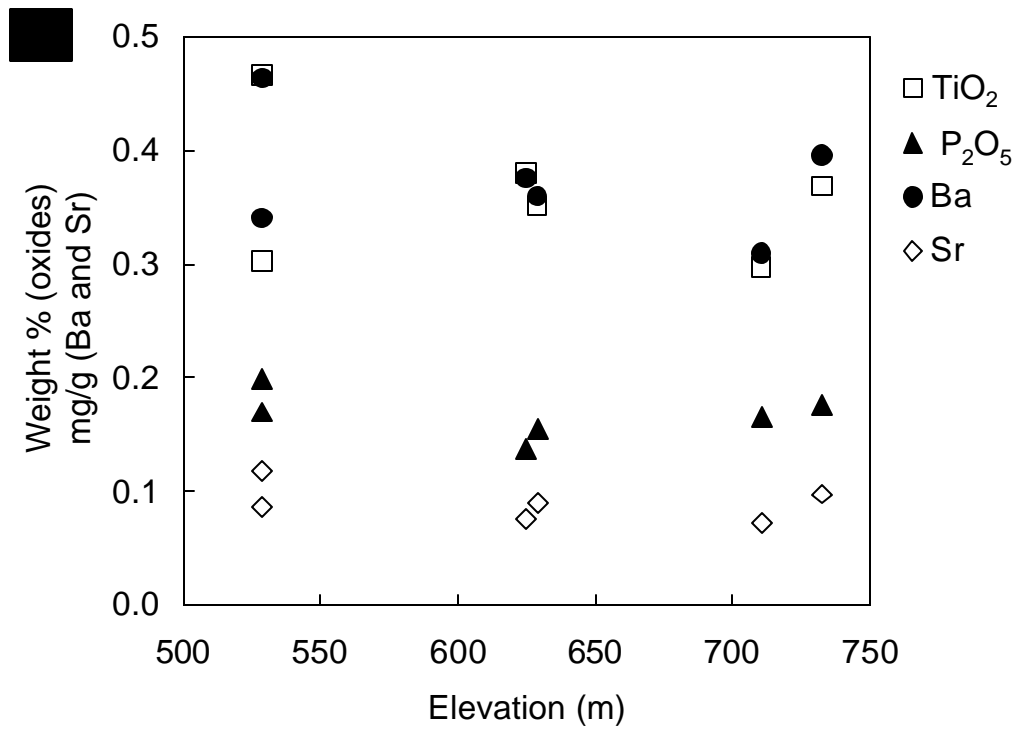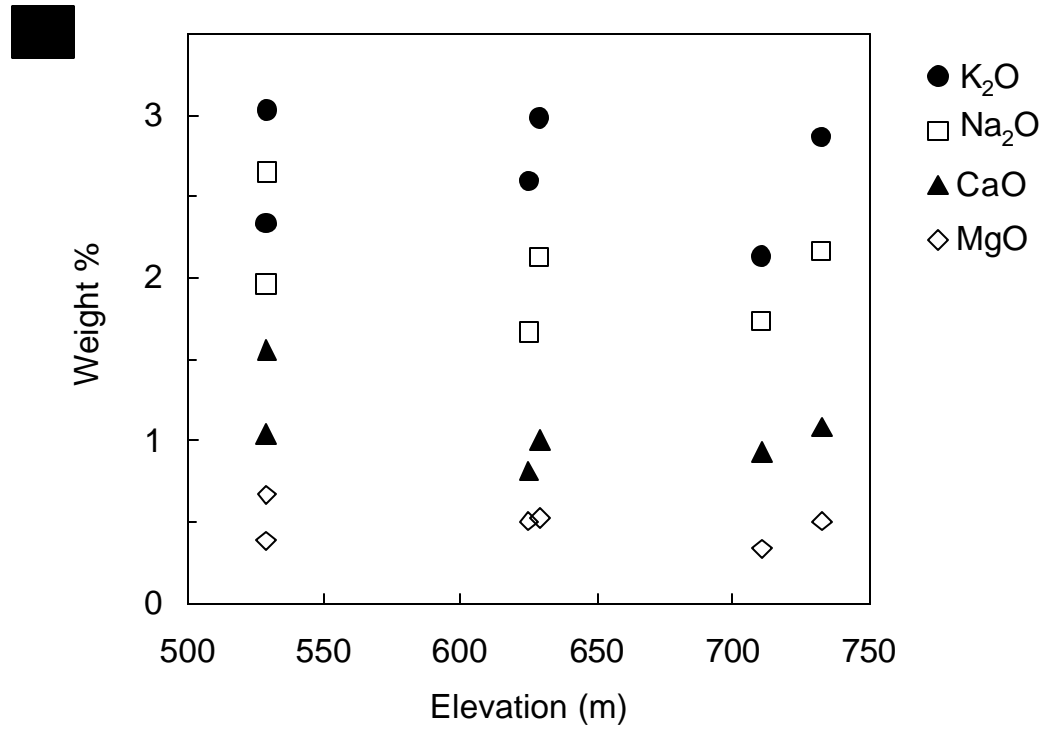
Figure 2-2. Concentration of major (a) and minor (b) cations in the six C horizon composite samples versus elevation.
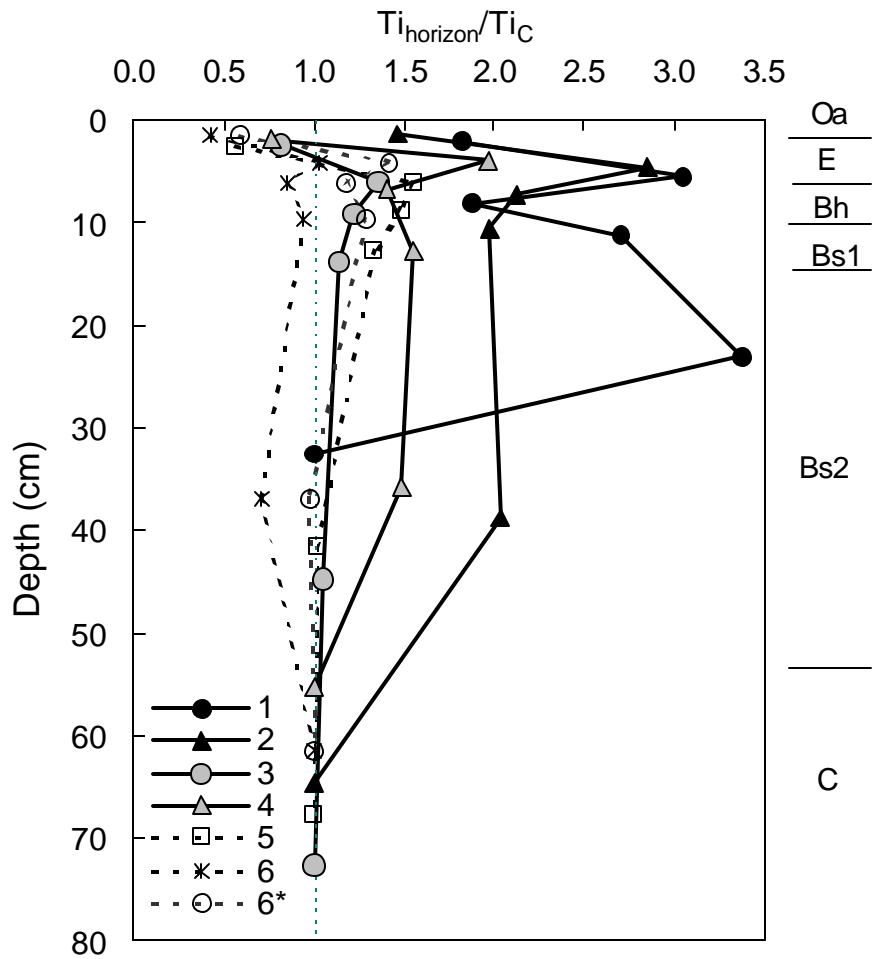
Figure 2-3. Titanium concentrations in the upper horizons normalized to the titanium concentration of the C horizon. The numbers in the legend indicate the regions of W-1 (see Figure 2-1). Data points are plotted at the mid-point depth of each horizon (Oa, E, Bh, Bs1, Bs2) or the mean upper boundary of the horizon (horizon C). Approximate horizon boundaries are marked to the right of the graph. The ratios for Region 6* were calculated by substituting the watershed mean of the C horizon chemical composition for that of the C horizon in Region 6.
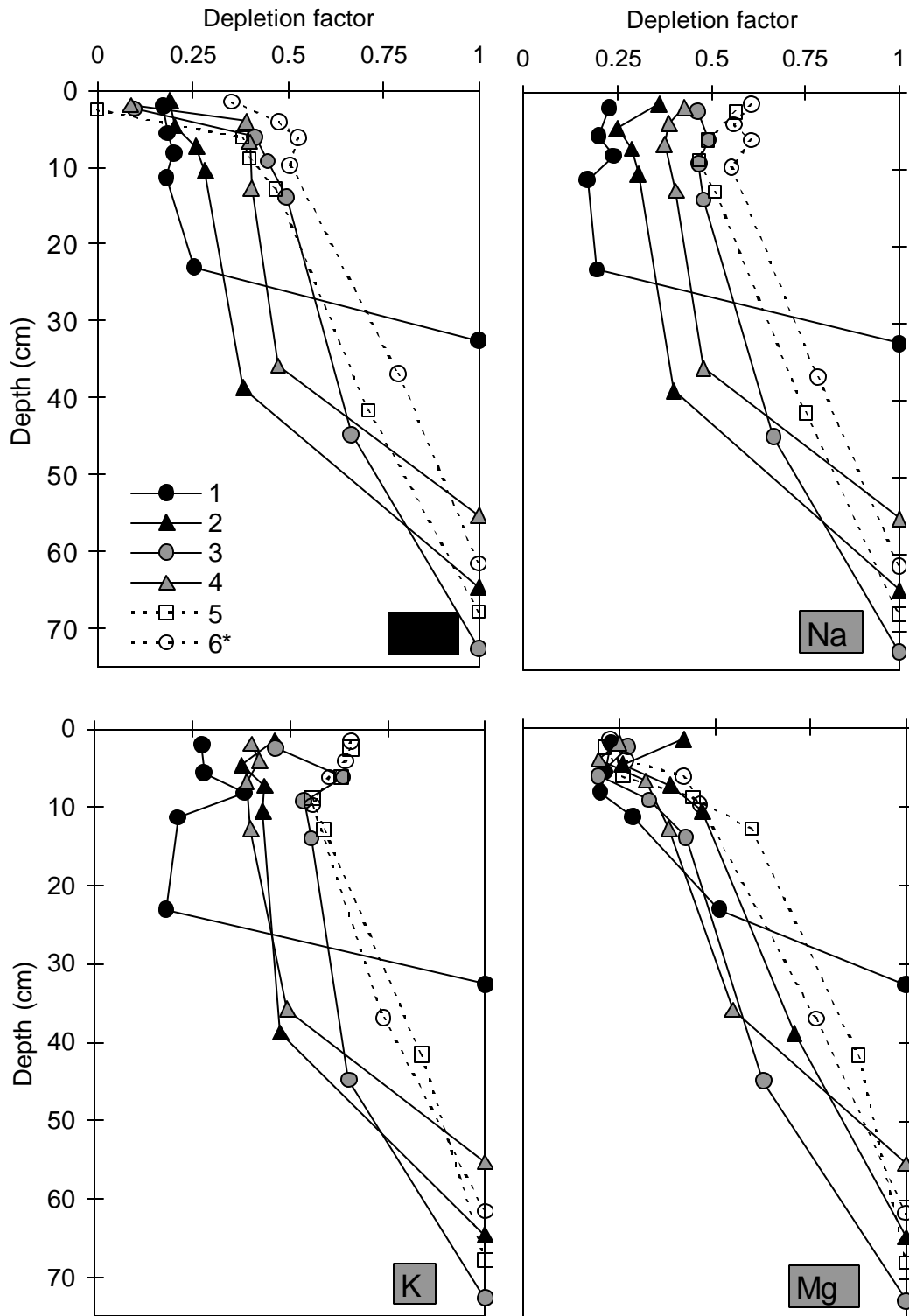
Figure 2-4. Depletion factors of base cations in Regions 1 through 6 of W-1 at the HBEF.
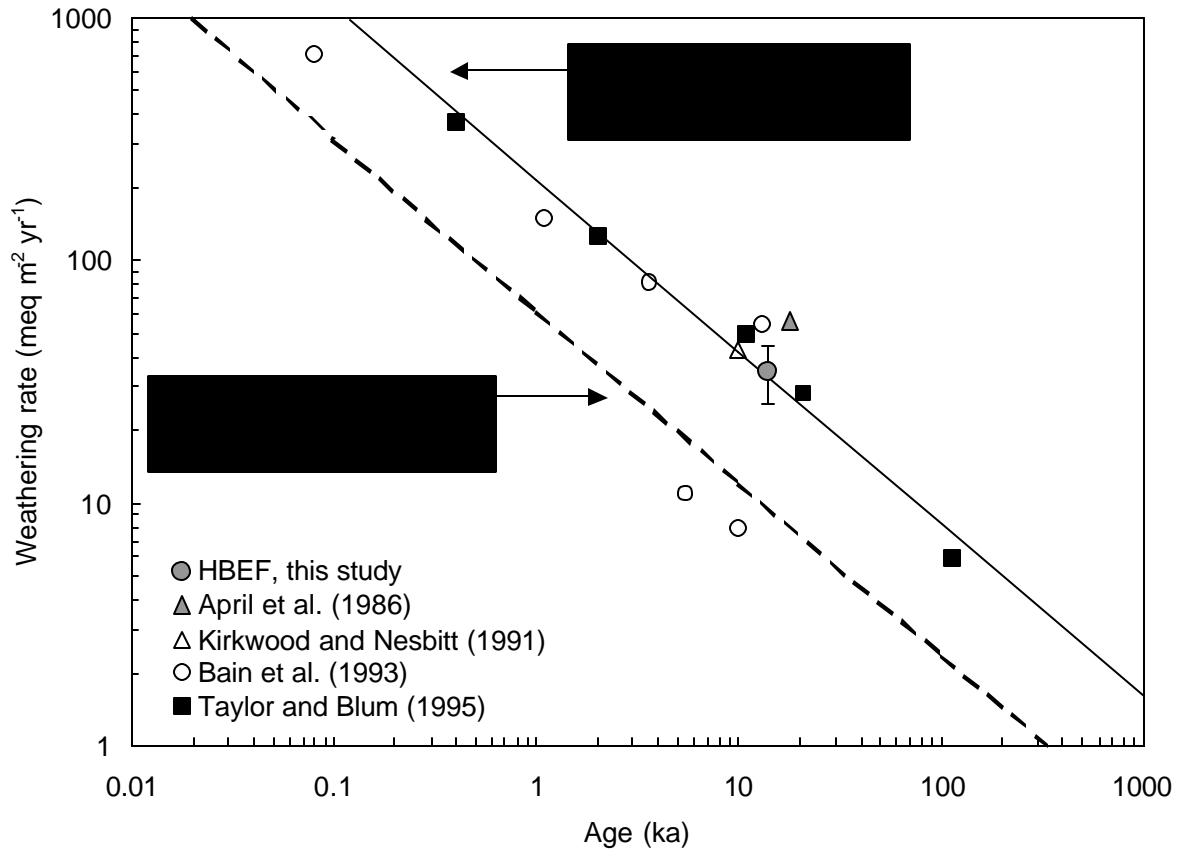
Figure 2-5. Long-term weathering rate (W_{LT}) as a function of age of soil (t) formed on a glacial deposit or a river terrace of granitoid lithology. The value for Hubbard Brook is the weighted average (± one standard deviation). The solid line is the best fit to the data of Taylor and Blum (1995). The dashed line is an estimate of short-term weathering rates determined by differentiating the equation for W_{LT}.
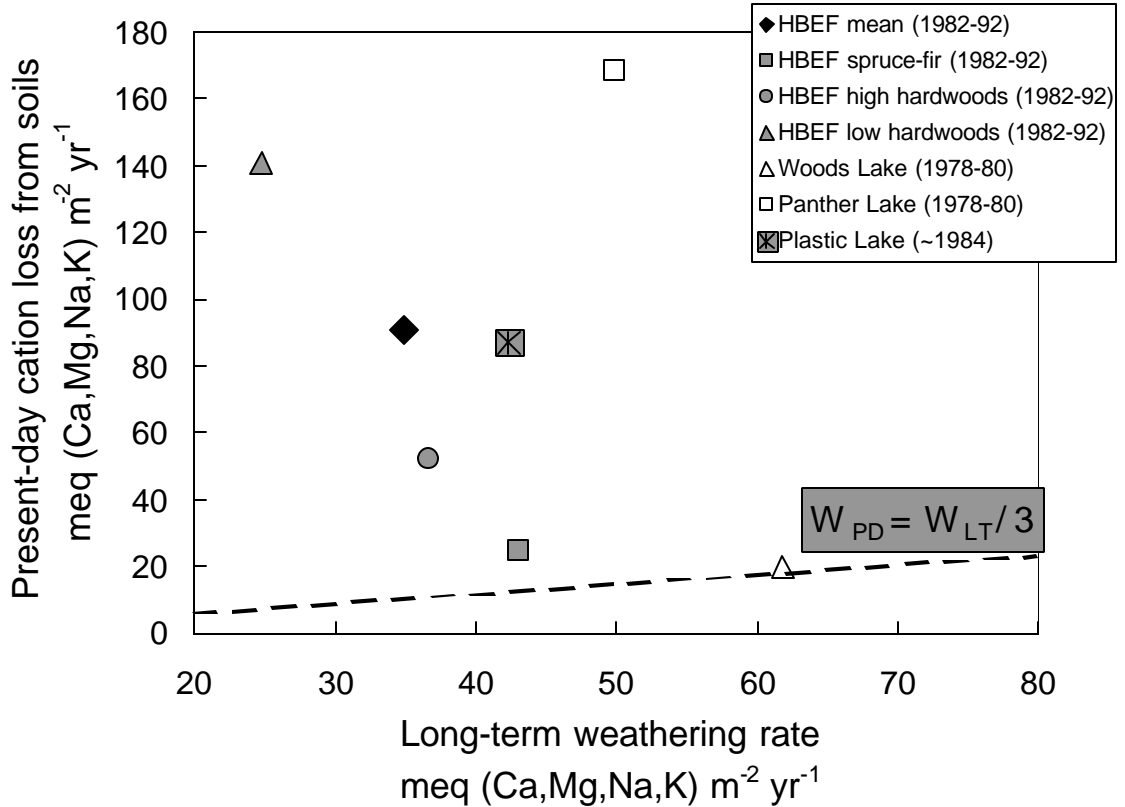
Figure 2-6. Present-day cation loss rates versus long-term weathering rates for granitoid watersheds. The present-day base cation loss from three vegetation zones in W-6 (Johnson et al., 2000) are plotted against the long-term weathering rates in the corresponding vegetation zones in W-1 (Table 2-5). The average long-term weathering rates are weighted by the area of each region. Data for Woods and Panther Lakes (Adirondack Mountains, New York) are from April et al. (1986a) and data for Plastic Lake (Ontario, Canada) are from Kirkwood and Nesbitt (1990). The time period for which present-day cation losses were determined is given in parentheses in the legend. The dashed line represents the relationship between the present-day weathering rate and the long-term weathering rate (see Section 5.3 for explanation). The points for Woods Lake and the spruce-fir zone in W-1 fall close to the WPD=WLT/3 line predicted by Taylor and Blum (1995) for an undisturbed watershed. All other points have a WPD that is much higher than predicted from WLT suggesting depletion of base cations from cation exchange pools.

48
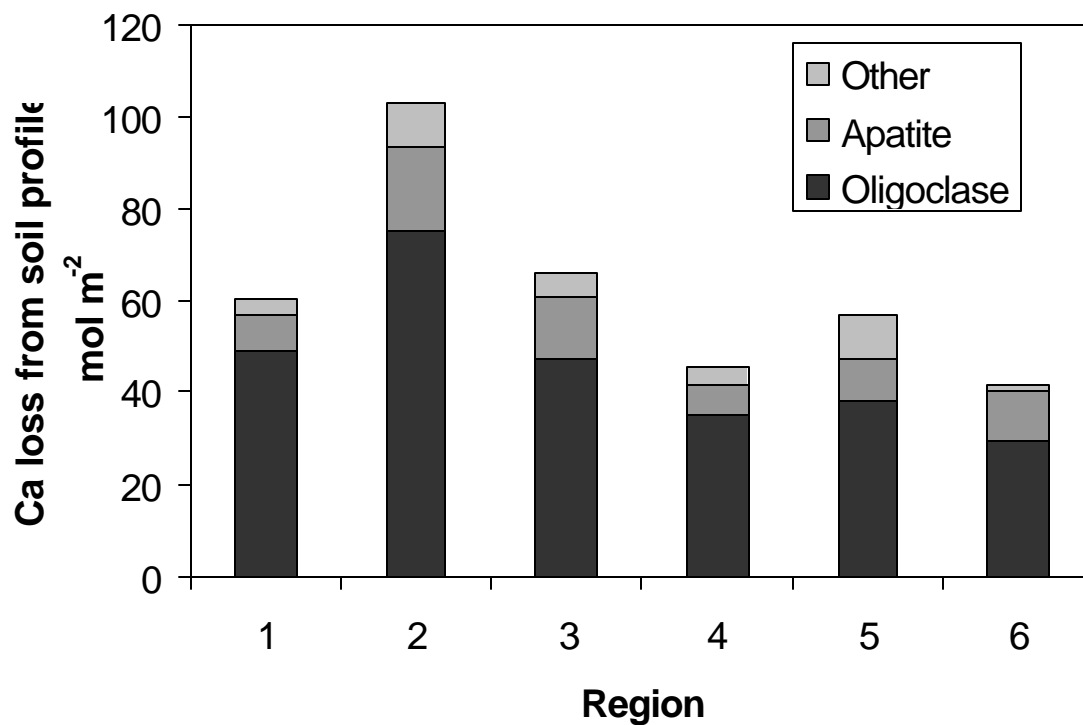
Figure 2-7. Ca loss from the W-1 soils over the last 14,000 years. The calcium losses due to oligoclase and apatite weathering were based on mineral stoichiometry and total element loss from each soil profile. Plagioclase weathering released most of the Ca from the soils (64-78%), but dissolution of apatite (<1% of the soil) accounted for a significant amount of calcium loss (12-22%).

References

April, R.H., Hluchy, M.M., Newton, R.M., 1986a. The nature of vermiculite in Adirondack soils and till. Clays and Clay Minerals 34, 549-556.

April, R.H., Newton, R.M., Coles, L.T., 1986b. Chemical weathering in two Adirondack watersheds: Past and present-day rates. Geological Society of America Bulletin 97, 1232-1238.

Augusto, L., Turpault, M.-P., Ranger, J., 2000. Impact of forest tree species on feldspar weathering rates. Geoderma 96 (3), 215-237.

Bailey, S.W., Buso, D.C., Likens, G.E., 2003. Implications of sodium mass balance for interpreting the calcium cycle of a northern hardwood ecosystem. Ecology 84 (2), 471-484.

Bain, D.C., Mellor, A., Robertson-Rintoul, M.S.E., Buckland, S.T., 1993. Variations in weathering processes and rates with time in a chronosequence of soils from Glen-Feshie, Scotland. Geoderma 57 (3), 275-293.

Bain, D.C., Mellor, A., Wilson, M.J., Duthie, D.M.L., 1994. Chemical and mineralogical weathering rates and processes in an upland granitic till catchment in Scotland. Water, Air, and Soil Pollution 73, 11-27.

Barton, C.C., Camerlo, R.H., Bailey, S.W., 1997. Bedrock Geologic Map of Hubbard Brook Experimental Forest, Miscellaneous Investigation Series Map I-2562. U.S. Department of Interior, U.S. Geological Survey.

Berner, R.A., Lasaga, A.C., Garrels, R.M., 1983. The carbonate-silicate geochemical cycle and its effect on atmospheric carbon dioxide over the past 100 million years. American Journal of Science 283, 641-683.

Blum, A.E., Stillings, L.L., 1995. Feldspar dissolution kinetics. In: A.F. White and S.L. Brantley (Editors), Chemical Weathering Rates of Silicate Minerals. Reviews in Mineralogy. Mineralogical Society of America, Washington, D.C., pp. 291-352.

Blum, J.D., Klaue, A., Nezat, C.A., Driscoll, C.T., Johnson, C.E., Siccama, T.G., Eagar, C., Fahey, T.J., Likens, G.E., 2002. Mycorrhizal weathering of apatite as an important calcium source in base-poor forest ecosystems. Nature 417, 729-731.

Brantley, S.L., Chen, Y., 1995. Chemical weathering rates of pyroxenes and amphiboles. In: A.F. White and S.L. Brantley (Editors), Chemical Weathering Rates of Silicate Minerals. Reviews in Mineralogy. Mineralogical Society of America, Washington, D.C., pp. 119-172.

Crews, T.E., Kitayama, K., Fownes, J.H., Riley, R.H., Herbert, D.A., Mueller-Dombois, D., Vitousek, P.M., 1995. Changes in soil phosphorous fractions and ecosystem dynamics across a long chronosequence in Hawaii. Ecology 76 (5), 1407-1424.

Davis, M.B., Ford, M.S., Moeller, R.E., 1985. Paleolimnology. In: G.E. Likens (Editor), An Ecosystem Approach to Aquatic Ecology: Mirror Lake and Its Environment. Springer-Verlag, New York, pp. 345-429.

Driscoll, C.T., Lawrence, G.B., Bulger, A.J., Butler, T.J., Cronan, C.S., Eagar, C., Lambert, K.F., Likens, G.E., Stoddard, J.L., Weathers, K.C., 2001. Acidic deposition in the northeastern United States: Sources and inputs, ecosystem effects, and management strategies. BioScience 51 (3), 180-198.

Hamburg, S.P., Cogbill, C.V., 1988. Historical decline of red spruce populations and climatic warning. Nature 331, 428-431.

Hodson, M.E., 2002. Experimental evidence for mobility of Zr and other trace elements in soils. Geochimica et Cosmochimica Acta 66, 819-828.

Hogan, J.F., Blum, J.D., 2003. Tracing hydrologic flow paths in a small forested watershed using variations in $^{87}Sr/^{86}Sr$, [Ca]/[Sr], [Ba]/[Sr] and $?^{18}O$. Water Resources Research 39, 1282.

Huntington, T.G., Hooper, R.P., Johnson, C.E., Aulenbach, B.T., Cappellato, R., Blum, A.E., 2000. Calcium depletion in a southeastern United States forest ecosystem. Soil Science Society of America Journal 64, 1845-1858.

Huntington, T.G., Johnson, C.E., Johnson, A.H., Siccama, T.G., Ryan, D.F., 1989. Carbon, organic matter, and bulk density relationships in a forested spodosol. Soil Science 148 (5), 380-386.

Hyman, M.E., Johnson, C.E., Bailey, S.W., April, R.H., Hornbeck, J.W., 1998. Chemical weathering and cation loss in a base-poor watershed. Geological Society of America Bulletin 110 (1), 85-92.

Johnson, C.E., Driscoll, C.T., Siccama, T.G., Likens, G.E., 2000. Element fluxes and landscape position in a northern hardwood forest watershed ecosystem. Ecosystems 3, 159-184.

Johnson, C.E., Johnson, A.H., Huntington, T.G., Siccama, T.G., 1991a. Whole-tree clear-cutting effects on soil horizons and organic-matter pools. Soil Science Society of America Journal 55, 497-502.

Johnson, C.E., Johnson, A.H., Siccama, T.G., 1991b. Whole-tree clear-cutting effects on exchangeable cations and soil acidity. Soil Science Society of America Journal 55, 502-508.

Jongmans, A.G., van Breemen, N., Lundstrom, U., van Hees, P.A.W., Finlay, R.D., Srinivasan, M., Unestam, T., Geisler, R., Melkerud, P.-A., Olsson, M., 1997. Rock-eating fungi. Nature 389, 682-683.

Kirchner, J.W., Lydersen, E., 1995. Base cation depletion and potential long-term acidification of Norwegian catchments. Environmental Science and Technology 29 (8), 1953-1960.

Kirkwood, D.E., Nesbitt, H.W., 1991. Formation and evolution of soils from an acidified watershed: Plastic Lake, Ontario, Canada. Geochimica et Cosmochimica Acta 55 (5), 1295-1308.

Lawrence, G.B., David, M.B., Shortle, W.C., 1995. A new mechanism for calcium loss in forest-floor soils. Nature 378, 162-165.

Likens, G.E., Driscoll, C.T., Buso, D.C., 1996. Long-term effects of acid rain: Response and recovery of a forest ecosystem. Science 272, 244-246.

Likens, G.E., Driscoll, C.T., Buso, D.C., Siccama, T.G., Johnson, C.E., Lovett, G.M., Fahey, T.J., Reiners, W.A., Ryan, D.F., Martin, C.W., Bailey, S.W., 1998. The biogeochemistry of calcium at Hubbard Brook. Biogeochemistry 41, 89-173.

Lovett, G.M., Thompson, A.W., Anderson, J.B., Bowser, J.J., 1999. Elevation patterns of sulfur deposition at a site in the Catskill Mountains, New York. Atmospheric Environment 33, 617-624.

Merritts, D.J., Chadwick, O.A., Hendricks, D.M., Brimhall, G.H., Lewis, C.J., 1992. The mass balance of soil evolution on late Quaternary marine terraces, northern California. Geological Society of America Bulletin 104, 1456–1470.

Meybeck, M., 1987. Global chemical weathering of surficial rocks estimated from river dissolved loads. American Journal of Science 287, 401-428.

Nagy, K.L., 1995. Dissolution and precipitation kinetics of sheet silicates. In: A.F. White and S.L. Brantley (Editors), Chemical Weathering Rates of Silicate Minerals. Reviews in Mineralogy. Mineralogical Society of America, Washington, D.C., pp. 173-233.

Pouchou, J.L., Pichoir, F., 1984. A new model for quantitative x-ray-microanalysis .1. Application to the analysis of homogeneous samples. Recherche Aerospatiale 3, 167-192.

Spear, R.W., Davis, M.B., Shane, L.C.K., 1994. Late Quaternary history of low- and mid-elevation vegetation in the White Mountains of New Hampshire. Ecological Monographs 64 (1), 85-109.

Taylor, A., Blum, J.D., 1995. Relation between soil age and silicate weathering rates determined from the chemical evolution of a glacial chronosequence. Geology 23 (11), 979-982.

Valsami-Jones, E., Ragnarsdottir, K.V., Putnis, A., Bosbach, D., Kemp, A.J., Cressey, G., 1998. The dissolution of apatite in the presence of aqueous metal cations at pH 2-7. Chemical Geology 151, 215-233.

van Breemen, N., Finlay, R., Lundstrom, U., Jongmans, A.G., Geisler, R., Olsson, M., 2000. Mycorrhizal weathering: A true case of mineral plant nutrition? Biogeochemistry 49, 53-67.

Velbel, M.A., 1993. Temperature dependence of silicate weathering in nature: How strong a negative feedback on long-term accumulation of atmospheric CO_2 and global greenhouse warming? Geology 21, 1059-1062.

Wallander, H., 2000. Uptake of P from apatite by *Pinus sylvestris* seedlings colonised by different ectomycorrhizal fungi. Plant and Soil 218, 249-256.

Wallander, H., Wickman, T., 1999. Biotite and microcline as potassium sources in ectomycorrhizal and non-mycorrhizal *Pinus sylvestris* seedlings. Mycorrhiza 9, 25-32.

Welch, S.A., Taunton, A.E., Banfield, J.F., 2002. Effect of microorganisms and microbial metabolites on apatite dissolution. Geomicrobiology Journal 19, 343-367.

Welch, S.A., Ullman, W.J., 1993. The effect of organic acids on plagioclase dissolution rates and stoichiometry. Geochimica et Cosmochimica Acta 57, 2725-2736.

Wesselink, L.G., Meiwes, K.-J., Matzner, E., Stein, A., 1995. Long-term changes in water and soil chemistry in spruce and beech forests, Solling, Germany. Environmental Science and Technology 29 (1), 51-58.

White, A.F., Blum, A.E., 1995. Effects of climate on chemical weathering in watersheds. Geochimica et Cosmochimica Acta 59 (9), 1729-1747.

Wright, R.F., 1988. Influence of acid rain on weathering rates. In: A. Lerman and M. Meybeck (Editors), Physical and Chemical Weathering in Geochemical Cycles. Kluwer Academic Publishers, pp. 181-196.

CHAPTER 3

A SEQUENTIAL EXTRACTION TO SELECTIVELY DISSOLVE APATITE FOR DETERMINATION OF SOIL NUTRIENT POOLS WITH AN APPLICATION TO HUBBARD BROOK EXPERIMENTAL FOREST, NEW HAMPSHIRE, USA

Abstract

Mineral weathering in soils is an important source of many nutrients to forest ecosystems. Apatite, a calcium phosphate mineral, occurs in trace amounts in virtually all igneous and metamorphic rocks and is often found as minute mineral inclusions in more resistant silicate minerals. To better understand the distribution of apatite in soils and its availability, a sequential extraction method was developed to selectively dissolve minerals from soils so that the chemical contribution of nutrients from the ion exchange pool, apatite, and a variety of silicate minerals could be distinguished and quantified. We explored the use of three molarities of HNO_3 (0.01, 0.1 and 1 M) at three temperatures (0, 10, or 20°C) and found that the extraction of apatite was optimized with 1 M HNO_3 at any of these temperatures. Soil, glacial till (i.e., soil parent material), and individual minerals collected from the Hubbard Brook Experimental Forest were subjected to a four-step sequential extraction. Chemical analyses of the extracts indicate that 1 M NH_4Cl (pH=7, 20°C) removes exchangeable ions, 1 M HNO_3 at 20°C primarily dissolves apatite, 1 M HNO_3 at 200°C primarily dissolves biotite and chlorite, and a mixture of concentrated HNO_3, HCl, and HF at 210°C dissolves the more refractory minerals including muscovite, alkali feldspar, plagioclase feldspar and quartz. This extraction

54

method was applied to soil profiles from the Hubbard Brook Experimental Forest to demonstrate that it could be used to interpret the abundance of apatite and other minerals as a function of depth and to assess the reservoirs of nutrient elements by soil horizon.

Introduction

Apatite, $Ca_5(PO_4)_3(F,Cl,OH)$, is an accessory mineral that is ubiquitous in igneous and metamorphic (i.e., crystalline) rocks, although it generally occurs in low abundance (<1 wt %) and as minute inclusions in larger silicate minerals. The dissolution of apatite is several orders of magnitude faster than most silicate minerals (Guidry and Mackenzie, 2003), and consequently its preferential dissolution may strongly influence the surface and groundwater chemistry of watersheds dominated by silicate minerals (Aubert et al., 2001; Hannigan and Sholkovitz, 2001; Oliva et al., 2004). In soils developed on crystalline rocks, apatite is the dominant P-bearing primary mineral. Because phosphorous is an essential and sometimes limiting nutrient for vegetation, apatite can be an important soil nutrient reservoir (Chapin III et al., 1994; Crews et al., 1995; Newman, 1995; Vitousek and Farrington, 1997; Schlesinger et al., 1998; Tanner et al., 1998). Apatite may also be a significant source of bioavailable Ca in some soils despite its relatively low abundance (Blum et al., 2002; Nezat et al., 2004; Yanai et al., 2005).

Apatite can be identified in petrographic thin sections of rocks by its optical properties or its chemical composition (e.g., by energy dispersive x-ray analysis), but its trace occurrence makes it difficult to quantify its abundance in rocks or soils with these methods. The total Ca and P in a bulk soil digest are insufficient to estimate the amount of apatite in soil because these elements are not exclusively found in apatite. For

example, soil organic matter and secondary Fe and Al oxides can contain significant amounts of P, and silicate minerals contain most of the Ca in soils derived from crystalline silicate parent material. The inclusion of apatite within unfractured silicate minerals presents another complication, because inclusions are not exposed to soil solutions until the host minerals are dissolved, such that the total apatite content of rocks and soils may overestimate the amount of apatite exposed to soil solutions.

Extraction methods exist to apportion P from sediments and soils into pools of differing availability, such as exchangeable, carbonate-bound, Al and Fe oxide-bound, organically bound, and primary apatite (Tessler et al., 1979; Williams et al., 1980; Hedley et al., 1982; Ruttenberg, 1992; Leleyter and Probst, 1999). However, some of the extracting solutions contain Na and Mg, the release of which is important to quantify in weathering studies. In addition, some soil extraction procedures may dissolve apatite during more than one step and are thus not selective (Leleyter and Probst, 1999; Aubert et al., 2004). Those methods that do selectively dissolve apatite use HCl (Williams et al., 1980; Ruttenberg, 1992), which form chloride molecular interferences that are problematic for analysis by inductively-coupled plasma mass spectrometry.

In previous investigations (Blum et al., 2002; Hamburg et al., 2003), we applied a sequential extraction procedure to soils containing Ca-bearing minerals to examine the relative availability of Ca pools. Based on the chemical composition of the extracts, we inferred that the four steps of the procedure dissolved Ca predominantly associated with the soil exchange pool, apatite, easily weathered silicates and more resistant silicate minerals. In this paper, we more fully evaluate the extraction procedure and determine the proportion of each major mineral that is dissolved during each step in the procedure.

We applied this procedure first to individual minerals separated from glacial till (i.e., soil parent material) collected at the Hubbard Book Experimental Forest to identify which minerals are dissolved during each step. Next, we identified the influence of acid strength and temperature on the isolation of apatite in the second extraction step. Finally, to interpret the chemical composition of sequential extracts of weathered soils and demonstrate the usefulness of the technique, we applied this method to soils from HBEF where the weathering of primary minerals and accumulation of secondary minerals in soil profiles had previously been characterized.

Methods

Soil sample collection

Soil and soil parent material (glacial till) were collected from Watershed 1 (W-1) of the Hubbard Brook Experimental Forest (HBEF) in the White Mountains of central New Hampshire (43°57'N, 71°44'W). The soils are relatively thin (mean of 50 cm), moderately well-drained Spodosols (Haplorthods) developed in basal till deposited by continental ice sheets that receded from the area ~14,000 years ago (Likens et al., 1977; Davis et al., 1985). The till is derived largely from local bedrock: Silurian-aged Rangeley Formation, a pelitic schist and meta-sandstone, and Devonian Kinsman granodiorite, a foliated granitoid rock with megacrysts of potassium feldspar (Barton et al., 1997). The vegetation of HBEF is characteristic of the northern hardwood forest (Bormann and Likens, 1979).

One large sample of deep and unweathered soil parent material was collected from a trench that had been previously excavated by backhoe just outside the boundary of

the lower part of W-1. A vertical face was cleared to create a fresh surface and soil was collected from a depth of 160 cm below the surface, ~90 cm below the top of the C horizon.

Forty-five randomly located soil pits were quantitatively excavated by Chris Johnson (Syracuse University) within W-1 during the summer of 1997 (Nezat et al., 2004). Samples were collected from six horizons (Oa, E, Bh, Bs1, Bs2, C), sieved through a 2‽mm screen, and oven-dried at 105°C. To reduce the total number of analyses but retain large-scale spatial patterns, the watershed was divided into six areas which include two areas in each of three elevation zones. Each area contained between four and eleven soil pits. For each area, a weighted composite sample was created for each horizon by combining 1% (by mass) of subsamples of like horizons from soil pits within that area. This procedure resulted in 36 soil samples (six horizons from each of six areas) for analysis.

Mineral separates

The large sample of soil parent material was crushed and the 100 to 300 µm size fraction was separated (using heavy liquids and a magnetic separator) into five samples highly enriched in apatite, potassium feldspar, plagioclase, muscovite, and biotite. To check the purity of the separates, a subsample of approximately 100 mineral grains from each separate was mounted on carbon tape and carbon coated. Minerals were identified using an energy dispersive spectrometer (EDS) on a Hitachi S3200N Scanning Electron Microscope (SEM); the area of mineral grains was calculated from digital images using image analysis software to estimate the relative abundance of each mineral. The apatite

separate was not checked for purity by SEM due to limited sample size; its purity was inferred from the chemistry of the digests of the separate.

Sequential extraction procedure

Representative 0.5 g subsamples of soils, glacial till, and mineral separates were sequentially reacted with each of the following ultra-pure solutions: 5 ml of 1 M NH_4Cl (pH=7) in a screw-top polypropylene tube at room temperature (~20°C) on a shaker table for 20 h; 5 ml of 1 M HNO_3 in a screw-top polypropylene tube at room temperature (~20°C) on a shaker table for 20 h; 15 ml of 1 M HNO_3 at 200 °C for 20 min (by microwave at ~20 Mpa); and, a solution of 8 ml of concentrated HNO_3, 1 ml HCl, and 1 ml HF at 210°C for 15 min (by microwave at ~20 Mpa; this is referred to as the 'HF solution' or 'HF extract'). The last two steps were performed in reinforced XP-1500 Teflon vessels in a CEM Microwave Accelerated Reaction System (MARS 5). After each extraction, the solution was centrifuged and the supernatant was pipetted into a Teflon beaker, evaporated to dryness on a hot plate, redissolved in 1 ml of concentrated HNO_3, evaporated again, and redissolved in 10-20 ml of 5% HNO_3 for chemical analysis. The mineral residue from each extraction step was carried to the subsequent step.

Isolation of apatite dissolution

To determine the optimal conditions for dissolving apatite while minimizing dissolution of other minerals, nine subsamples of C horizon soil were used. First, the exchangeable fraction was removed by adding 5 mL of 1 M NH_4Cl solution (pH=7) to 0.5 g of dried C horizon soil and shaking for 20 h at room temperature (~20°C). Next, each subsample was treated with a different combination of molarity and temperature of

extracting solution. The three molarities were 0.01 M, 0.1 M and 1 M HNO_3 (pH of 2, 1 and 0, respectively), and the three temperatures were 0, 10 and 20°C.

Chemical analysis of extracts

Extracts were analyzed on a Perkin Elmer Optima 3300DV Inductively Coupled Plasma-Optical Emission Spectrometer (ICP-OES) using NIST-traceable standard solutions and five- to eight-point calibration curves. The elements Al, Ca, Fe, K, Mg, Na, P, Si, Sr and Ti were analyzed. Silicon is not reported for the final extract because Si is volatilized during extraction with HF. The lack of contamination during the sequential extraction was confirmed by multiple analyses of procedural blanks. Analysis of High Purity certified reference materials (Soil Solution A and River Sediment Solution B) indicate that the accuracy of our chemical analysis was within ±5%.

To distinguish subtle differences in the relative dissolution of minerals such as apatite and biotite, $^{87}Sr/^{86}Sr$ ratios were measured in the extracts obtained at different temperatures and molarities from C horizon samples (described above) and the apatite separate. Sample aliquots containing ~100 ng of Sr were eluted through quartz columns with Eichrom Sr-Spec resin. Strontium fractions were loaded with 1 µl of H_3PO_4 and Ta_2O_5 powder on tungsten filaments. Fifty to two hundred $^{87}Sr/^{86}Sr$ ratios were measured for each sample on a Finnigan MAT 262 multiple-collector Thermal Ionization Mass Spectrometer (TIMS) in static mode, yielding internal precisions of at least ±0.000030 (2s). The $^{87}Sr/^{86}Sr$ ratios were normalized to a $^{86}Sr/^{88}Sr$ value of 0.1194. Measurements of NBS987 had a mean $^{87}Sr/^{86}Sr$ ratio of 0.710238 ± 0.000025 (2s, n=26) during the period of analysis.

Results

Sequential extraction of mineral separates

The density and magnetic separations of minerals from the glacial till parent material yielded separates that varied in purity (Table 3-1). Separation of minerals was not complete because some minerals have similar physical properties (e.g., alkali feldspar, plagioclase, and quartz), are intergrown (e.g., biotite and muscovite), or have mineral inclusions (e.g., apatite included within biotite). We applied the sequential extraction procedure to each mineral separate and to the glacial till from which the minerals were separated (Table 3-2).

Calcium and P were the dominant elements in all extracts of the apatite mineral separate, indicating that the separate was ~98% pure (Table 3-2, Figure 3-1a). The first extract, a 1 M NH_4Cl solution, removed <0.01 % of the Ca and P in the bulk sample. The 1 M HNO_3 extract at 20°C and 200°C removed ~40% and ~60%, respectively, of the total Ca and P in a Ca:P ratio of 5:3 (the stoichiometric ratio in apatite). The only other element released in significant quantity was Al, which was removed mainly in the HF solution and accounted for only ~1% of the total of the elements analyzed.

Most of the plagioclase separate was extracted by the HF solution (Table 3-2, Figure 3-1b). The 1 M NH_4Cl extraction step removed only ~0.04% of the total of the elements analyzed. The 1 M HNO_3 extract (at 20°C) removed some Al, Ca, Fe, and P, presumably from apatite inclusions and Fe and Al oxides, but these accounted for only ~3% of the total of the elements analyzed (Table 3-1). The 1 M HNO_3 extract of plagioclase (at 200°C) dissolved Al, Ca, K and Na totaling ~6% of the separate. The HF solution extracted more than 90% of the separate and contained Al, Ca, K and Na. The K

is presumably derived from alkali feldspar which constitutes 13% of the total feldspars in the plagioclase separate (Table 3-2); small amounts of Fe, Mg, and P in the HF extract indicate the presence of mineral inclusions (Figure 3-1b).

Like the plagioclase separate, most of the alkali feldspar separate was extracted by the HF solution (Table 3-2, Figure 3-1c). The 1 M NH_4Cl removed only ~0.2% of the total of the elements analyzed. The 1 M HNO_3 (at 20°C) extracted small amounts of Al, Ca, Fe, and P, which accounted for ~1% of the total of the elements analyzed, and the 1 M HNO_3 (at 200°C) dissolved some Al, Fe, and Mg, which totaled ~2% of the total of the elements analyzed. The HF solution, which extracted 97% of the total of the elements analyzed, contained predominantly Al, Ca, K and Na from the dissolution of alkali feldspar and plagioclase, the latter of which constituted 17% of the alkali feldspar separate.

Most of the muscovite separate was dissolved by the HF solution (Table 3-2, Figure 3-1d). The 1 M NH_4Cl extraction of muscovite removed only ~0.01% of the total of the elements analyzed. As in the extraction of the feldspar separates, the 1 M HNO_3 (at 20°C) extract dissolved Al, Ca, Fe and P, amounting to <4% of the total of the elements analyzed. The 1 M HNO_3 extract (at 200°C) dissolved ~18% of the total of the elements analyzed and had high concentrations of Al, Fe, K and Mg. These elements are in biotite, chlorite, and hornblende, minerals that are present in the muscovite separate as impurities. The HF solution dissolved most of the muscovite separate and contained Al, Ca, Fe, K, Mg, and Na, indicating dissolution of muscovite along with the plagioclase and alkali feldspar that were present as impurities (Table 3-1).

In contrast to the feldspars and muscovite separates, a significant proportion of the biotite separate was dissolved by the 1 M HNO_3 (at 200°C) extraction (Table 3-2, Figure 3-1e). The 1 M NH_4Cl extraction removed only ~0.01% of the total of the elements analyzed. The 1 M HNO_3 (at 20°C) removed ~6% of the total of the elements analyzed, most of which was Al, Ca, Fe, and P (Figure 3-1e). The 1 M HNO_3 (at 200°C) and the HF solution extracted roughly equal portions of the total elements analyzed (Table 3-1). The 1 M HNO_3 extract (at 200°C) contained Al, Fe, K and Mg, elements present in biotite, muscovite, chlorite, and hornblende. The HF solution extracted Al, Ca, Fe, K, Mg, and Na, indicative of the dissolution of plagioclase, alkali feldspar, and muscovite.

Sequential extraction of glacial till

The chemical composition of the bulk glacial till reflects the dissolution of all of the minerals in the mineral separates, combined in their naturally occurring proportions. The 1 M NH_4Cl extracted <0.1% of the total of the elements analyzed. The second step in the sequential extraction method (1 M HNO_3 at 20°C) was intended to target the dissolution of apatite. The 1 M HNO_3 (at 20°C) removed ~10% of the total of the elements analyzed, and was composed mostly of Al, Ca, Fe, and P; small amounts of K, Mg, Si and Ti were also released (Figure 3-1f). The 1 M HNO_3 (at 200°C) extracted ~15%, and the HF solution ~75%, of the total of the elements analyzed in the glacial till samples.

Effect of HNO_3 molarity and temperature on apatite dissolution

The extraction of glacial till at three HNO_3 molarities and three temperatures tested the effect of the concentration and temperature of HNO_3 on the specificity and

63

congruency of apatite dissolution (Table 3-3, Figure 2). At the HNO_3 concentration of 0.01 M, apatite did not dissolve appreciably at any of the temperatures investigated (0, 10, or 20°C). In the 0.1 M HNO_3 extract, a considerable amount of Ca was released into solution at all three temperatures, but much less P than expected from congruent dissolution of apatite (represented by the dashed line in Figure 3-2a). The 1 M HNO_3 extract removed the highest concentrations of Ca and P, and had a Ca:P ratio identical to that of apatite (5:3), indicating the congruent dissolution of apatite.

Temperature had little effect on the efficacy of apatite dissolution with 1 M HNO_3 (Figure 3-2a). The most important influence of temperature on these extracts was on the minor amount of other elements released into solution in the 1 M HNO_3 extracts (Figure 3-2c,d): between extractions at the temperatures of 0°C and 20°C, Fe, K, Mg and Ti were higher by a factor of 2.4, 2.9, 12, and 2.4, respectively.

Sequential extraction of soil profiles

We applied the sequential extraction procedure to the six composite soil profiles that were derived from 45 soil pits from at HBEF, to extend our interpretations of the sequential extracts of parent materials to weathered horizons and to demonstrate how this method can be used to provide insight into soil-forming processes.

The 1 M NH_4Cl extract represented a very small fraction (<1%) of the total soil chemical inventory and was dominated by Ca, K and Mg (Figure 3-3). The cation concentrations in the 1 M NH_4Cl extracts were highest in the Oa horizon, lowest in the E and C horizons and intermediate in the Bh, Bs1 and Bs2 horizons.

The 1 M HNO$_3$ extract (at 20°C) was dominated by Fe released from the Bh, Bs1 and Bs2 horizons and Ca and P released from the C horizon (Figure 3-3). Potassium, Mg and Na were very low in this extract in all horizons.

A large proportion of the Fe and Mg in the soil was released by the 1 M HNO$_3$ extract (at 200°C). Large amounts of P were also removed by the 1 M HNO$_3$ extract (at 200°C) in the organic and B horizons. In contrast, Ca, Na and K concentrations in this extract represent only a small fraction of the total soil pools (Figure 3-3). The composition of this extract showed little variation with depth.

The HF/HCl/HNO$_3$ solution extracted most of the Ca, K, and Na in each soil horizon (Figure 3-3). Magnesium and Fe were released in amounts approximately equal to the 1 M HNO$_3$ extract (at 200°C), and P concentrations were relatively low in this extract. This extract also showed little variation in composition with depth, with the exception that Ca and Na were higher in the C horizon, and Mg was higher in the Oa horizon.

Discussion

Comparison of sequential extracts of minerals and soil parent material with mineral compositions

To determine which minerals were dissolved during each step in the extraction procedure, the chemical composition of the extracts of the impure mineral separates were plotted on ternary diagrams with the apices Ca, Mg, and Na+K (Figure 3-4), along with the compositions of the individual minerals previously determined by electron microprobe analysis (Nezat et al., 2004). The 1 M NH$_4$Cl extracts were not plotted

because they make up a very small fraction of the total of each element extracted (<0.1%) and they represent an exchangeable pool not associated with the soil mineral pools.

Apatite is the only mineral dissolved in abundance in the 1 M HNO_3 (at 20°C) extracts of the silicate mineral separates and bulk glacial till (Figure 3-1). This extract of plagioclase, alkali feldspar, muscovite and the glacial till plots near the apatite composition on the ternary diagrams (Figure 3-4), and has P/Ca, Sr/Ca and Na/Ca ratios similar to those of the apatite separate (Table 3-2). This reflects the selective dissolution of apatite inclusions that occurred in each of these silicate minerals and were in contact with the extraction solutions. Because the minerals were crushed to 100-300μm prior to separation, apatite that was previously enclosed in minerals was exposed. The 1 M HNO_3 (at 20°C) extract of the biotite separate plots between the compositions of apatite and hornblende (an 11% impurity in the biotite separate, Table 3-1), indicating that some hornblende was dissolved along with apatite in this extract (Table 3-2).

The composition of the 1 M HNO_3 (at 200°C) extracts of the silicate mineral separates reflects the preferential dissolution of biotite and chlorite (and the apatite inclusions that commonly occur within them) compared to plagioclase, alkali feldspar and muscovite (Figure 3-4a-e), as predicted by mineral dissolution kinetics (e.g., Ganor et al., 2005). Although neither biotite nor chlorite was detected in 100 grains analyzed from the alkali feldspar mineral separate by SEM-EDS (Table 3-1), the composition of this extract suggests that one or both of these minerals is present as an impurity, as is the case for the plagioclase separate, or as inclusions in the alkali feldspar.

The HF extract compositions of each mineral separate (except biotite) plot close to the compositions for the sum of the extracts (Figure 3-4) as one would expect, because

most of the Ca, Mg, K, and Na – the four elements plotted on the ternary diagram – was released in the HF extract (Table 3-2). The HF digest of the biotite separate is an exception to this, and instead plots near the impurity minerals plagioclase, alkali feldspar, and muscovite, because the biotite was largely removed by the previous 1 M HNO_3 (at 200°C) extract.

To illustrate the utility of the sequential extraction for natural samples, extractions of six composite C horizon samples are compared to the composition of primary minerals (Figure 3-4f). These samples were not crushed, and therefore only minerals exposed to soil solutions were extracted by each step. Calcium from apatite as well as some Mg from hornblende and/or chlorite was extracted from the C horizon soils by 1 M HNO_3 (at 20°C). According to the Ca:P ratios in this extract, the source of Ca can be identified as apatite (Figure 3-5). The scatter of the six data points for this extract indicates that the relative proportions of apatite and hornblende/chlorite in the C horizon varied somewhat across the watershed (i.e., W-1 at HBEF).

The composition of the 1 M HNO_3 (at 200°C) extracts of C horizon samples (Figure 3-4f) was quite different from the composition of the 1 M HNO_3 (at 20°C) extracts and can be explained by a mixture of apatite (±hornblende), biotite and feldspars. Although apatite was largely removed by the 1 M HNO_3 (at 20°C) extracts, biotite can contain numerous apatite inclusions and thus the dissolution of biotite in the 1 M HNO_3 (at 200°C) extract probably exposes additional apatite to dissolution.

The compositions of the HF extracts of C horizon samples were dominated by K+Na and had a composition similar to that of plagioclase, potassium feldspar, and muscovite (Figure 3-4f). Because plagioclase, alkali feldspar and quartz are the dominant

67

minerals in Hubbard Brook soils (Nezat et al., 2004), the sum of the digests had a composition similar to that of the HF digests, but was shifted slightly toward the composition of the weaker acid extracts.

Isolation of apatite dissolution

Dilute HNO_3 concentrations of 0.01M and 0.1M were evaluated as potential reagents for the dissolution of apatite from soil parent material, because we sought to minimize the accompanying dissolution of silicate minerals. However, we found that these solutions were too dilute to dissolve apatite and inhibit P re-adsorption, and thus that 1M HNO_3 was required for apatite extraction. In the 0.01M HNO_3 (Table 3-3, Figure 3-2), the high ratios of $^{87}Sr/^{86}Sr$ and (Fe+K+Na)/(Ca+Na), and the low Ca/Sr ratio of the minor amount of dissolution product suggest that some biotite dissolution occurred (Taylor et al., 2000; Erel et al., 2004).

The 0.1M HNO_3 extracts dissolved large amounts of Ca and P (Table 3-3, Figure 3-2), but the Ca:P ratios were considerably higher (~12:3) than that the 5:3 ratio of apatite. However, the Ca/Sr and $^{87}Sr/^{86}Sr$ ratios of the 0.1 M extracts are similar to that of the apatite separate (Figure 3-2b), confirming that the Ca was derived from apatite. The deficit of P in the 0.1 M extract is probably due to the adsorption of P onto Fe and Al oxides (e.g., Dreibus and Haubold, 2004). The Fe content of the 0.1M extracts are quite low, indicating that Fe oxides were not dissolved under these conditions. Silicate minerals were also not dissolved significantly at this molarity (Table 3-3).

The 1 M HNO_3 extract removed the highest concentrations of Ca and P, had a Ca:P ratio identical to that of apatite (5:3), and had Ca/Sr and $^{87}Sr/^{86}Sr$ ratios similar to that of the apatite separate (Figure 3-2b). Relatively high concentrations of K, Mg, Fe

and Ti suggest that biotite is also partially dissolved at this molarity (Table 3-3, Figure 3-2c,d). The 1 M HNO_3 dissolved ~40 times more Fe than the 0.1 M solution (Table 3-3). Thus, the 1 M HNO_3 solution probably dissolved Fe oxides from mineral surfaces, which allowed P to remain in solution (Figure 3-2c). We conclude that to dissolve apatite and keep both Ca and P in solution in an extract, at least a 1 M HNO_3 acid strength is necessary.

We found that temperature had a measurable effect on the extraction of K, Mg, Fe and Ti by 1 M HNO_3 (Table 3-3, Figure 3-2), suggesting a minor enhancement of biotite dissolution at higher temperature. Similarly, Bullen and Bailey (2005) found that a 1 M HNO3 extract of similar soils performed at a range of temperatures (0 to 30°C) yielded higher K and Mg concentrations and $^{87}Sr/^{86}Sr$ ratios at higher temperatures, which they attributed to enhanced biotite dissolution.

We suggest that a 1 M HNO_3 extract of soil is optimal for assessing the amount of apatite that is potentially available to plants by mineral weathering. About 80% of the P in the C horizons of soils was dissolved by these extracts (Figure 3-3). The remaining ~20% of P was probably derived from the more resistant (Williams et al., 1980) and less abundant phosphate mineral monazite $[(Ce,La,Y,Th)PO_4]$ and from apatite that is entirely included within silicate minerals and thus shielded from the 1 M HNO_3 (at 20°C) solution until the host minerals are dissolved in later steps of the extraction.

Although apatite was nearly completely dissolved in the soil samples, only ~40% of the apatite mineral separate dissolved in the 1 M HNO_3 (at 20°C); the remaining apatite was released by the 1 M HNO_3 extracted at 200°C. Results from the geochemical modeling program, Solmin88, indicate that the 1 M HNO_3 extract at 20°C became

saturated with respect to apatite; at natural abundances (<1%) apatite in soils should be completely dissolved during this step.

In the case of the plagioclase and alkali feldspar mineral separates, the HF solution also extracted some P, but in amounts much less than predicted by the Ca:P of ratio of apatite, due to Ca also being released from feldspar (Figure 3-4). The source of P may be apatite and monazite inclusions as in the case of the C horizon samples as discussed above. The lack of P in the HF digest of biotite and muscovite results indicate that apatite inclusions in the biotite and muscovite were largely dissolved by the 1 M HNO_3 extracts at 20°C and 200°C.

It should be kept in mind that apatite included in more resistant minerals will not be dissolved until the host minerals are broken down. Thus the sequential extraction described here allows identification of the amount of apatite in contact with soil solutions, and the amount included within silicate minerals with varying degrees of resistance to weathering. To quantify the total amount of apatite in a soil or rock sample, the sample should be finely powdered before extraction to fully expose apatite inclusions to the 1 M HNO_3 extract (at 20°C).

Interpreting extracts of soil profiles

Interpreting the sequential extraction of soil profiles can be complicated because soils contain exchangeable cations, labile and refractory organic matter, and secondary minerals such as Fe and Al oxides, in addition to primary minerals. Elemental concentrations for each extract of each horizon for one representative composite soil profile are shown in Figure 3-4, and a few illustrative chemical parameters for each soil horizon from all six composite soil profiles investigated are plotted on Figs. 5 and 6.

The Ca and P contents of the 1 M HNO_3 (at 20°C) extracts of soil horizons indicate that apatite is present only at depth in HBEF soils (Figs. 3a,f and 5). In our experiments on mineral separates, we verified that 1 M HNO_3 (at 20°C) dissolved apatite congruently (Figure 3-1a). The Bs2 and C horizons have the highest concentrations of Ca and P in the 1 M HNO_3 (at 20°C) extracts and they are released at the apatite Ca:P ratio of 5:3 (Figure 3-5). Above the Bs2 horizon, the low concentrations and lack of correlation between Ca and P indicates that these elements reside in different pools (Figure 3-5).

As soils develop, primary apatite is weathered from the soil. After release by weathering, Ca is taken up by vegetation, held on the exchange complex, or dissolved in groundwater and lost from the ecosystem. Due to its relative mobility following release, Ca in the 1 M HNO_3 (at 20°C) extracts of the upper horizons has a lower concentration than deeper in the soil where less apatite weathering has occurred. In contrast, P is comparatively immobile in HBEF soils (Wood et al., 1984), and after being released by weathering of apatite is retained in the soil complexed with organic matter and secondary minerals (Walker and Syers, 1976; Smeck, 1985; Cross and Schlesinger, 1995; Johnson et al., 2003), resulting in a relatively constant concentration above the C horizon. In the organic horizon (Oa), some P is extracted by 1 M HNO_3 (at 20°C), but little Al or Fe, suggesting that the P is associated with relatively labile organic matter. In the B horizon, elevated concentrations of P accompanied by Al and Fe in the 1 M HNO_3 (at 20°C) extract suggest that P is associated with secondary Al and Fe oxides.

Large amounts of P were also removed by the 1 M HNO_3 extract (at 200°C) in the organic and B horizons. Phosphorus in these horizons is correlated with soil organic

matter content, measured as loss on ignition (Figure 3-6), which suggests that it is associated with more refractory organic matter.

Magnesium concentrations in the 1 M HNO_3 extract (at 20°C) are highest in the B and C horizons (Figure 3-3). Common Mg-bearing minerals in the HBEF soils are biotite, chlorite, and hornblende. The high Mg and Fe concentrations and low K:Mg ratio (0.2-0.4) of this extract suggest that the source of Mg is chlorite or altered biotite (hydrobiotite/vermiculite), rather than biotite (K:Mg ~ 1; Nezat et al., 2004). The low Na concentration suggests that hornblende is not a major source of Mg in this extract (Figure 3-3).

Calcium, Na and K concentrations in the 1 M HNO_3 extract (at 200°C) represent only a small fraction of the total soil pools (Figure 3-3) because plagioclase and alkali feldspar are not dissolved appreciably by this extract. In contrast, most of the Mg is released by this extract due to the dissolution of Mg-bearing minerals such as biotite, chlorite, and hornblende.

Based on comparison with the composition of sequential extractions of the mineral separates, we conclude that the HF/HCl/HNO_3 solution digests mainly plagioclase and alkali feldspar (Figure 3-1d,e), which are the dominant minerals in HBEF soil parent materials (besides quartz). Assuming that the C horizon represents the initial composition of the upper soil horizons, the decrease in Ca, Na and K towards the soil surface represents the depletion of alkali and plagioclase feldspars by mineral weathering. The extraction method does not reveal quartz (SiO_2) dissolution because Si is lost during the HF digestion, but the lack of information on quartz dissolution is not a major limitation because quartz does not contain any important nutrient elements.

Application to other soil and rock types

The sequential extraction method described in this study is appropriate for application to igneous and silicate-dominated metamorphic rocks. In the current study, the sequential extraction method was performed on relatively young soils (~14 ka) developed on silicate crystalline rock soil parent materials in a temperate climate. In another study (Nezat et al., In preparation), we tested this sequential extraction technique on C horizon soils developed on a variety of igneous, metamorphic and sedimentary soil parent materials of varying age from across the northeastern U.S.A. The 1 M HNO_3 (at 20°C) extractions of nearly all soils developed on crystalline silicate rocks exhibited a Ca:P ratio similar to that of apatite, the presence of which was confirmed by mineralogical analysis. In soils developed on sedimentary carbonate rocks and shales, large amounts of Ca and Mg were released by the 1 M HNO_3 (at 20°C) extract, which dissolves carbonate minerals. The release of Ca from carbonate is not accompanied by the release of P and is therefore easily distinguished from an apatite source.

Conclusions

We developed and tested a sequential extraction method to determine the amount of apatite in contact with soil solutions and to identify its presence as inclusions in more resistant silicate minerals. Applying this method to mineral separates indicated that 1 M HNO_3 (at 20°C) dissolved mainly apatite; 1 M HNO_3 (at 200°C) dissolved mainly biotite and chlorite; and a solution of concentrated HF, HCl and HNO_3 dissolved muscovite, alkali feldspar and plagioclase feldspar. We demonstrated that the apatite extraction could not be carried out with an acid strength of less than 1 M HNO_3 because this

molarity is required to assure solubilization of Fe and Al oxides that would otherwise adsorb P.

The sequential extraction method can be applied to soil profiles to provide information about the amount and distribution of pools of mineral-derived nutrients in soils. For example, the amount of apatite can be quantified by the amount of Ca and P extracted by 1 M HNO_3 (at 20°C), whereas the Ca and Na concentration of the sum of the extracts can be used to indicate the plagioclase content, because plagioclase is the dominant Ca and Na-bearing mineral. Bulk phosphorous concentrations of soils (or the sum of the sequential extracts) cannot be used to determine the presence of apatite because P is also associated with organic matter and Fe and Al oxides. Hence, sequential extractions can indicate more accurately than bulk soil composition the amount of nutrients held in specific minerals and the potential for these nutrients to be released by weathering.

Acknowledgments

Table 3-1. Mineral composition of separates determined by scanning electron microscopy and energy dispersive spectrometry

	Plagioclase separate	Alkali feldspar separate	Muscovite separate	Biotite separate
	(% of each mineral in separate)[a]			
Plagioclase	**55.2**	17.1	5.3	6.0
Alkali feldspar	7.0	**82.6**	2.1	2.6
Muscovite	1.1	ND	**58.3**	4.7
Biotite	6.7	ND	18.5	**62.5**
Chlorite	ND	ND	1.8	4.6
Quartz	26.8	0.3	11.0	4.3
Hornblende	ND	ND	2.3	10.8
Other[b]	3.2	ND	0.7	4.5
Total	96.8	100.0	99.3	95.5

[a] ND indicates not detected.

[b] "Other" minerals include apatite, ilmenite, zircon and epidote.

Table 3-2. Chemical composition of extractions of mineral separates and glacial till

	Al	Ca	Fe	K	Mg	Na	P	Si	Sr	Ti
					?mol/g					
1 M NH₄Cl extract										
Apatite	BDL[a]	BDL	BDL	BDL	BDL	BDL	BDL	BDL	BDL	BDL
Plagioclase	BDL	0.9	0.173	0.121	0.512	BDL	BDL	BDL	BDL	BDL
Alkali feldspar	BDL	0.7	0.0130	0.109	0.380	BDL	BDL	BDL	BDL	BDL
Muscovite	BDL	BDL	BDL	0.342	BDL	BDL	BDL	BDL	BDL	BDL
Glacial till	BDL	BDL	0.373	0.394	BDL	BDL	BDL	BDL	BDL	0.037
1 M HNO₃ extract (at 20°C)										
Apatite[b]	40.8	3459	11.2	3.87	3.57	10.0	2190	45.1	1.31	0.469
Plagioclase	45.4	41.5	9.77	1.28	2.57	BDL	26.2	22.9	0.0204	0.332
Alkali feldspar	38.3	8.08	7.15	1.01	1.02	BDL	6.23	16.2	0.0026	0.170
Muscovite	113	35.3	31.8	2.57	6.94	BDL	21.0	47.3	0.0245	0.690
Biotite	238	51.0	179	1.51	31.8	BDL	27.3	79.2	0.0610	3.95
Glacial till	97.0	26.0	26.8	3.10	9.43	BDL	15.9	43.0	0.00848	0.837
1 M HNO₃ extract (at 200°C)										
Apatite	20.3	5315	3.89	4.81	0.587	14.6	3279	42.7	1.29	0.571
Plagioclase	140	37.1	26.9	11.4	14.1	36.9	4.16	109	0.161	2.44
Alkali feldspar	56.4	1.32	13.7	19.2	5.62	15.4	2.04	52.5	0.0204	0.625
Muscovite	353	25.6	310	58.2	172	12.0	2.51	115	0.0833	12.2
Biotite	1294	22.9	1583	258	759	15.9	13.5	414	0.0697	53.6
Glacial till	125	3.86	98.3	33.8	52.1	5.43	2.32	137	0.0121	5.94
HF/HCl/HNO₃ extract										
Apatite	129	13.2	0.384	12.9	BDL	18.2	17.5	NR[c]	0.00899	4.46
Plagioclase	2298	531	26.5	204	14.0	1204	5.33	NR	2.85	15.3
Alkali feldspar	3312	73.5	4.58	1928	3.01	1083	7.88	NR	1.55	1.65
Muscovite	2164	174	191	830	60.4	690	BDL	NR	1.25	63.4
Biotite	1609	231	498	458	213	669	BDL	NR	1.99	169
Glacial till	1663	167	104	700	26.4	793	4.48	NR	0.972	27.9
Sum of extracts										
Apatite	190	8788	15.4	21.6	4.16	42.8	5486	NR	2.62	5.52
Plagioclase	2483	610	63.4	217	31.2	1241	35.7	NR	3.03	18.1
Alkali feldspar	3406	83.6	25.5	1948	10.0	1099	16.2	NR	1.57	2.45

Muscovite	2630	234	533	892	239	702	23.6	NR	1.36	76.2
Biotite	3141	305	2260	717	1004	685	40.7	NR	2.12	226
Glacial till	1884	197	230	737	88.0	799	22.7	NR	0.992	34.7
Ideal chemical composition of minerals[d]										
Apatite	------	9920	------	------	------	------	5952	-------	------	------
Plagiocalse	4600	657	------	------	------	3113	------	10459	------	------
Alkali feldspar	3597	------	------	3597	------	------	------	10791	------	------
Muscovite	7538	------	------	2513	------	------	------	7538	------	------
Biotite	3985	------	3454	1689	1589	------	------	6156	------	411

[a]BDL indicates "below detection limit."

[b]The $^{87}Sr/^{86}Sr$ of the 1 M HNO_3 extract of the apatite separate is 0.715281.

[c]NR indicates "not reported." Si concentrations in the $HF/HCl/HNO_3$ extract and the sum of extracts are not reported because Si is volatilized during HF digestion.

[d]The chemcial compositions of plagioclase and biotite were measured by microprobe analysis and reported in Nezat et al. (2004). Apatite, alkali feldspar, and muscovite were assumed to have the following compositions: $Ca_5(PO_4)_3F$, $KAlSi_3O_8$, and $KAl_2(AlSi_3O_{10})(OH)_2$, respectively. Except for Ti in biotite, the concentrations of only major elements were calculated. Dashed lines indicate values not calculated.

Table 3-3. Chemical composition of extracts (performed at various molarities and temperatures) of a C horizon sample

Temp °C	HNO$_3$ M	Al	Ca	Fe	K	Mg	Na	P	Si	Sr	Ti	^{87}Sr/^{86}Sr
					?mol/g sample					mmol/g sample		
20	0.01	2.75	0.0247	0.445	0.107	0.0758	0.0233	0.0321	1.26	<0.17	25.1	0.74389
20	0.1	77.8	15.2	0.508	0.109	0.0822	0.132	2.46	8.25	5.04	10.3	0.71965
20	1	172	18.1	21.4	0.499	2.57	0.338	12.0	15.5	6.85	512	0.72152
10	0.01	3.96	0.160	0.649	0.104	0.0973	0.0384	0.110	1.34	<0.17	30.3	0.74686
10	0.1	80.0	13.4	0.307	0.0925	0.0501	0.125	3.37	6.81	4.74	10.9	0.71727
10	1	143	15.2	12.8	0.272	0.563	0.274	9.79	4.55	6.76	297	0.72075
0	0.01	3.51	0.134	0.571	0.0888	0.0825	0.0237	0.116	4.57	<0.17	27.8	0.75223
0	0.1	72.8	11.6	0.229	0.0748	0.0476	0.0862	3.08	7.57	4.78	10.5	0.71847
0	1	167	18.3	8.83	0.169	0.208	0.197	12.1	24.5	6.68	215	0.71698
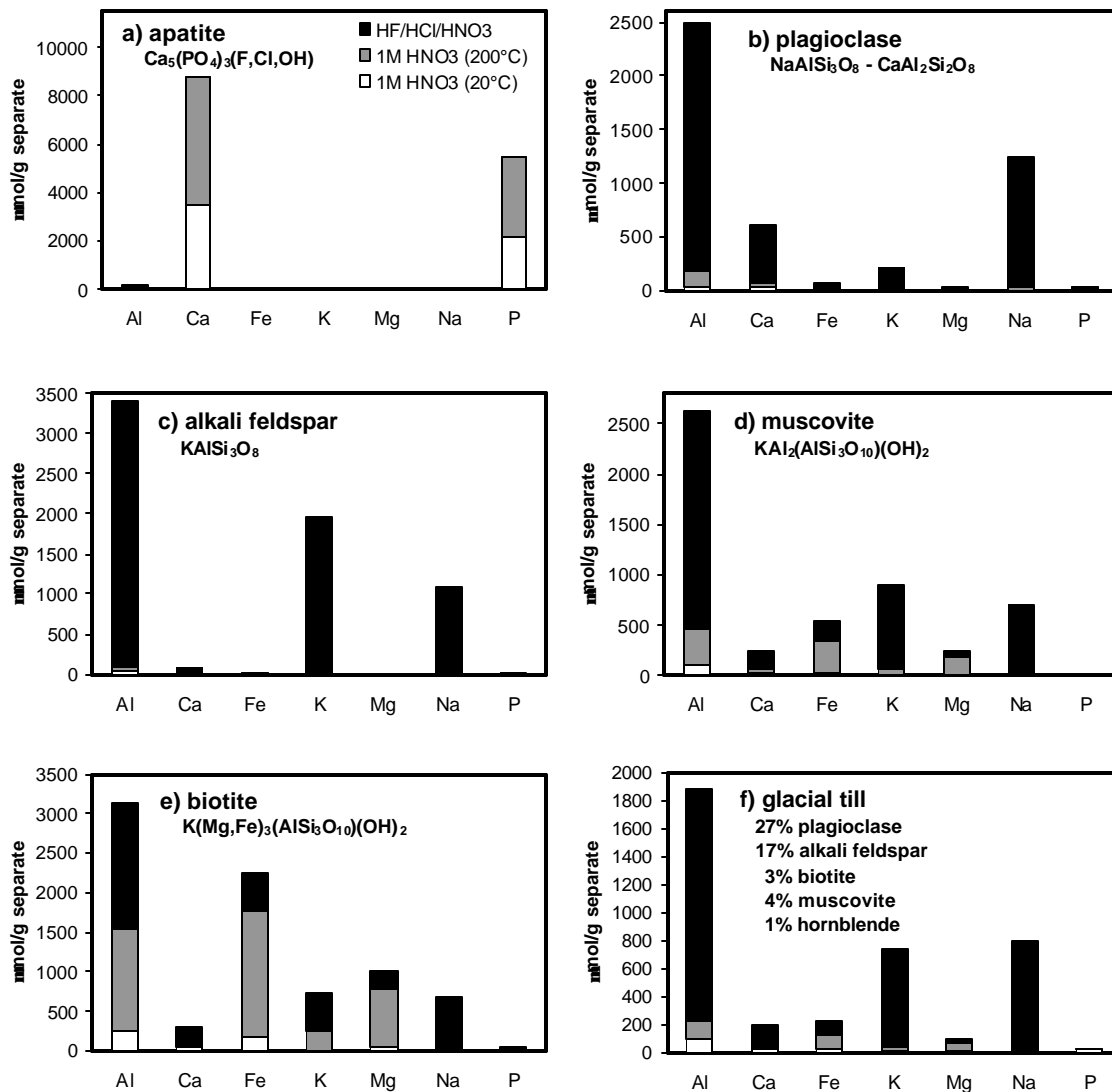
Figure 3-1. Chemical composition of sequential extracts of minerals separated from HBEF glacial till. Mineral separates are not pure (Table 3-1), but are named according to the dominant mineral in the separate. The general formula for each mineral is given. The sequential extract of the bulk glacial till is shown for comparison; the composition of the glacial till is from Nezat et al.(2004). The 1 M NH4Cl extracts are not included because they are <<1% of the total, and too small to be seen at this scale.

79
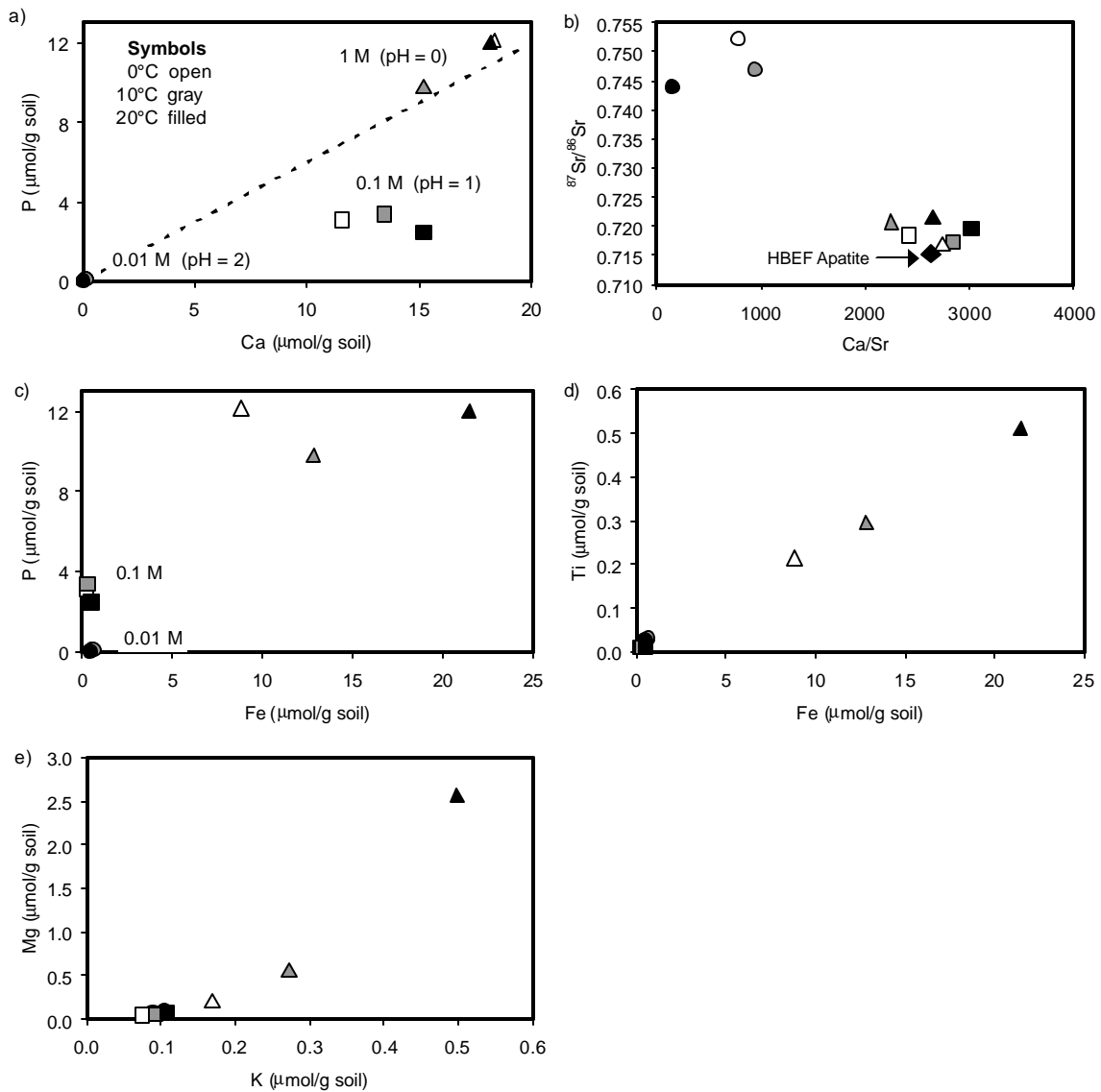
Figure 3-2. Chemical composition of C horizon soil extracted by 0.01 M, 0.1 M, or 1 M HNO_3 solution at 0, 10 or 20 °C. The pH of the solutions are 2, 1, and 0, respectively. The 0.01 M, 0.1 M, and 1 M HNO_3 are represented by circles, squares, and triangles, respectively; the extracts at 0, 10 and 20 °C are represented by open, gray, and black symbols, respectively. a) P versus Ca concentrations. The dashed line represents the P:Ca ratio of apatite (0.6). b) $^{87}Sr/^{86}Sr$ versus Ca/Sr. c) P versus Fe concentrations. d) Ti versus Fe concentrations. e) Mg versus K concentrations.
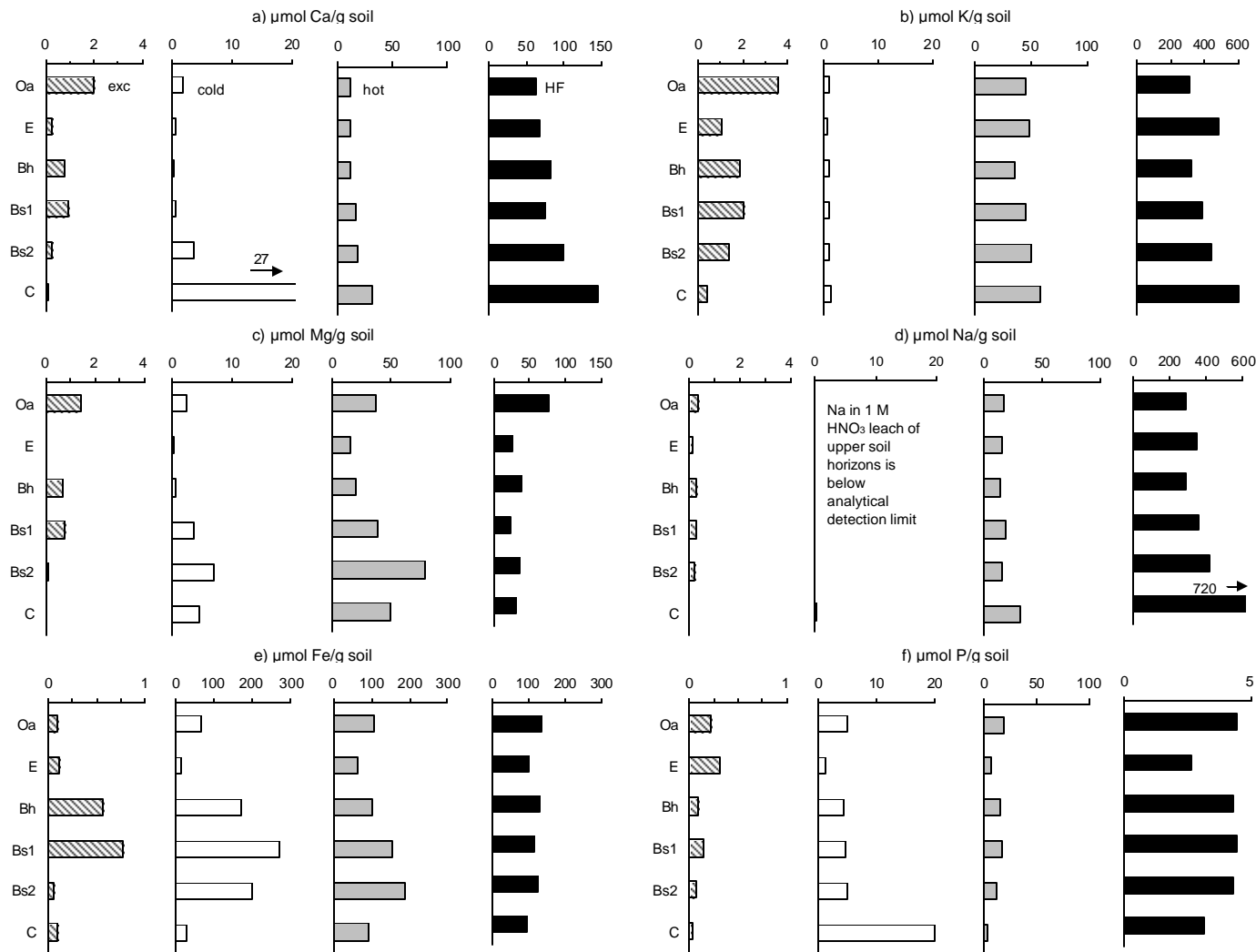
Figure 3-3. Distribution of elements with depth in a composite soil profile at Hubbard Brook Experimental Forest. The chemical composition of this composite profile is represented by black symbols in Figure 3-4 and enlarged symbols in Figs. 5 and 6.
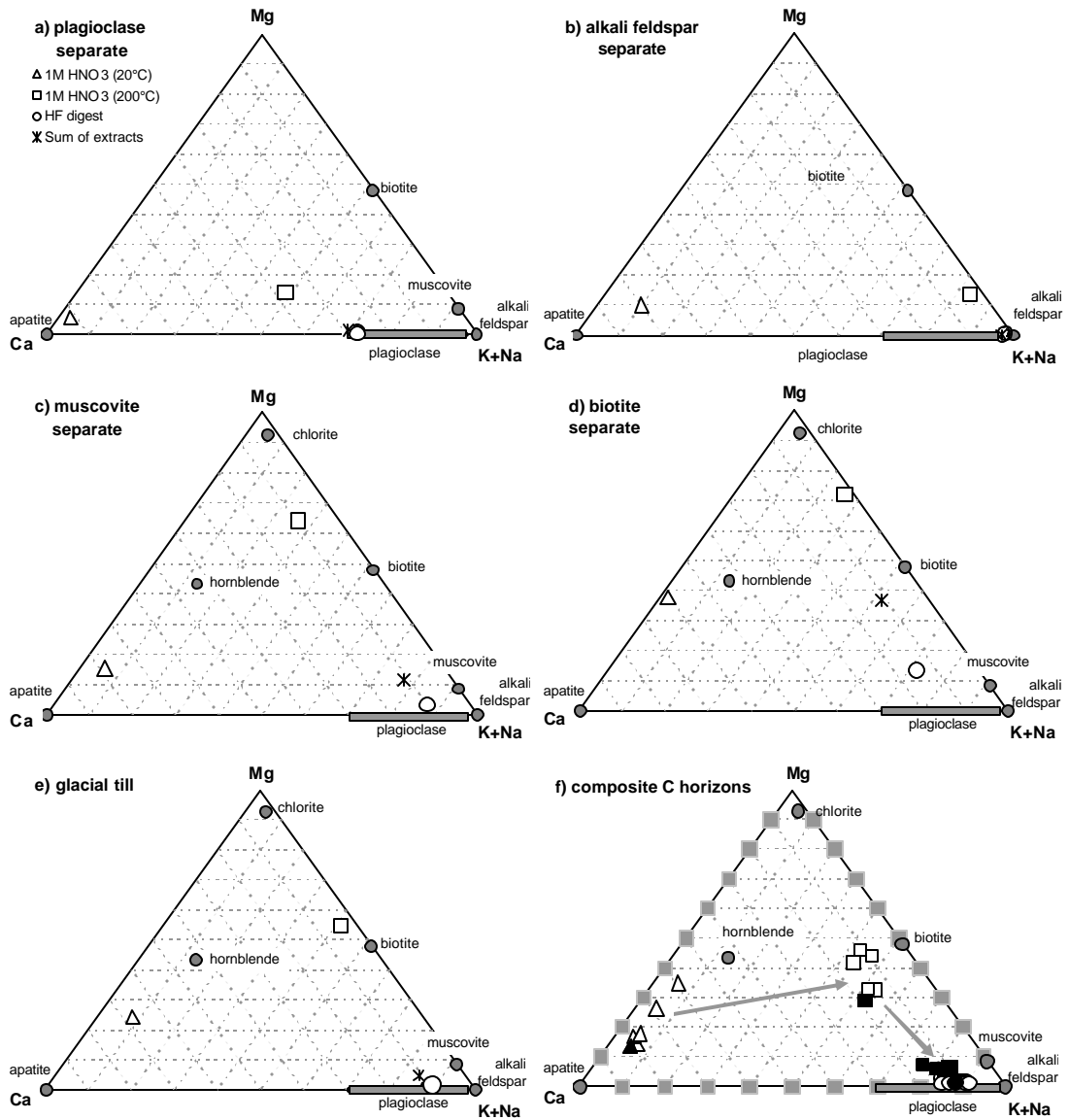
Figure 3-4. Ternary diagram comparing chemical composition of sequential extracts of mineral separates, glacial till (from which the minerals were separated), and C horizons to composition of individual minerals. The gray symbols represent the composition of individual mineral as determined from microprobe analysis; the rectangle indicates the range of plagioclase composition in the HFEB soils (data from Nezat et al., 2004). Extracts of the apatite separate are not plotted but would plot on the Ca apex (Table 3-2). A) Plagioclase separate. b) Alkali feldspar separate. c) Muscovite separate. d) Biotite separate. e) Glacial till from which the minerals were separated. f) C horizon composite soils representing six regions in Watershed 1 at the Hubbard Brook Experimental Forest. The black symbols represent extracts of the C horizon soil that is plotted in Figure 3-3. Gray arrows indicate the sequence of extracts from weakest to strongest.

82
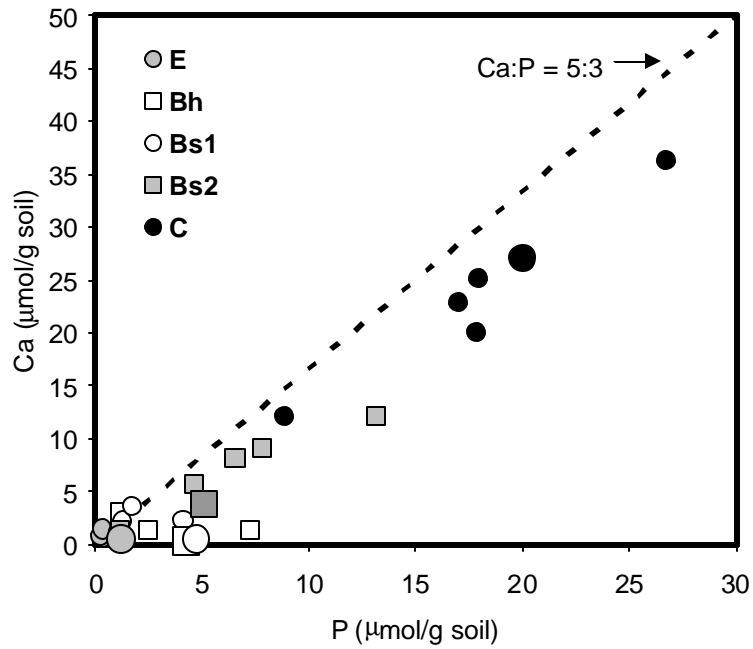
Figure 3-5. Calcium versus phosphorous extracted from HBEF mineral soil horizons using 1 M HNO_3 at 20°C. These data represent six composite soil profiles from HBEF. The variability in chemical composition of the soil horizons is due to differences in vegetation and rates of soil development across the watershed (Nezat et al., 2004). The dashed line represents the Ca:P ratio of apatite (5:3). The enlarged symbols represent the composite soil profile plotted in Figure 3-3.
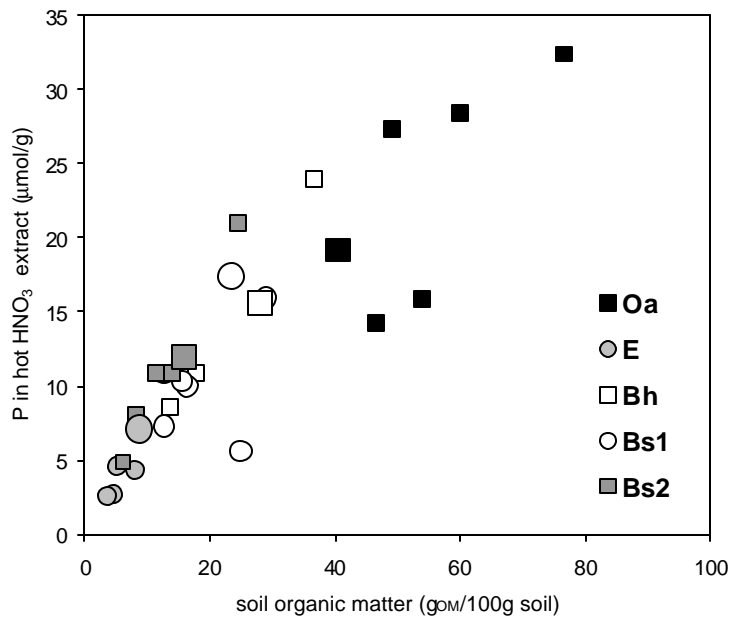
Figure 3-6. Phosphorous extracted from HBEF soil horizons by 1 M HNO_3 at 200°C plotted as a function of soil organic matter (measured by loss on ignition; data from Nezat et al., 2004). These data represent six composite soil profiles from HBEF. The enlarged symbols represent horizons from the composite soil profile plotted in Figure 3-3.

References

Aubert, D., Probst, A., Stille, P., 2004. Distribution and origin of major and trace elements (particularly REE, U and Th) into labile and residual phases in an acid soil profile (Vosges Mountains, France). Applied Geochemistry 19 (6), 899-916.

Aubert, D., Stille, P., Probst, A., 2001. REE fractionation during granite weathering and removal by waters and suspended loads: Sr and Nd isotopic evidence. Geochimica et Cosmochimica Acta 65 (3), 387-406.

Barton, C.C., Camerlo, R.H., Bailey, S.W., 1997. Bedrock Geologic Map of Hubbard Brook Experimental Forest, Miscellaneous Investigation Series Map I-2562. U.S. Department of Interior, U.S. Geological Survey.

Blum, J.D., Erel, Y., 1997. Rb-Sr isotope systematics of granitic soil chronosequence: The importance of biotite weathering. Geochimica et Cosmochimica Acta 61 (15), 3193-3204.

Blum, J.D., Klaue, A., Nezat, C.A., Driscoll, C.T., Johnson, C.E., Siccama, T.G., Eagar, C., Fahey, T.J., Likens, G.E., 2002. Mycorrhizal weathering of apatite as an important calcium source in base-poor forest ecosystems. Nature 417, 729-731.

Bormann, F.H., Likens, G.E., 1979. Pattern and Process in a Forested Ecosystem. Springer-Verlag, New York, 253 pp.

Bullen, T.D., Bailey, S.W., 2005. Identifying calcium sources at an acid deposition-impacted spruce forest: a strontium isotope, alkaline earth element multi-tracer approach. Biogeochemistry 74, 63-99.

Chapin III, F.S., Walker, L.R., Fastie, C.L., Sharman, L.C., 1994. Mechanisms of primary succession following deglaciation at Glacier Bay, Alaska. Ecological Monographs 64 (2), 149-175.

Crews, T.E., Kitayama, K., Fownes, J.H., Riley, R.H., Herbert, D.A., Mueller-Dombois, D., Vitousek, P.M., 1995. Changes in soil phosphorous fractions and ecosystem dynamics across a long chronosequence in Hawaii. Ecology 76 (5), 1407-1424.

Cross, A.F., Schlesinger, W.H., 1995. A literature review and evaluation of the Hedley fractionation: Applications to the biogeochemical cycle of soil phosphorus in natural ecosystems. Geoderma 64, 197-214.

Davis, M.B., Ford, M.S., Moeller, R.E., 1985. Paleolimnology. In: G.E. Likens (Editor), An Ecosystem Approach to Aquatic Ecology: Mirror Lake and Its Environment. Springer-Verlag, New York, pp. 345-429.

Dreibus, G., Haubold, R., 2004. Phosphorous sorption by terrestrial basalt and granite and implications for the martian crust. Icarus 167, 166-169.

Erel, Y., Blum, J.D., Roueff, E., Ganor, J., 2004. Lead and strontium isotopes as monitors of experimental granitoid mineral dissolution. Geochimica et Cosmochimica Acta 68 (22), 4649-4663.

Ganor, J., Roueff, E., Erel, Y., Blum, J.D., 2005. The dissolution kinetics of a granite and its minerals - Implications for comparison between laboratory and field dissolution rates. Geochimica et Cosmochimica Acta 69 (3), 607-621.

Guidry, M.W., Mackenzie, F.T., 2003. Experimental study of igneous and sedimentary apatite dissolution: control of pH, distance from equilibrium, and temperature on dissolution rates. Geochimica et Cosmochimica Acta 67 (16), 2949-2963.

Hamburg, S.P., Yanai, R.D., Arthur, M.A., Blum, J.D., Siccama, T.G., 2003. Biotic control of calcium cycling in northern hardwood forests: acid rain and aging forests. Ecosystems 6 (4), 399-406.

Hannigan, R.E., Sholkovitz, E.R., 2001. The development of middle rare earth element enrichments in freshwaters: weathering of phosphate minerals. Chemical Geology 175, 495-508.

Hedley, M.J., Stewart, J.W.B., Chauhan, B.S., 1982. Changes in inorganic and organic soil phosphorus fractions induced by cultivation practices and by laboratory incubations. Soil Science Society of America Journal 46 (5), 970-976.

Johnson, A.H., Frizano, J., Vann, D.R., 2003. Biogeochemical implications of labile phosphorous in forest soils determined by the Hedley fractionation procedure. Oecologia 135, 487-499.

Kalinowski, B.E., Schweda, P., 1996. Kinetics of muscovite, phlogopite, and biotite dissolution and alteration at pH 1-4, room temperature. Geochimica et Cosmochimica Acta 60 (3), 367-385.

Leleyter, L., Probst, J.-L., 1999. A new sequential extraction procedure for the speciation of particulate trace elements in river sediments. International Journal of Environmental Analytical Chemistry 73 (2), 109-128.

Likens, G.E., Bormann, F.H., Pierce, R.S., Eaton, J.S., Johnson, N.M., 1977. Biogeochemistry of a Forested Ecosystem. Springer-Verlag, New York, 146 pp.

Newman, E.I., 1995. Phosphorus inputs to terrestrial ecosytems. Journal of Ecology 83 (4), 713-726.

Nezat, C.A., Blum, J.D., Klaue, A., Johnson, C.E., 2004. Influence of landscape position and vegetation on long-term weathering rates at the Hubbard Brook Experimental

Forest, New Hampshire, USA. Geochimica et Cosmochimica Acta 68 (14), 3065-3078.

Nezat, C.A., Blum, J.D., Yanai, R.D., Hamburg, S.P., In preparation. The importance of soil mineralogy to plant nutrient availability in the northeastern USA.

Oliva, P., Dupré, B., Martin, F., Viers, J., 2004. The role of trace minerals in chemical weathering in a high-elevation granitic watershed (Estibére, France): Chemical and mineralogic evidence. Geochimica et Cosmochimica Acta 68 (10), 2223-2244.

Ruttenberg, K.C., 1992. Development of a sequential extraction method for different forms of phosphorus in marine sediments. Limnology and Oceanography 37 (7), 1460-1482.

Schlesinger, W.H., Bruijnzeel, L.A., Bush, M.B., Klein, E.M., Mace, K.A., Raikes, J.A., Whittaker, R.J., 1998. The biogeochemistry of phosphorous after the first century of soil development on Rakata Island, Krakatau, Indonesia. Biogeochemistry 40, 37-55.

Smeck, N.E., 1985. Phosphorus dynamics in soils and landscapes. Geoderma 36, 185-199.

Tanner, E.V.J., Vitousek, P.M., Cuevas, E., 1998. Experimental investigation of nutrient limitation of forest growth on wet tropical mountains. Ecology 79 (1), 10-22.

Taylor, A.S., Blum, J.D., Lasaga, A.C., MacInnis, I.N., 2000. Kinetics of dissolution and Sr release during biotite and phlogopite weathering. Geochimica et Cosmochimica Acta 64 (7), 1191-1208.

Tessler, A., Campbell, P.G.C., Bisson, M., 1979. Sequential extraction procuedure for the speciation of particulate trace metals. Analytical Chemistry 51, 844-851.

Vitousek, P.M., Chadwick, O.A., Crews, T.E., Fownes, J.H., Hendricks, D.M., Herbert, D., 1997. Soil and ecosystem development across the Hawaiian islands. GSA Today 7 (9), 2-8.

Walker, T.W., Syers, J.K., 1976. The fate of phosphorous during pedogenesis. Geoderma 15, 1-19.

Williams, J.D.H., Mayer, T., Nriagu, J.O., 1980. Extractability of phosphorus from phosphate minerals common in soils and sediments. Soil Science Society of America Journal 44 (3), 462-465.

Wood, T., Bormann, F.H., Voigt, G.K., 1984. Phosphorous cycling in a northern hardwood forest: biological and chemical control. Science 223, 391-393.

Yanai, R.D., Blum, J.D., Hamburg, S.P., Arthur, M.A., Nezat, C.A., Siccama, T.G., 2005. New insights into calcium depletion in northeastern forests. Journal of Forestry 103 (1), 14-20.

CHAPTER 4

THE DISTRIBUTION OF APATITE IN SOIL PARENT MATERIALS IN THE NORTHEAST USA

Abstract

Apatite, $Ca_5(PO_4)_3(F,Cl,OH)$, is the dominant P-bearing mineral in crystalline

silicate rocks. Because Ca and P are essential nutrients for vegetation, apatite may be an

important nutrient reservoir. To explore the regional availability of apatite in soils across

the northeastern United States, we collected and sequentially extracted soil parent

material derived from crystalline silicate and sedimentary rocks from 20 sites. The first

extract, a 1 M HNO_3 extract performed at 10°C, selectively dissolved apatite from soils.

The dissolution of apatite was identified by a Ca:P ratio of 5:3 and a lack of Na, Al and Si

in the extract. Most of the soil parent materials derived from crystalline silicate rocks

contained apatite; the Maine soils had the lowest apatite content and those from the

Adirondacks had the highest (ranging from 4 to 42 ? mol Ca/g soil and 2 to 27 ? mol P/g

soil). Shale and sandstone-derived soils contained the smallest amount of leachable Ca

(averaging 7 ? mol/g soil) and P (2 ? mol/g soil) suggesting that these rocks did not

contain appreciable amounts of apatite or carbonate. Large amounts of Ca (140 ? mol/g

soil) but very little P (4 ? mol/g soil) were dissolved from carbonate-derived soils

indicating that apatite was not much more prevalent in these materials than in the other

sedimentary parent materials. The second extract, performed with concentrated HNO_3 at

120°C, removed more weathering-resistant minerals such as hornblende. The chemical composition of the residual fraction was determined as the difference between a $LiBO_2$ flux of bulk soil and the sum of the sequential extracts. The residual, which included feldspars, had more than 90% of the total Ca in the crystalline silicate rocks. Although the residual fraction contained most of the Ca, the 1M HNO_3 extract removed most of the P, and the Ca fraction that is most accessible for dissolution. Apatite is clearly important for explaining the availability of P in soils, and may be important for Ca as well, because of its greater accessibility for dissolution.

INTRODUCTION

Apatite, $Ca_5(PO_4)_3(F,Cl,OH)$, is the dominant P-bearing primary mineral in soils derived from crystalline silicate rocks. Both Ca and P are essential nutrients for vegetation, and their availability in soils is important to the health of terrestrial ecosystems. Recent studies suggest that Ca may be a limiting nutrient in forest ecosystems in the northeast USA where Ca has been leached from the soil exchangeable pool (Likens et al., 1998; Lawrence et al., 1999; Huntington et al., 2000). In these soils, base cation-poor silicates are the dominant minerals and weather too slowly to replenish the exchangeable pool (Likens et al., 1998; Nezat et al., 2004). Apatite has been identified as a potentially important source of Ca for vegetation at Hubbard Brook Experimental Forest (Blum et al., 2002). Although it is only present in trace amounts (~1%) in Hubbard Brook soils, apatite may be a more accessible source of Ca because it dissolves much more rapidly than plagioclase (Valsami-Jones et al., 1998; Welch et al., 2002; Köhler et al., 2005). Thus identifying the distribution of apatite may provide

insight into forest management practices and vegetative adaptation to disturbance such as logging and acid deposition.

Bulk soil analyses indicates the total Ca content of soils, but does not identify trace minerals such as apatite. We have developed a procedure to sequentially leached soil parent materials to extract minerals of increasing resistance to chemical weathering. In earlier study, we confirmed that a 1M HNO_3 solution dissolved apatite but only dissolved ~3% of plagioclase, the mineral that holds most of the Ca in crystalline silicate-derived soils (Nezat et al., In review). Although bulk soil analysis indicates the total Ca content of soils, it does not identify trace minerals, such as apatite, which may be an important source of calcium. Our objective was to collect soils from different soil parent materials across the northeastern USA and test for the presence of easily weathered minerals such as apatite and carbonates. In addition, we digested the soils with solutions of increasing acidity at higher temperatures to identify less easily weathered mineral pools of base cations and phosphorus.

Geologic Setting of Northeast U.S.

Most of the northeast U.S. extending from parts of northern Pennsylvania to Maine is covered by glacial till deposited by the Laurentide Ice Sheet during the Wisconsinan Glacial Stage. The general direction of ice sheet advance ranged from southwest to southeast depending on the regional topography and bedrock texture (Isachsen et al., 2000). In the Adirondack Mountains (NY), White Mountains (NH) and northeastern Pennsylvania, the glacial till is composed of local bedrock, often found less than 15 km away (Crowl and Sevon, 1999; Isachsen et al., 2000; Bailey et al., 2003).

In order to sample a range of crystalline and sedimentary bedrock compositions, twenty locations in New York, Pennsylvania, New Hampshire and Maine were selected according to their bedrock geology. To take into account the direction of glacial advance, we assumed that the glacial deposits at each location were composed predominantly of bedrock within 10 km northward of each site (Figure 1, Table 1).

Sampling sites with metamorphic or igneous bedrock were located in the Adirondack Mountains (New York), White Mountains (New Hampshire) and Maine. Two of the sites, Hubbard Brook and Bartlett, are experimental forests and are located in the White Mountains in New Hampshire on base-poor silicate bedrock. The Hubbard Brook Experimental Forest is underlain by a pelitic schist, meta-sandstone and granodiorite (Barton et al., 1997). The Bartlett Experimental Forest is underlain by granites and syenites of the White Mountain plutonic series (Lyons et al., 1997). The sampling sites in Maine are underlain by gneiss and granite (Osberg et al., 1985). The Adirondack Mountains, located in northeastern New York, are underlain by charnockite, anorthosite and mangerite; in the northwest region, marble, calcsilicate rock and quartzite are common (Isachsen et al., 2000).

Several sites underlain by sedimentary bedrock were selected. Rock types in Finger Lakes region of New York include dolomite, limestone, shale, siltstone and sandstone (Isachsen et al., 2000). The two sites in Pennsylvania are underlain by sandstone, shale, limestone, chert, conglomerate, clay and coal (Survey, 2000).

In the northeastern US, the glacial till is usually at least several meters thick and ~10,000 years old (Isachsen et al., 2000; Bailey et al., 2003). Due to its relatively recent deposition, the glacial till has fresh mineral surfaces and the soils developed are much

younger than those developed on older bedrock south of the glacial advance. Most of the soils in the region are spodosols (Johnson et al., 2000; Yanai et al., 2005b; Sullivan et al., 2006).

Methods

Between July 2002 and February 2004, soil pits were excavated to the C horizon and soils were collected at every 10 cm depth. For the purpose of this study, only the C horizon soils (soil parent material) were analyzed. At the Hubbard Brook and Bartlett Experimental Forests, C horizon samples were collected from multiple depths to observe changes in C horizon composition. All samples were dried at 105°C and sieved through a 2-mm screen.

To identify selected pools of base cations (Ca, Mg, K, Na), P, Al, Fe, Sr and Ti, soils were sequentially extracted using a procedure modified from Blum et al. (2002) and Nezat et al. (In review). A representative ~0.5 g of soil was sequentially leached with the following solutions: 5 mL of 1 M NH_4Cl for ~18 hours on a shaker table at room temperature, 1 M HNO_3 acid for 18 hours at 10°C on a shaker table, and concentrated HNO_3 acid for 3 hours on a hot plate at 120°C. After each leach, the mixture was centrifuged and the supernatant was collected and filtered through a 0.45 µm membrane. Each extract was evaporated to dryness on a hot plate and redissolved in 5% HNO_3 acid. The remaining soil was carried on to the next step.

Because the sequential extraction procedure did not completely dissolve the soils, a bulk soil digest was performed by $LiBO_2$ fusion on another aliquot of soil. About 1 g of technical grade $LiBO_2$ and ~0.1 g of soil were mixed in a graphite crucible and heated

for 20 minutes at 1100 °C. The molten bead was dissolved in ~60 mL of trace metal grade 5% HNO_3 on a magnetic stir plate. The solution was filtered with cellulose fiber paper (25 µm pore size) to remove any graphite. To check the accuracy of this method, several USGS standards were also digested and analyzed. The "residual fraction" is defined as the bulk soil digest minus the sum of the soil leaches.

The sequential leach procedure separates the soil into 1) exchangeable ions, 2) apatite and other easily dissolved minerals, 3) less resistant silicate minerals such as hornblende and biotite, and 4) relatively weathering resistant minerals such as feldspars and quartz (Nezat et al., In review). The first extract, the 1 M NH_4Cl solution, also dissolves calcite and gypsum (Hendershot et al., 1993), which are present in sedimentary rocks at some of our sampling locations. To accurately represent the easily-leached minerals (apatite and carbonate) in the soils, we combined the chemical compositions of the 1 M NH_4Cl and 1 M HNO_3 leaches and refer to this as the "leachable fraction." In the soil parent materials derived from crystalline silicate rocks, exchangeable cations represent less than 1% of base cations in the bulk soil (Yanai et al., 2005a). Thus, the sum of these two fractions does not differ significantly from the 1 M HNO_3 extract for these soils.

All solutions were analyzed on a Perkin Elmer Optima 3300DV Inductively Coupled Plasma-Optical Emission Spectrometer (ICP-OES) using a five- to eight-point calibration curve. Calibration standards, external check standards and sequential extracts of soils were diluted with 2% HNO_3 acid prior to analysis. The $LiBO_2$ fluxes were analyzed separately and $LiBO_2$ was added to the calibration standards and external check standards to match the matrix of the $LiBO_2$ fluxes. Analysis of High Purity certified

reference material Soil Solution A indicated an accuracy of ±5%. $LiBO_2$ fluxes of USGS standard reference materials (ScO-1, STM-1, QLO-1 and RGM-1) were within 5% of the certified values for Al, Ca, Fe, K, Mg, Na, and Sr; Ti concentrations were within 10%. Recovery of P in the $LiBO_2$ fluxes of USGS standards was low (40 to 80%). However, there was a linear relationship between the certified and measured concentrations of P in the four USGS standards (r^2=0.99). We used this relationship to correct the measured P concentrations.

To verify the presence of apatite in the crystalline silicate-derived soils, polished thin sections were made from a subsample of the 250 µm – 2 mm size fraction that had been impregnated with epoxy. Thin sections were made from soil parent materials collected from the sampling sites in Maine, New Hampshire (excluding Bartlett) and the Adirondack Mountains, NY. Apatite was identified by an energy dispersive spectrometer (EDS) on a Hitachi S3200N Scanning Electron Microscope (SEM).

Results

The Ca concentrations in the bulk soils and sequential leaches varied across the northeastern USA (Table 2, Figure 2). Generally, the soils derived from crystalline silicate bedrock had higher total Ca concentrations. The soils in the Adirondack Mountains had the highest bulk Ca (200-1300 µmol/g); more than 90% of the total Ca was in the residual fraction. Among the crystalline silicate-derived soils, the Adirondack soils also had the highest leachable Ca concentrations (up to 42 µmol/g); soils at Hubbard Brook had 27 µmol leachable Ca/g while Bartlett and Maine soils had lower concentrations. Soils derived from clastic sedimentary rocks had the least amount of both

bulk Ca (21-106 µmol/g) and leachable Ca (0.4-17 µmol/g). Not surprisingly, the soils derived from dolostone (Site #379 in the Finger Lakes region of NY) had a high Ca concentration (187µmol/g) of which 76% was leachable (142 µmol/g). The hot HNO_3 removed <5 % of the total Ca from all sites except for the Tioga Forest soil (13%) suggesting there is a small amount of Ca-bearing minerals in these soils that are of intermediate resistance to weathering.

More P was found in the leachable fraction of soils derived from crystalline silicate-derived soils (except for two of the six Adirondack locations) than the hot HNO_3 digest. On the other hand, more P resided in the hot HNO_3 fraction of the sedimentary-derived soils than the leachable fraction.

Bulk Mg concentrations are lower than Ca in the crystalline silicate-derived soils and higher than Ca in the sedimentary sites. There was less than 5 µmol/g of leachable Mg in the soils except for the soil containing dolostone which contained 18 µmol/g, or 4% of bulk Mg. Unlike Ca, which resides mostly in the residual fraction of the crystalline silicate soils, a significant amount of Mg (up to 47%) was extracted by the hot HNO_3 solution.

Only small amounts of other base cations (Na and K) were found in the leachable fraction (<2% of total Na and K) and hot HNO_3 fraction (<1% of total Na, and <5% of total K except for 14% at site T30 at Bartlett). The small amount of Na and K along with Al and Fe in the leachable fraction suggests that silicate minerals are not attacked by this leach. Large amounts of Fe (mean ~50%) were extracted by the hot HNO_3 solution.

Apatite was identified using EDS on a SEM. Apatite was found in all soil parent materials derived from crystalline silicate rocks, including the Adirondacks (NY),

Hubbard Brook (NH) and the two samples collected in Maine. Apatite was either found as an individual grain or included in quartz or feldspar (Figure 1b).

Discussion

Hubbard Brook

In earlier studies, we showed that apatite, an easily-weathered, calcium phosphate mineral, was present in trace amounts in Hubbard Brook soils (Blum et al., 2002; Nezat et al., 2004). Blum et al. (2002) noted that the chemical composition of a 1 M HNO_3 extract of relatively unweathered soils from Hubbard Brook was similar to that of apatite: that is, Ca and P were the dominant elements in the extract, the Ca:P ratio was similar to that found in apatite (5:3), and there were insignificant amounts of Na, K, and Si in the extract. For this study, we lowered the temperature at which the extract was performed (from 20°C to 10°C) to minimize biotite dissolution, a small amount of which occurs at 20°C (Bullen and Bailey, 2005; Nezat et al., In review).

To show the apatite content in soils as a function of soil depth, we plotted Ca versus P concentrations of the 1 M HNO_3 of soils collected from several depths from the top of the mineral soil to the C horizon (some data from Blum et al., 2002 and Nezat et al., In review). The Ca:P ratio indicates that apatite is present in the Bs2 and C horizons but has been weathered from the upper horizons where chemical weathering in soil is more intense (Figure 3). Multiple samples from one soil pit indicate that there are small increases in apatite with depth even in the C horizon.

Although the 1 M HNO_3 extract of the Hubbard Brook soils is a small percentage of the total Ca (Figure 2), it is the mineral fraction that may be most readily solubilized.

Apatite is less than 1% of the minerals in the soil but a mass balance suggests that up to 20% of the Ca lost from the soils has been due to apatite dissolution (Nezat et al., 2004). Because the soils are base-poor and the base saturation is low (Johnson et al., 2000), easily weathered minerals such as apatite may be an important source of Ca for vegetation.

Apatite in northeast U.S. soils

After confirming that apatite was present in Hubbard Brook soils, we investigated whether apatite was an important Ca-bearing mineral in other acid-sensitive soils. The Ca and P concentrations in the 1 M HNO_3 leach of C horizons collected across the northeast U.S. are plotted on Figure 4. Measurable amounts of Ca and P and the similarity between the Ca:P ratio in apatite and the 1M HNO_3 leach of soils suggests apatite is present in other soils in the northeast United States. The soils developed on crystalline bedrock had a Ca:P ratio of 5:3, the stoichiometric ratio in apatite. The clastic sedimentary-derived soils typically had the lowest concentrations of Ca and P and the Ca:P ratios (>5:3) suggest that both carbonate and apatite account for the leachable Ca in these soils. The soil developed on dolostone bedrock had a high Ca concentration and a small P concentration indicating that carbonate dissolution was responsible for most of the leachable Ca.

According to the Ca and P concentrations, the Adirondack soils generally had the highest content of apatite with Wolf Pond and Old Squaw soils having the highest of the sites. These two sites are located next to each other near the center of the Adirondacks and overlie charnockite and granitic and quartz syenite gneiss bedrock. Sand Pond and

Altamont have intermediate concentrations of apatite. Sand Pond, which lies in east-central Adirondacks, is underlain by charnockite and anorthosite. Altamont lies in north-central Adirondacks and is underlain by mangerite gneiss and granite.

Besides bedrock type, the amount of apatite in soils is also dependent on the degree of weathering of the upper C horizon. As can be seen in Hubbard Brook soils, soils exhibit an increase in apatite with depth. Two of the Adirondack sites, Day and Hopkinton, have low concentrations of apatite. The high concentrations of leachable Al and Fe in the soils suggests that these horizons have secondary Al and Fe minerals and thus have weathered appreciably (Nezat et al., In review). In addition, these two sites have measurable amounts of exchangeable Ca, also suggesting that the soil at this depth was weathered. Day and Hopkinton soils are also different than other soils developed on crystalline rocks because the leachable fraction contained only ~20% of the total P (compared to 70% in the other soils) and the hot HNO_3 solution removed the remaining 80%. The high Fe content in the hot HNO_3 suggests that P was adsorbed to Fe in the soils (e.g., Giesler et al., 2005) and was released when the secondary Fe minerals were dissolved by the hot HNO_3 solution. Thus, at these two sites, apatite concentrations may be greater in deeper soils where less weathering has occurred. Despite low Ca and P concentrations, individual apatite grains were found in thin section at these sites (Figure 1b).

Because the Ca:P ratio in the leachable fraction of crystalline silicate rocks is similar to that of apatite, we can assume that most of the leachable P is due to apatite dissolution. However, monazite, a Ce-phosphate mineral, is also present in these soils. Monazite is found in igneous and metamorphic rocks but is more resistant to weathering.

Williams et al. (1980) found that monazite was not dissolved by a dilute HCl leach suggesting that our dilute HNO_3 leach would also not extract monazite. Thus, P extracted by the hot HNO_3 solution may be from monazite, apatite inclusions in minerals dissolved during this step, or P sorbed to Fe and Al oxyhydroxides.

Availability of extractable fraction

The current methods of measuring Ca availability in soils are insufficient to explain the Ca mobilized during forest regrowth. For example, ecosystem budgets of forests in Hubbard Brook Experimental Forest (HBEF, New Hampshire, U.S.) suggest a significant amount of Ca (2-3 g m^{-2} y^{-1}) is removed from the soil during forest regrowth (Hamburg et al., 2003; Yanai et al., 2005a). Mineral weathering rates of plagioclase, the dominant Ca-bearing mineral in the HBEF soils, account for only ~10% of the Ca loss from the soil (0.2-0.3 g m-2 y-1; Likens et al., 1998) and are not affected by forest disturbance or regrowth (Bailey et al., 2003). Based on these calculations, it would appear that the exchangeable Ca pool at Hubbard Brook (<10 g m^{-2}) would be depleted during a few years of forest regrowth. The occurrence of forest regrowth suggests that weathering of apatite or other Ca-bearing minerals is accelerated during this stage.

The calcium in apatite may be plant-available through dissolution by fungi. Ectomycorrhizal fungi, a type of fungi that is symbiotically associated with certain tree species, may weather minerals directly and transport the dissolved nutrients to the tree roots (Jongmans et al., 1997; Landeweert et al., 2001; Wallander, 2000). Laboratory experiments indicate that the rate of apatite dissolution is faster when ectomycorrhizal fungi are present (Wallander, 2000). More research is needed to determine if fungi

increase the dissolution rate of apatite in order to adapt to low concentrations of soil exchangeable calcium.

Conclusions

The distribution of apatite in soils is important for understanding the availability of P and Ca for vegetation. Apatite can be extracted from soils and quantified using a 1 M HNO_3 solution and geochemically identified using the Ca:P ratio of the extract. Using this technique, apatite was found in soils collected from crystalline silicate-derived glacial till. Soils developed on sedimentary rocks generally had a lower apatite content. The apatite content in soils was not related to the bulk Ca concentration indicating that bulk Ca, the majority of which is in plagioclase, should not be used as an indicator of plant-available calcium.

Acknowledgements

References

Bailey, S.W., Buso, D.C., Likens, G.E., 2003. Implications of sodium mass balance for interpreting the calcium cycle of a northern hardwood ecosystem. Ecology 84 (2), 471-484.

Barton, C.C., Camerlo, R.H., Bailey, S.W., 1997. Bedrock Geologic Map of Hubbard Brook Experimental Forest, Miscellaneous Investigation Series Map I-2562. U.S. Department of Interior, U.S. Geological Survey.

Blum, J.D., Klaue, A., Nezat, C.A., Driscoll, C.T., Johnson, C.E., Siccama, T.G., Eagar, C., Fahey, T.J., Likens, G.E., 2002. Mycorrhizal weathering of apatite as an important calcium source in base-poor forest ecosystems. Nature 417, 729-731.

Bullen, T.D., Bailey, S.W., 2005. Identifying calcium sources at an acid deposition-impacted spruce forest: a strontium isotope, alkaline earth element multi-tracer approach. Biogeochemistry 74, 63-99.

Crowl, G.H., Sevon, W.D., 1999. Quaternary. In: C.H. Shultz (Editor), Geology of Pennsylvania. Pennsylvania Geological Survey and Pittsburgh Geological Survey, Harrisburg, pp. 225-231.

Giesler, R., Andersson, T., Lövgren, L., Persson, P., 2005. Phosphate sorption in aluminum- and iron-rich humus soils. Soil Science Society of America Journal 69, 77-86.

Hamburg, S.P., Yanai, R.D., Arthur, M.A., Blum, J.D., Siccama, T.G., 2003. Biotic control of calcium cycling in northern hardwood forests: acid rain and aging forests. Ecosystems 6 (4), 399-406.

Hendershot, W.H., Lalande, H., Duquette, M., 1993. Ion exchange and exchangeable cations. In: M.R. Carter (Editor), Soil Sampling and Methods of Analysis. Lewis, Boca Raton, pp. 167-176.

Huntington, T.G., Hooper, R.P., Johnson, C.E., Aulenbach, B.T., Cappellato, R., Blum, A.E., 2000. Calcium depletion in a southeastern United States forest ecosystem. Soil Science Society of America Journal 64, 1845-1858.

Isachsen, Y.W., Landing, E., Lauber, J.M., Rickard, L.V., Rogers, W.B. (Editors), 2000. Geology of New York: A Simplified Account. New York State Museum, Albany, 294 pp.

Johnson, C.E., Driscoll, C.T., Siccama, T.G., Likens, G.E., 2000. Element fluxes and landscape position in a northern hardwood forest watershed ecosystem. Ecosystems 3, 159-184.

Köhler, S.J., Harouiya, N., Chaïrat, C., Oelkers, E.H., 2005. Experimental studies of REE fractionation during water-mineral interactions: REE release rates during apatite dissolution from pH 2.8 to 9.2. Chemical Geology 222, 168-182.

Lawrence, G.B., David, M.B., Lovett, G.M., Murdoch, P.S., Burns, D.A., Stoddard, J.L., Baldigo, B.P., Porter, J.H., Thompson, A.W., 1999. Soil calcium status and the response of stream chemistry to changing acidic deposition rates. Ecological Applications 9 (3), 1059-1072.

Likens, G.E., Driscoll, C.T., Buso, D.C., Siccama, T.G., Johnson, C.E., Lovett, G.M., Fahey, T.J., Reiners, W.A., Ryan, D.F., Martin, C.W., Bailey, S.W., 1998. The biogeochemistry of calcium at Hubbard Brook. Biogeochemistry 41, 89-173.

Lyons, J.B., Bothner, W.A., Moench, R.H., Thompson Jr., J.B., 1997. Bedrock geologic map of New Hampshire. U.S. Department of the Interior, U.S. Geological Survey.

Nezat, C.A., Blum, J.D., Klaue, A., Johnson, C.E., 2004. Influence of landscape position and vegetation on long-term weathering rates at the Hubbard Brook Experimental Forest, New Hampshire, USA. Geochimica et Cosmochimica Acta 68 (14), 3065-3078.

Nezat, C.A., Blum, J.D., Yanai, R.D., Hamburg, S.P., In review. A sequential extraction to selectively dissolve apatite for determination of soil nutrient pools with an application to Hubbard Brook Experimental Forest, New Hampshire, USA. Chemical Geology.

Osberg, P.H., Hussey, A.M., Boone, G.M., 1985. Bedrock Geologic Map of Maine. Maine Geological Survey, Department of Conservation.

Sullivan, T.J., Fernandez, I.J., Herlihy, A.T., Driscoll, C.T., McDonnell, T.C., Nowicki, N.A., Snyder, K.U., Sutherland, J.W., 2006. Acid-base characteristics of soils in the Adirondack Mountains, New York. Soil Science Society of America Journal 70, 141-152.

Survey, B.o.T.a.G., 2000. Geologic Map of Pennsylvania. Department of Conservation and Natural Resources.

Valsami-Jones, E., Ragnarsdottir, K.V., Putnis, A., Bosbach, D., Kemp, A.J., Cressey, G., 1998. The dissolution of apatite in the presence of aqueous metal cations at pH 2-7. Chemical Geology 151, 215-233.

Wallander, H., 2000. Uptake of P from apatite by *Pinus sylvestris* seedlings colonised by different ectomycorrhizal fungi. Plant and Soil 218, 249-256.

Welch, S.A., Taunton, A.E., Banfield, J.F., 2002. Effect of microorganisms and microbial metabolites on apatite dissolution. Geomicrobiology Journal 19, 343-367.

Williams, J.D.H., Mayer, T., Nriagu, J.O., 1980. Extractability of phosphorus from phosphate minerals common in soils and sediments. Soil Science Society of America Journal 44 (3), 462-465.

Yanai, R.D., Blum, J.D., Hamburg, S.P., Arthur, M.A., Nezat, C.A., Siccama, T.G., 2005a. New insights into calcium depletion in northeastern forests. Journal of Forestry 103 (1), 14-20.

Yanai, R.D., Phillips, R.P., Arthur, M.A., Siccama, T.G., Hane, E.N., 2005b. Spatial and temporal variation in calcium and aluminum in northern hardwood forest floors. Water, Air, and Soil Pollution 160 (1-4), 109-118.

Table 4-1. Characteristics of sampling sites.

Location	Property of	Latitude			Longitude			Glaciated	Bedrock
Bartlett Experimental Forest (H1)	EF	44 °	3 '	12 "	71 °	16 '	40 "	yes	granite, syenite
Bartlett Experimental Forest (H4)	EF	44 °	2 '	52 "	71 °	16 '	48 "	yes	granite, syenite
Bartlett Experimental Forest (T30)	EF	44 °	8 '	46 "	71 °	14 '	9 "	yes	pelitic schist
Hubbard Brook Experimental Forest	EF	43 °	57 '	14 "	71 °	43 '	19 "	yes	granodiorite, pelitic schist
Tioga State Forest, Gleason, PA	ST	41 °	38 '	33 "	76 °	55 '	52 "	?	sandstone, shale, limestone, chert, conglomerate, clay, coal
Patterson Park, Galeton, PA	ST	41 °	41 '	42 "	77 °	53 '	42 "	?	sandstone, shale, limestone, chert, conglomerate, clay, coal
Sand Pond, NY	FP	43 °	56 '	50 "	73 °	53 '	50 "	yes	metanorthosite; anorthositic gneiss
Wolf Pond, NY	FP	43 °	53 '	40 "	74 °	20 '	50 "	yes	charnockite; granitic & quartz syenite gneiss
Day, NY	IP	43 °	19 '	30 "	74 °	3 '	5 "	yes	biotite & hbl granitic gneiss; undivided metasedimentary rock; migmatite
Hopkinton, NY	IP	44 °	30 '	55 "	74 °	35 '	35 "	yes	charnockite; granitic & quartz syenite gneiss
Altamont, NY	IP	44 °	15 '	55 "	74 °	26 '	30 "	yes	mangerite; pyroxene-hbl syenite gneiss; charnockite; metasedimentary rock; granitic gneiss
Old Squaw, NY	FP	43 °	44 '	0 "	74 °	22 '	0 "	yes	gabbroic metanorthosite; anorthositic gneiss; mangerite to charnockitic gneiss
Chain of Ponds, ME	IP	45 °	19 '	20 "	70 °	37 '	0 "	yes	gneiss; granite
Osborn, ME	IP	44 °	47 '	45 "	68 °	16 '	0 "	yes	alkali feldspar granite
CH#164, NY	CH	42 °	13 '	44 "	77 °	0 '	55 "	yes	shale, sandstone
CH#201, NY	CH	42 °	37 '	38 "	76 °	23 '	36 "	yes	shale
CH#342, NY	CH	43 °	30 '	25 "	75 °	57 '	55 "	yes	sandstone, shale
CH#379, NY	CH	43 °	0 '	48 "	76 °	22 '	17 "	yes	limestone, dolomite
CH#395, NY	CH	42 °	33 '	33 "	76 °	24 '	39 "	yes	shale

EF = Experimental Forest; ST=state; FP=Finch-Pruyn; IP = International Paper; CH=Cotton Hanlon

Table 4-2. Chemical composition of bulk soil digest.

	Al	Ca	Fe	K	Mg	Na	P	Sr	Ti
				μmol/g soil (bulk soil)					
HBEF, NH									
Trench, 100 cm	2183	196	197	619	91	752	21.4	1.05	34.1
Trench, 115 cm	1967	189	158	530	76	780	19.7	1.00	28.4
Trench, 130 cm	2062	206	191	623	163	716	21.6	0.99	33.6
Trench, 140 cm	2133	198	163	671	91	762	22.8	1.03	34.8
Trench, 150 cm	1995	189	160	584	84	760	22.0	0.98	34.7
Trench, 162 cm	2046	186	213	645	109	683	24.2	1.00	38.0
W-1, hardwoods									
Bartlett, NH									
H1-2 C0-25	2347	69	304	873	35	1150	4.05	0.57	35.5
H1-2 C25-50	2713	89	358	1000	52	1283	2.19	0.77	45.1
H1-2 C50+	2391	82	368	868	43	1135	6.26	0.67	46.8
H4-3 C0-25	2440	158	337	738	77	1072	7.19	1.20	50.3
T30-1 C0-25	2677	148	476	572	219	624	17.8	1.80	72.3
T30-1 C25-50	2908	145	562	630	282	574	15.5	1.76	78.3
T30-1 C50+	3304	152	634	774	330	640	17.1	1.88	84.5
Adirondacks, NY									
Sand Pond	1791	566	1418	638	440	624	17.4	1.48	351
Wolf Pond	3993	1296	744	222	401	1147	39.1	5.88	184
Day	2068	372	927	521	337	472	14.3	1.18	210
Hopkinton	1522	252	511	546	131	588	17.6	1.53	115
Altamont	1544	198	454	527	113	529	13.0	1.36	92.5
Old Squaw	2473	571	819	688	303	889	25.2	2.59	185
Maine									
Chn of Ponds	2075	266	297	359	179	727	10.8	2.35	62.1
Osborn	2019	132	292	590	183	649	10.4	0.72	61.9
Northern PA									
Tioga Forest	1873	21	604	368	162	99	28.3	0.39	97.3
Patterson	3369	22	525	839	210	75	10.4	0.76	125
Finger Lakes, NY									
164	2564	41	621	564	285	307	8.24	1.12	126
201	1874	106	429	431	209	404	15.8	1.29	82.2
395	2176	40	554	476	278	303	12.7	0.88	108
342	1505	29	399	377	244	287	9.31	0.58	56.6
379	2499	187	679	760	421	195	23.7	0.73	66.8

Table 4-3. Chemical composition of sequential leaches. Note that we have published the

composition of some of these soils using a different sequential extraction procedure

(Yanai et al., 2005a). The sequential extraction method was modified to better isolate the

apatite fraction (Nezat et al., In review).

Soil Pit Location	Depth cm	Al	Ca	Fe	K	Mg	Na	P	Sr	Ti	Al	Ca	Fe	K	Mg	Na	P	Sr	Ti
		umol/g soil (leachable fraction)									umol/g soil (hot nitric digest)								
HBEF, NH																			
Trench#	100	148	23.4	16.1	0.6	1.2	2.8	16.0	0.019	0.36	85	1.2	83.0	16.5	39.4	1.0	1.1	0.002	2.86
Trench	115	136	20.7	15.3	0.5	1.0	0.9	14.2	0.013	0.32	86	0.9	85.0	15.3	45.0	0.8	1.0	0.002	2.46
Trench	130	98	24.5	15.0	1.1	1.5	0.6	16.3	0.008	0.27	109	1.5	109.5	29.1	53.2	1.3	1.2	0.002	3.73
Trench	140	94	24.9	11.5	1.1	1.2	0.5	16.5	0.014	0.25	102	1.0	92.9	28.5	47.5	1.2	0.8	0.002	3.62
Trench	150	74	25.7	11.0	1.2	1.3	0.5	16.8	0.009	0.24	97	1.2	91.6	24.7	46.4	1.1	0.8	0.002	3.05
Trench	162	79	27.1	11.5	1.3	1.4	0.6	17.7	0.010	0.27	130	1.6	122.5	34.6	61.5	1.3	1.0	0.004	4.44
W-1, hardwoods		160	16.2	18.5	0.5	1.3	0.6	11.8	0.006	0.53	164	1.0	144.8	28.7	72.8	1.1	1.7	0.003	5.05
Bartlett, NH																			
H1-2 C0-25	80-105	100	2.9	19.4	1.2	1.0	0.6	2.0	0.005	1.20	95	1.2	105.5	7.0	15.5	0.7	1.3	0.004	2.07
H1-2 C25-50	105-130	52	6.2	20.8	1.7	1.1	0.7	3.1	0.011	1.47	151	1.6	141.4	12.0	18.2	1.0	1.8	0.008	2.56
H1-2 C50+	130+	49	9.9	34.6	2.0	3.6	0.7	5.0	0.015	2.71	106	1.3	138.6	11.4	16.2	0.8	1.6	0.007	3.47
H4-3 C0-25	80	160	8.2	48.3	1.5	3.1	1.0	6.0	0.006	2.54	59	1.3	87.8	7.3	20.1	0.6	1.3	0.008	1.53
T30-1 C0-25	40-65	241	12.2	38.9	3.7	5.6	1.0	9.0	0.012	1.93	441	1.9	339.7	78.7	163.3	2.4	6.8	0.026	6.57
T30-1 C25-50	65-90	226	8.5	28.3	5.7	5.3	0.9	7.5	0.010	2.07	334	1.9	289.5	49.2	125.8	1.7	7.1	0.023	5.41
T30-1 C50+	90+	140	5.0	26.1	5.9	6.7	1.1	5.7	0.023	2.64	589	2.1	388.3	103.1	195.2	3.2	7.6	0.035	8.18
Adirondacks, NY																			
Sand Pond	53	62	29.1	19.0	0.3	2.1	0.4	18.9	0.010	0.42	66	5.2	112.5	1.8	43.7	0.7	2.5	0.006	1.48
Wolf Pond	102	391	42.3	12.2	0.2	1.5	1.8	26.6	0.046	0.34	114	19.6	61.3	0.8	37.3	10.6	2.3	0.059	1.07
Day	154	525	4.7	86.1	0.3	0.7	0.3	2.0	0.004	0.61	137	1.3	212.7	2.3	29.6	1.7	8.0	0.002	2.83
Hopkinton	32	358	6.7	83.2	0.5	1.4	0.4	2.1	0.010	1.24	127	1.1	219.9	2.9	31.3	0.6	8.7	0.002	4.71
Altamont	51	31	15.4	5.7	0.1	1.2	0.3	10.4	0.007	0.32	25	1.2	34.9	1.1	17.4	0.4	0.9	0.002	1.03
Old Squaw	93	121	40.9	10.5	0.4	1.4	0.6	27.1	0.016	0.38	39	3.1	57.4	1.7	15.5	1.4	1.9	0.003	1.27
Maine																			
Chn of Ponds	25	212	7.6	18.0	0.3	4.5	0.4	7.1	0.009	1.11	133	2.2	129.2	13.4	82.0	0.6	2.6	0.009	4.87
Osborn	51	94	4.2	9.0	0.9	4.3	0.7	5.5	0.006	0.91	218	2.1	165.5	17.2	90.3	0.9	2.3	0.006	4.53
Northern PA																			
Tioga Forest	50	108	1.3	46.3	0.9	0.9	0.2	2.9	0.002	0.12	438	2.6	407.6	7.2	78.6	0.3	19.1	0.012	<0.18
Patterson	40	82	0.4	15.4	1.5	0.4	0.2	0.1	0.001	0.00	223	0.1	227.0	7.8	37.7	0.2	3.5	0.006	<0.15
Finger Lakes, NY																			
164	35	37	17.2	26.7	1.5	5.4	0.5	0.4	0.026	0.08	401	1.2	485.8	9.8	151.7	0.7	4.2	0.006	<0.17
201	65	137	8.4	35.9	0.3	1.2	0.3	6.9	0.019	0.49	290	1.6	287.7	3.9	115.8	0.6	3.7	0.010	<0.16
395	44	35	12.5	26.8	0.9	5.0	0.4	1.6	0.021	0.07	421	0.6	441.9	5.1	172.0	0.5	5.6	0.006	<0.16
342	93	48	2.1	23.7	0.6	2.0	0.3	2.5	0.016	0.09	423	0.4	400.5	6.5	220.6	0.5	4.7	0.004	<0.15
379	77	99	141.7	46.0	4.1	18.1	0.8	3.6	0.115	0.07	335	9.1	517.3	13.5	119.1	0.4	18.3	0.021	<0.18

\# 1N HNO3 leach only

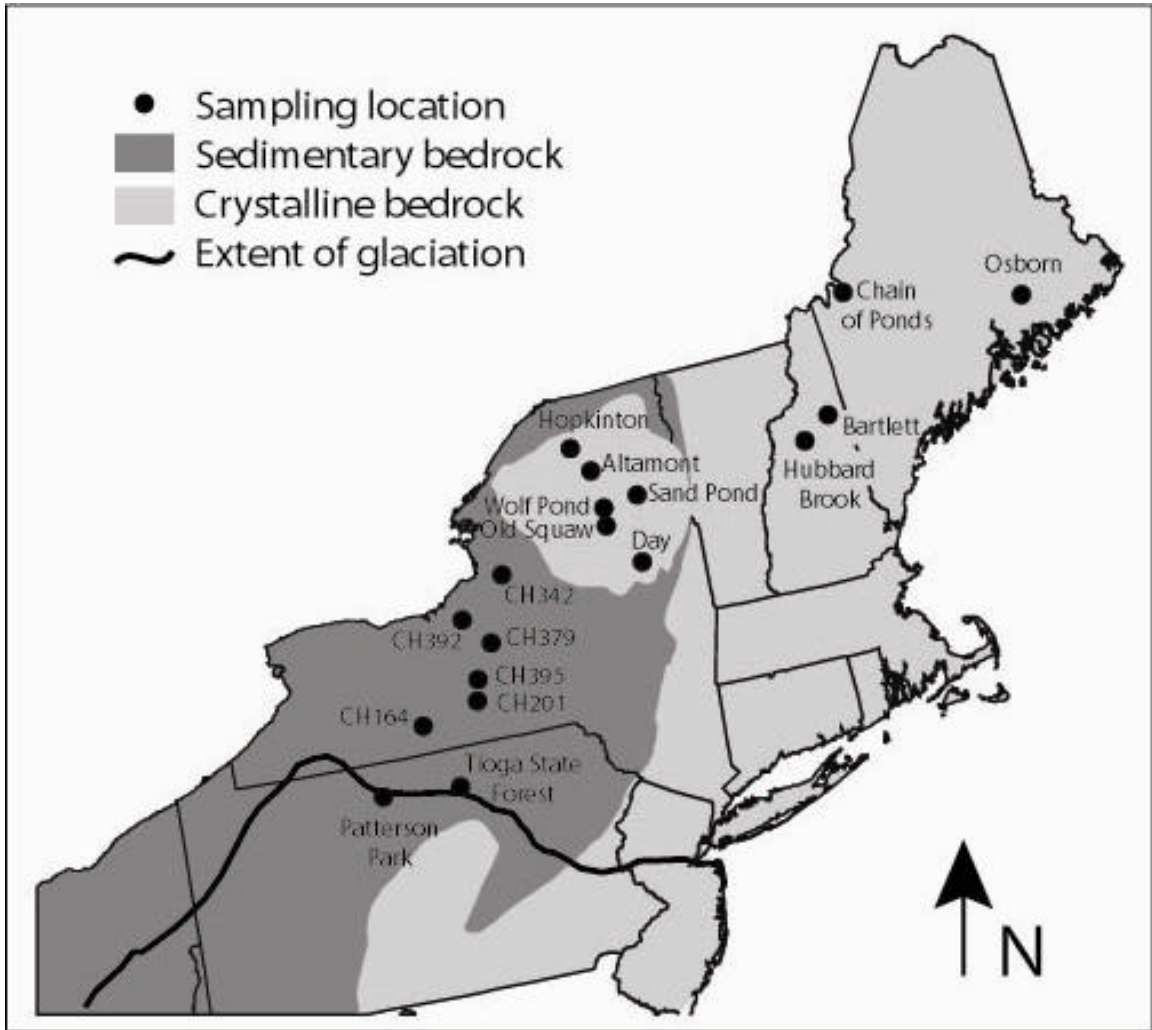Figure 4-1. Location of sample locations in the northeast USA.

Figure 4-2. SEM images of apatite in Adirondack soils. The scale bar is 100 µm long.
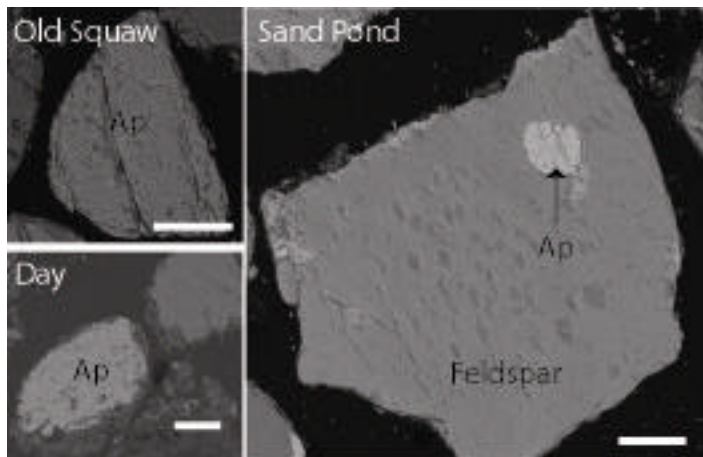
Figure 4-3. Amount of Ca and P in the leachable, hot HNO$_3$, and residual fractions of the soil. The sites are divided by bedrock type: crystalline silicate, clastic sedimentary and carbonate (abbreviated "carb") sedimentary. The residual fraction is the bulk soil digest minus the sum of the leaches.
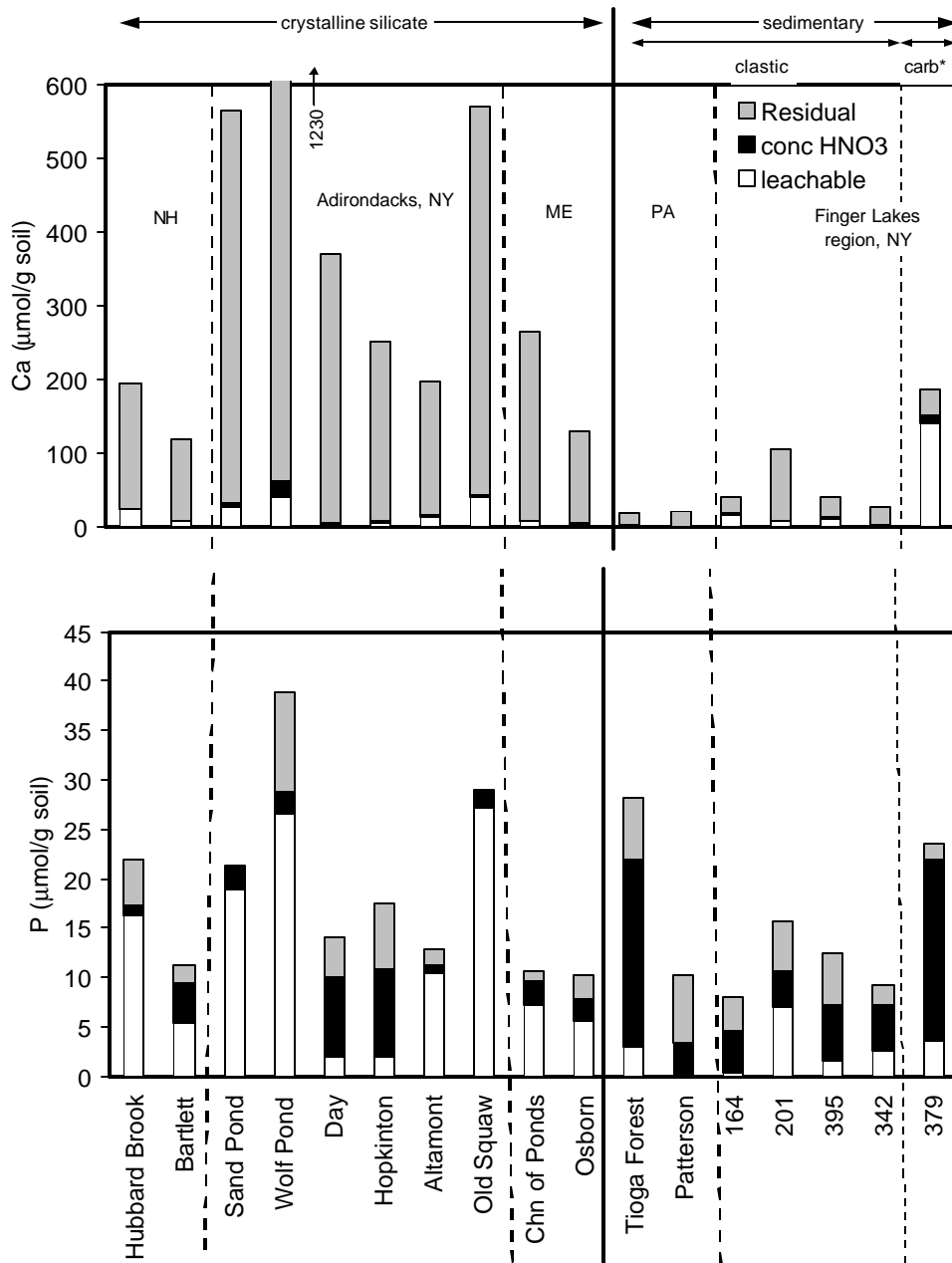
Figure 4-4. P versus Ca in the 1 M HNO$_3$ leach of soils collected at Hubbard Brook Experimental Forest. The grey circles represent a series of progressively deeper C horizon soils (100 – 162 cm) collected from one location (Table 3). The open symbols represent soils that were collected by horizon from six different locations at the Hubbard Brook Experimental Forest (data from Blum et al., 2002 and Nezat et al., In review). The dashed line represents P:Ca ratio in apatite (3:5).
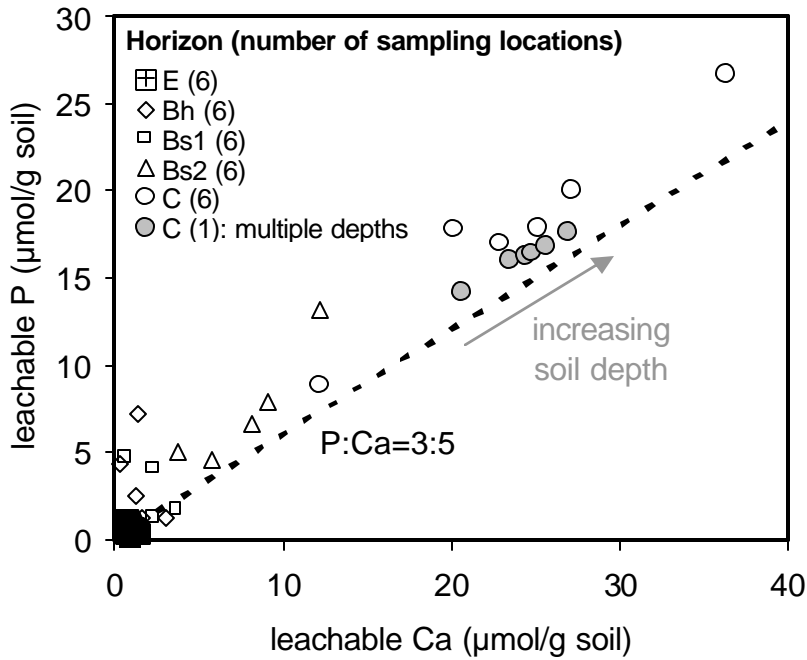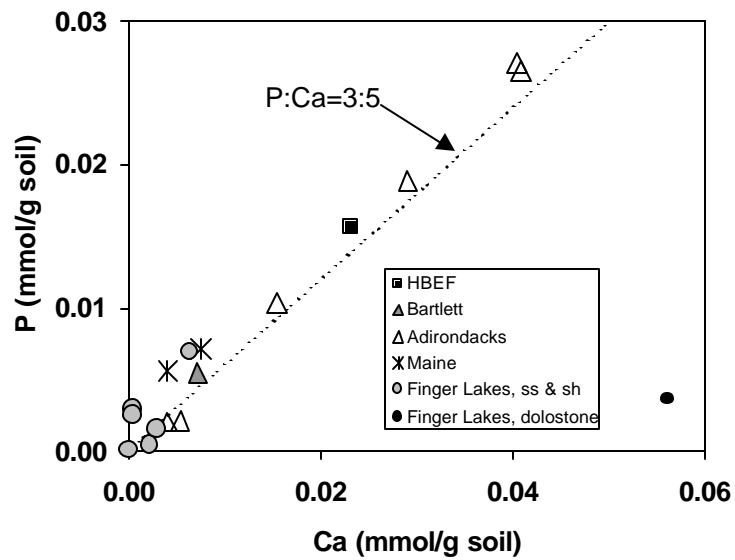
Figure 4-5. P versus Ca of 1 M HNO_3 leach (at 10 °C) of C horizon samples from across the northeast U.S. Dolostone has a high Ca concentration as expected and little P. The other sites fall along the dashed line that represents P:Ca = 3:5, the stoichiometric ratio in apatite.

CHAPTER 5

EXPERIMENTAL EVIDENCE FOR MICROBIAL RESPONSE TO CA- AND P-BEARING MINERALS IN A NORTHERN HARDWOOD FOREST

Abstract

Calcium and phosphorous are essential nutrients for vegetation. Many trees are symbiotically associated with fungi that transport nutrients from the soil to the tree roots and it has been suggested that some of these fungi may obtain nutrients directly from minerals via their hyphae. To test the microbial response to Ca- and/or P-bearing minerals, mesh bags containing quartz plus 1% wollastonite ($CaSiO_3$) or 1% apatite ($Ca_5(PO_4)_3F$) were buried in soil for two growing seasons in spruce/fir, beech and sugar maple stands. Microbial community composition and biomass in the mesh bags and surrounding soil were characterized and quantified using phospholipid fatty acid (PLFA) analysis. Total bacterial and fungal biomass in the soil and control bags (which contained only quartz) did not differ significantly among stand types. This suggests that background microbial composition and biomass were similar among stand types. The degree of fungal colonization in apatite- and wollastonite-amended bags depended on stand type. In the beech stands, the fungal biomass was significantly greater in the apatite-amended bags than in those containing wollastonite. In the spruce-fir stands, the total fungal biomass did not vary as a function of the mineral assemblage. In the sugar maple stands, the fungal biomass had a negative response to the presence of wollastonite.

The different response in each stand may be related to the type of fungi present as well as the nutrient status of the soils. Interestingly, under all three stand types, the molar fraction of 18:1?7c, an individual PLFA found in Gram negative bacteria and arbuscular mycorrhizal fungi, was significantly greater in the wollastonite-amended bags than in the control and apatite-amended bags. This may be important for evaluating the effects of a wollastonite addition to a watershed neighboring the study site for this field experiment.

Introduction

Trees have access to soil nutrients through root uptake as well as through fungi with which they form symbiotic associations. Trees with symbiotic fungi have better access to nutrients and are more tolerant to moisture-related stress and pathogens (Raina et al., 2000). The two most common types of symbiotic fungal-tree associations are ectomycorrhizae and arbuscular mycorrhizae. Ectomycorrhizal fungi (EcM) form a sheath around the tree root and extend hyphae (threadlike filaments) into the soil (Lakhanpal, 2000). These fungi are symbiotically associated with pine (*Pinus*), spruce (*Picea*), fir (*Abies*), birch (*Betula*), and beech (*Fagus*). Arbuscular mycorrhizae are commonly associated with angiosperms such as maples (*Acer*). Arbuscular mycorrhizae surround and penetrate root cells but typically do not extend their hyphae as far away from the roots as ectomycorrhizae. The extent of a fungi's hyphal network, or mycelium, in the soil varies with host species (Raina et al., 2000).

Laboratory and field investigations suggest that mycorrhizal fungi may be able to dissolve minerals directly and absorb the released nutrients. Fungal hyphae seem to be able to aquire nutrients from minerals such as biotite, hornblende, apatite and microcline

115

by exuding low molecular weight organic acids (Jongmans et al., 1997; Wallander, 2000; Landeweert et al., 2001). As a result, the presence of nutrient-bearing minerals such as apatite can stimulate mycelial biomass and plant growth and result in greater concentrations of nutrients in fungi and plants (Wallander, 2000; Hagerberg et al., 2003; Wallander et al., 2003). In field investigations, tubular micropores (3-10 µm in diameter), some of which contained hyphae, were found in feldspar and hornblende grains collected from E horizon soils beneath European conifers (Jongmans et al., 1997; Hoffland et al., 2002). Ectomycorrhizae have been found as deep as 4m within fractured granitic bedrock (Bornyasz et al., 2005).

In environments where Al concentrations in soil solutions are toxic to vegetation, it has been speculated that mycorrhizae may allow trees to bypass the soil solution and obtain nutrients from minerals directly via dissolution (van Breemen et al., 2000). Calcium and phosphorous are essential nutrients for vegetation. In most forest ecosystems, nitrogen is the limiting nutrient. However, in the northeastern USA, decades of nitrogen deposition and loss of calcium from the soil exchange complex could result in a shift toward Ca or P limitation.

To test the microbial response to P- and/or Ca-bearing minerals, we buried mesh bags containing one of three different mineral assemblages: quartz only, quartz plus apatite ($Ca_5(PO_4)_3(F,Cl,OH)$) or quartz plus wollastonite ($CaSiO_3$). Mesh bags with only quartz served as controls. Because there is a difference in root and hyphae diameters, mesh can been used to create a root-free environment to study microbial communities.

One way to study fungal community composition and biomass in soils is through the use of phospholipid fatty acids (PLFAs). Phospholipids are the main component of

cell membranes in organisms and represent living microbial biomass. Each phospholipid contains two fatty acids. A fatty acid is a carbon chain with a carbon at one end of the chain bonded to an oxygen atom and a hydroxide molecule. Fatty acids are identified by the number of carbon atoms, the number and location of double bonds, and the location of methyl branches along the carbon chain. Certain PLFAs are specific to bacteria and fungi. For example, saturated and monounsaturated PLFAs are common in bacteria while an 18-carbon, polyunsaturated PLFA is only found in fungi (e.g., Frostegård and Bååth, 1996).

The objective of this study were to identify the fungal and bacterial colonization in response to a Ca- and P-bearing mineral (apatite) and a Ca-bearing mineral (wollastonite) under ectomycorrhizal conifers (spruce-fir), ectomycorrhizal hardwoods (beech), and arbuscular mycorrhizal hardwoods (sugar maple). We hypothesized that apatite, because it contains both Ca and P, would stimulate more microbial colonization than quartz or wollastonite. In addition, if the ecosystem is Ca-limited, we should see a fungal increase in bags containing wollastonite relative to the control. We also hypothesized that there would be a greater fungal response to apatite and/or wollastonite in the ectomycorrhizal stands (spruce-fir and beech) due to the greater extent of ectomycorrhizae in the soil.

Site Description

The Hubbard Brook Experimental Forest (HBEF) is located in the White Mountains of central New Hampshire, USA. The vegetation is predominantly northern hardwood forest, dominated by American beech (*Fagus grandifolia* Ehrh.), sugar maple

(*Acer saccharum* Marsh), and yellow birch (*Betula alleghaniensis* Britton). White birch (*Betula papyrifera* Marsh.), red spruce (*Picea rubens* Sarg.) and balsam fir (*Abies balsamea* L.) are dominant at higher elevations (Fig. 1). The dominant soils are well-drained Spodosols (haplorthods) extending to about 60 cm depth. The soils are developed on glacial till composed of underlying bedrock and bedrock to the north of the Hubbard Brook valley, which includes pelitic schist, meta-sandstone and granodiorite (Barton et al., 1997).

Stands of beech and sugar maple were chosen across a range of elevation in Watershed 3, which lies at the eastern end of the Hubbard Brook valley. Mixed stands of spruce and fir were selected along the ridge less than 1 km west of Watershed 3. These sites have not been disturbed or experimentally manipulated since logging in the early 1900's. The sites range in elevation from ~550 to 730 m above sea level (Fig. 1).

Methods

Methods for constructing mesh bags were adapted from Wallander et al. (2001) and Hagerberg et al. (2003). Bags were made of 50 µm nylon mesh, which is hydrophyilic and has large enough openings to allow fungal hyphae (= 10 µm diameter) to enter the bag but small enough to prevent roots from entering the bag. The bags were ~5 cm by 5 cm and contained one of three mineral assemblages: 50 g quartz, 50 g quartz plus 0.5 g apatite, or 50 g quartz plus 0.5 g wollastonite. Because quartz is expected to be inert in soils over this time period, the bags with only quartz served as a control.

The quartz was purchased from Fisher Scientific as Ottawa Sand, which contained less than 1% impurities. The quartz was pre-cleaned with 1M HNO_3 on a shaker table

overnight to remove any reactive impurities, and sonicated repeatedly in deionized water to remove finer particles. Apatite (from Durango, Mexico) and wollastonite (from the Willsboro-Lewis skarns, New York) were purchased from Ward's Natural Science, crushed with a mortar and pestle, sieved to 100 - 250 µm, and ultrasonically cleaned in ethanol several times to remove fine particles adhered to grain surfaces. Mineral surfaces were examined using a scanning electron microscopy to confirm the lack of fine particles on mineral surfaces.

In order to assess the fungal and bacterial response to Ca- and/or P-bearing minerals, mesh bags with each mineral assemblage (apatite + quartz, wollastonite + quartz, or quartz only) were buried in triplicate at nine sites in May 2004. Sites were chosen based on their dominant tree species: spruce-fir (ectomycorrhizal), beech (ectomycorrhizal), and sugar maple (non-ectomycorrhizal). At each site, we marked a line that was roughly perpendicular to the slope of the terrain; nine holes were spaced ~15 cm apart along this line. The forest floor was removed as a block and then the mineral soil was excavated. Mineral bags were buried in the upper B soil horizon (~10 cm below the top of the Oa horizon) where apatite is present naturally. Also, at this depth saprotrophic fungi, which derive their nutrients from decaying organic matter, are in relatively low abundance. A bag was placed horizontally in each hole and the hole was then refilled with the original mineral soil and the forest floor block was replaced with as little disruption as possible.

One set of mesh bags (that is, one bag of each mineral assemblage for a total of 3 bags per site) was retrieved from each of the nine sites in October 2005 before leaf senescence. The second set of bags will be collected in summer 2006 and the last set in

summer 2007 to determine microbial biomass changes over time. During retrieval of each mineral bag, a soil sample was collected within a few centimeters above the mineral bag in order to compare the microbial composition between the inside and outside of the bag. The mesh bags and soil were stored in a cool, dark container in the field until they could be frozen at -80°C and lyophilized.

Microbial composition and biomass were estimated using phospholipid fatty acid analysis. We used a 20 g subsample of the mesh bag, and 2 g subsample of soil. Phospholipids were extracted with a single-phase, phosphate buffered solution of $CHCl_3$ and CH_3OH (modified Bligh and Dyer method). Polar lipids were separated using silicic acid chromatography, and converted to fatty acid methyl esters (FAMEs) with a solution of methanol and KOH (0.28 g KOH/25 mL methanol). The FAMEs were separated using a Finnigan Delta plus mass spectrometer with a GC/C III interface (Thermofinnigan). A standard with known concentrations of four to five FAMEs was analyzed periodically (every four samples) during each run; the regression between the known concentrations and peak areas of the FAME mix was used to convert peak area of sample PLFAs to concentrations. To correct for any loss of PLFAs during the assay, phosphatidylcholine (Avanti), a synthetic polar lipid containing two 21:0 fatty acids per mole, was added as an internal standard to each sample before lipid extraction. Concentrations of PLFAs were corrected using the recovery of the 21:0 fatty acids.

Specific PLFAs are characteristic of certain microbes. We assigned PLFAs to various microbes based on earlier studies. Branched-chain fatty acids (i15:0, a15:0, i16:0 and 10Me16:0) are common in Gram-positive bacteria (O'Leary and Wilkinson, 1988); even-carbon unsaturated fatty acids (16:1?7 and 16:1?9) and cylcopropanes (cy17:0 and

cy19:0) are dominant in Gram-negative bacteria (Wilkinson, 1988). Other fatty acids

specific to bacteria include a17:0 and i17:0 (Frostegård and Bååth, 1996). The PLFAs

16:0 and 18:0 are general biomarkers for all organisms including bacteria and fungi

(Larsen et al., 1998; Olsson and Melkerud, 2000). Fungal biomarkers are 18:2?6 and

18:1?9 (Frostegård and Bååth, 1996; Klamer and Bååth, 2004). The fatty acids, 16:1?5

and 18:1?7, are found in both arbuscular mycorrhizal fungi and bacteria (Wilkinson,

1988; Graham et al., 1995).

Statistical Analysis

Using a one-way analysis of variance (ANOVA), we tested the null hypothesis

that mineral assemblage did not affect the molar fractions of PLFA or biomass in the

mesh bags. Data for each stand type was analyzed individually with mineral assemblage

as the criterion variable. To determine if pairs of mean values were significantly

different, we used a student's t test. Significance was accepted at $p<0.05$.

Results

When the mesh bags were retrieved, we observed minimal disturbance to the

forest floor, and found that roots had grown into the soil column above the mesh bags.

At the time of bag harvesting, the soil was saturated due to extensive rain for several days

prior to sampling. Fe-oxide staining was present on the outside of the bags. A small

number of hyphae were the only type of organic matter that was visible inside the bags.

Total microbial biomass and composition

The presence of PLFAs in the mesh bags indicates that microbial colonization

occurred in the mesh bags after two growing seasons (Figure 2). The amount of PLFAs

in the mesh bags, represented as nmol PLFA per gram quartz, did not differ significantly among stand type. In all stands, the microbial community within and outside the control bags was dominated by bacterial biomass relative to fungal biomass (Figure 3). The difference between the bacterial and fungal fractions was more pronounced in the soil than in its corresponding control bag, especially in the beech stands.

Effects of mineral assemblage on microbial biomass

Total microbial biomass was not significantly affected by the presence of apatite or wollastonite in the mesh bags (Figure 4). Bacterial biomass was also not significantly different among treatments except for the smaller bacterial fraction in the wollastonite bags located under sugar maple. In the beech stands, the fungal PLFA fraction was significantly greater in the apatite bags than in the wollastonite bags but both bags were not statistically different than the control. In the spruce-fir and sugar maple stands, the fungal biomass did not differ as a function of mineral assemblage.

Effects of mineral assemblage on microbial community composition

Among the treatments, the microbial community compositions were not significantly different except for a few individual PLFAs (Figure 4a-c). Under the beech stand, the molar fraction of 16:1?7c and 18:1?7c was significantly higher in the wollastonite-amended bags relative to the control bag, the apatite-amended bag and the surrounding soil (Figure 4a). Under the spruce-fir stands, 16:1?9c was higher in the apatite-amended bags (Figure 4b). Under the sugar maple, 18:1?7c was significantly higher in the wollastonite bags; there was no detectable a15:0 and 16:1?5c in the wollastonite bags making the molar percent of these PLFAs significantly lower than the control bags (Figure 4c).

The soil surrounding the mesh bags had a greater fraction of some individual PLFAs than the interior of the mesh bags. In the soil in the beech stands, there was a greater fraction of PLFAs representing Gram negative bacteria (i16:0 and 10Me16:0) and Gram positive bacteria (cy19:0 and 16:1?9c) relative to the bags. Under spruce-fir stands, the surrounding soil had a greater molar fraction of cy19:0 than the bags but a lower fraction of 16:1?5c and 18:0. Under sugar maple, the surrounding soil had higher 10Me16:0 and cy19:0 but smaller amounts of 16:1?7c, 18:2?6, 16:0 and 18:0.

Discussion

Site conditions

The mesh bags were buried ~3-17 cm below the Oie horizon. Across most of the Hubbard Brook watershed, the depths to the Bh, Bs1 and Bs2 horizons average ~7, 10 and 14 cm, respectively (Nezat et al., 2004). We buried the bags at a depth of 10-15 cm unless we encountered a rock or root and then the bag was buried at a shallower depth. At Hubbard Brook, apatite is present naturally in the B horizon (Nezat et al., In review). At this depth, sapotrophic fungi are expected to be less abundant than in the organic horizon.

The larger difference between the molar fractions of fungi and bacteria in the mesh bags compared to the adjacent soil may be due to the lack of sapotrophic fungi in the mesh bags. A quartz medium, which we chose for the contents our mesh bags, is not favorable for growth of sapotrophic fungi because the bags did not accumulate a visible amount of organic matter (Wallander et al., 2001). Another possibility is that the difference in fungal and bacterial fractions between the inside and outside of the bag is

due to disturbance of the soil when the bags were originally placed in the soil. To test the effects of disturbance on microbial composition of the soil, in the future we will analyze the PLFA composition of a soil near the site of the experiment that has not been disturbed by the experiment. Also, if the pronounced difference between the fungal and bacterial fractions is due to disturbance, bags collected in the future should show a fungal:bacterial ratio more similar to that of the overlying soil.

Dissolution of apatite and wollastonite

Apatite and wollastonite may be dissolved by organic acids released by fungi and bacteria colonizing a mesh bag, and/or by inorganic and organic acids in the soil solution that move through the mesh bag. At pH of ~4, the pH of soils at HBEF, the dissolution rates of wollastonite and apatite are in the same order of magnitude. Results of laboratory experiments indicate that at pH 4 the dissolution of apatite is $10^{-8.5}$ mol m^{-2} s^{-1} (Valsami-Jones et al., 1998). Based on the Ca release rate, the dissolution rate of wollastonite is $10^{-8.0}$ mol m^{-2} s^{-1} and is independent of pH (Weissbart and Rimstidt, 2000). Peters et al. (2004) calculated that wollastonite that was added to a watershed at Hubbard Brook had a similar dissolution rate ($10^{-8.7}$ to $10^{-8.4}$ mol m^{-2} s^{-1}) as those established by laboratory experiments. In comparison, the dissolution of oligoclase, the most common Ca-bearing mineral in HBEF soils, is 10^{-12} mol m^{-2} s^{-1}, three to four orders of magnitude slower than apatite or wollastonite (Oxburgh et al., 1994). Because apatite and wollastonite were not pre-weathered before they were placed in the field, the initial dissolution rates are expected to be somewhat higher than laboratory rates due to ion exchange processes on freshly cleaved mineral surfaces.

Microbial response in different stand types

Beech, spruce and fir are associated with ectomycorrhizal fungi which extend hyphae into the soil; sugar maple have arbuscular mycorrhizal associations. Because ectomycorrhizae usually extend mycelia farther away from the root, we hypothesized that the mesh bags placed in the beech, spruce and fir stands would have more fungal production than those in the sugar maple stands. However, the fungal biomass in the control bags does not differ significantly among the stand types (Figure 4). For the same reason, we also expected that ectomycorrhizal fungi associated with beech, spruce and fir might respond to the presence of apatite and/or wollastonite but that arbusucular mycorrhizal fungi in the sugar maple stands would not. Fungal biomass varied in the bags in the beech stands but did not differ among mineral assemblages in the spruce-fir stands (Figure 4c). Although not statistically significant, the fungi in the sugar maple stands had a negative response to the presence of apatite and wollastonite.

There are a few reasons why spruce and fir may not have responded to the presence of apatite or wollastonite. First, if plant-available P is higher in the soils in the spruce-fir stands, then ectomycorrhizae may not respond to P-bearing minerals. The low pH of the soils in the spruce-fir zone and the high concentration of inorganic Al (Johnson et al., 2000) suggest that phosphate may be more mobile in this region. Secondly, the bags in the spruce-fir stands were typically buried at shallower depths (Table 1) where saprotrophic fungi are more abundant. Because saprotrophic fungi may represent a large proportion of total fungi in the bags, changes in ectomycorrhizal biomass may not be detectable. Additional research is needed to determine the lack of preferential colonization of fungi in the apatite- and wollastonite-amended bags.

Although the fungal community in the spruce and fir soils did not respond to apatite or wollastonite, laboratory and field experiments indicate that ectomycorrhizal fungi do respond to apatite additions under certain conditions. For example, a study by Wallander et al. (2000) found that more apatite was weathered from soils containing ectomycorrhizal fungi associated with Scots pine (*Pinus sylvestris*). In turn, the biomass of seedlings with ectomycorrhizal fungi increased faster than those without ectomycorrhizae. In another study, mesh bags containing quartz and 1% apatite (50-630 μm from Madagascar) were buried in the organic horizon in Norway spruce (*Picea abies*) stands that varied in nutrient status (Hagerberg et al., 2003). In all of the stands, fungal biomass increased in apatite-amended bags compared to quartz control bags. However, the abundance of ectomycorrhizal roots on the outside of the bags differed among the sites; in the P-deficient stand, the roots were more abundant.

In fall 1999, wollastonite was added to the forest floor of an entire watershed at Hubbard Brook. During the first six months, calcium was released from the mineral surface faster than silica (Peters et al., 2004). The dissolution of wollastonite increased the pH of the Oa horizon (organic horizon beneath the leaf litter) from 3.9 to 4.2 (Juice et al., 2006). Three years after the wollastonite addition, the pH of the forest floor was still 4.2 (Fisk et al., 2006). The Ca fertilization stimulated arbuscular mycorrhizal colonization of sugar maple seedlings and mature sugar maple (Juice et al., 2006). The authors did not have enough data to conclude whether the improved health of sugar maple and increased mycorrhizal colonization was causative or correlative (Juice et al., 2006). In our study, the wollastonite appeared to suppress both fungal and bacterial colonization in the mesh bags. Our results suggest that AM fungi do not benefit directly

from the presence of wollastonite but that the AM growth increases found by (Juice et al., 2006) were due to healthier sugar maple, which benefited from other effects of the wollastonite addition (increased pH, exchangeable Ca, etc.).

Response of individual PLFAs

The PLFA cy19:0, which is indicative of Gram negative bacteria, was more prevalent in the soil than in the mesh bags. Its greater fraction in the soil suggests that 1) it is associated with the rhizosphere because roots were present in the soil but not the mesh bags, or 2) current conditions in the mesh bags were not conducive for the type of Gram negative bacteria that are dominated by this PLFA. Gram negative, rod-shaped bacteria and *Pseudomonas* are more abundant in the rhizosphere than in root-free soil because the release of root exudates is conducive for rapidly growing bacteria (Atlas and Bartha, 1987 and references within). Future PLFA analysis of bags that will be collected in the next year and have remained in the soil longer may reveal whether the bags become more habitable for the cy10:0-bearing bacteria.

The molar fraction of 18:1?7c, which is found in bacteria and arbuscular mycorrhizae, was greater in the wollastonite-amended bags in all three stands. Of all the PLFAs, it exhibited the strongest response to a treatment. Interestingly, the same PLFA showed no preference for the apatite-amended bag relative to the control bag. If Ca were the nutrient needed, then it seems that there should have been an increase in 18:1?7c in the apatite bag as well. However, laboratory experiments indicate that wollastonite dissolves slightly faster than apatite at a pH of 4. The faster release of Ca from wollastonite may stimulate a response mycorrhizae are Ca-limited. These results suggest

a shift may have occurred in the microbial composition in the watershed that received the wollastonite addition. PLFA analysis of those soils would be able to test for this.

Conclusions

Fungal and bacterial responses to the presence of apatite and wollastonite differed depending on stand type. In the beech stands apatite, but not wollastonite, stimulated fungal colonization suggesting that P was a nutrient in high demand. In the spruce-fir stands, there was no difference in fungal response to the different mineral assemblages suggesting that spruce and fir are neither Ca- or P-limited. In the sugar maple stands, apatite did not affect the total fungal biomass relative to the control. Wollastonite appeared to suppress fungal colonization in the beech and sugar maple stands. Additional research is needed to develop a causal understanding of the observed responses.

The PLFA 18:1?7, which is found in arbuscular fungi and bacteria, was greater in wollastonite bags under all three stand types. This may be important for evaluating the ecosystem response to a wollastonite addition in a watershed that is adjacent to the study site for the field experiment here.

Table 1. Characteristics of sites where in- growth mesh bags were buried.

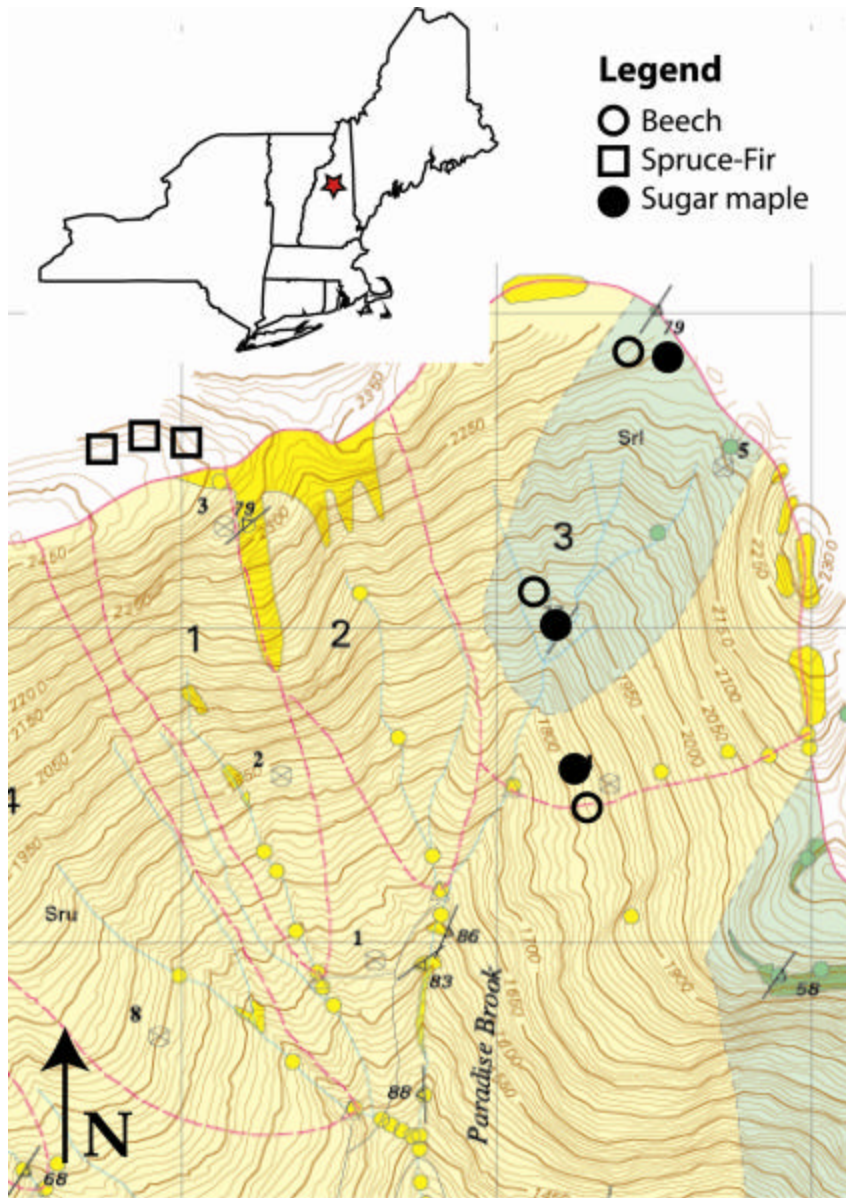|	Latitude		Longitude		Qtz	Ap	Woll	Overstory
	°	'	°	'		Depth (cm)		
BE1	43	57.5	71	43.3	17	12	12	**American beech (*Fagus**
BE2	43	57.7	71	43.3	11	10	8	***grandifolia* Ehrh.)**
BE3	43	57.3	71	43.3	5	7	7	
SF1	43	57.6	71	43.8	5	3	4.5	**Red spruce (*Picea rubens***
SF2	43	57.6	71	43.8	9	7	7	**Sarg.), balsam fir (*Abies***
SF3	43	57.6	71	43.8	7	4	4	***balsamea* L.), yellow birch**
								(*Betula alleghaniensis*
								Britton), white birch (*Betula*
								***papyrifera* Marsh.)**
SM1	43	57.7	71	43.3	8	11	12	**Sugar maple (*Acer saccharum***
SM2	43	57.4	71	43.3	9	10	14	**Marsh)**
SM3	43	57.4	71	43.3	12	7	9	

Fig. 5-1. Location of buried bags at Hubbard Brook Experimental Forest, NH.
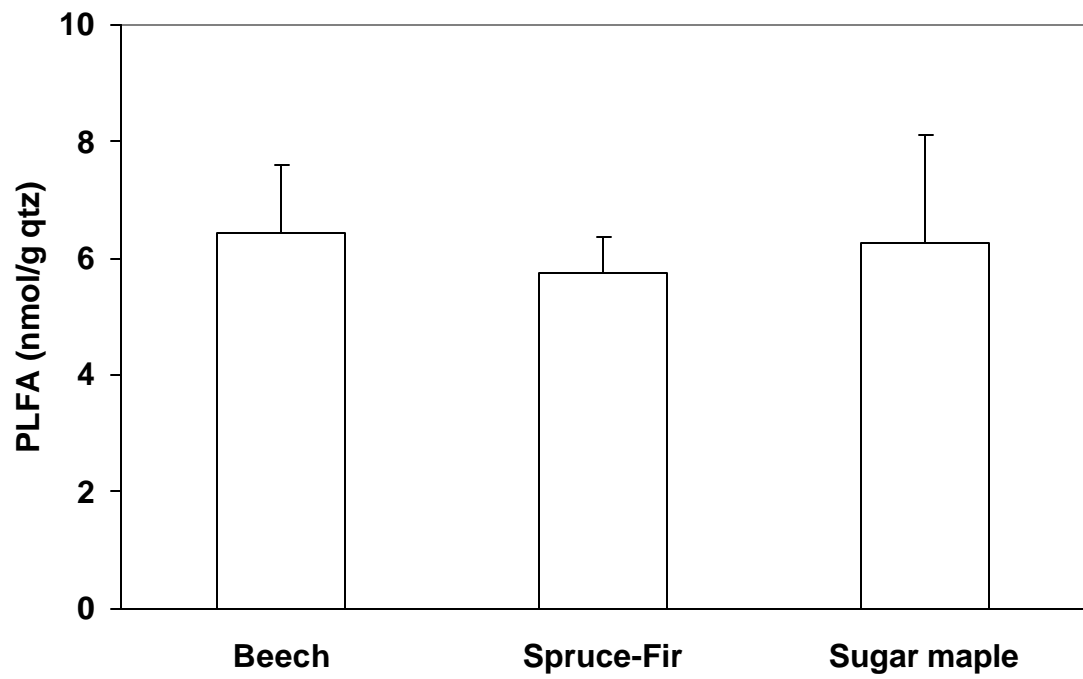
Figure 5-2. Total amount of phospholipid fatty acids in control bags after two growing

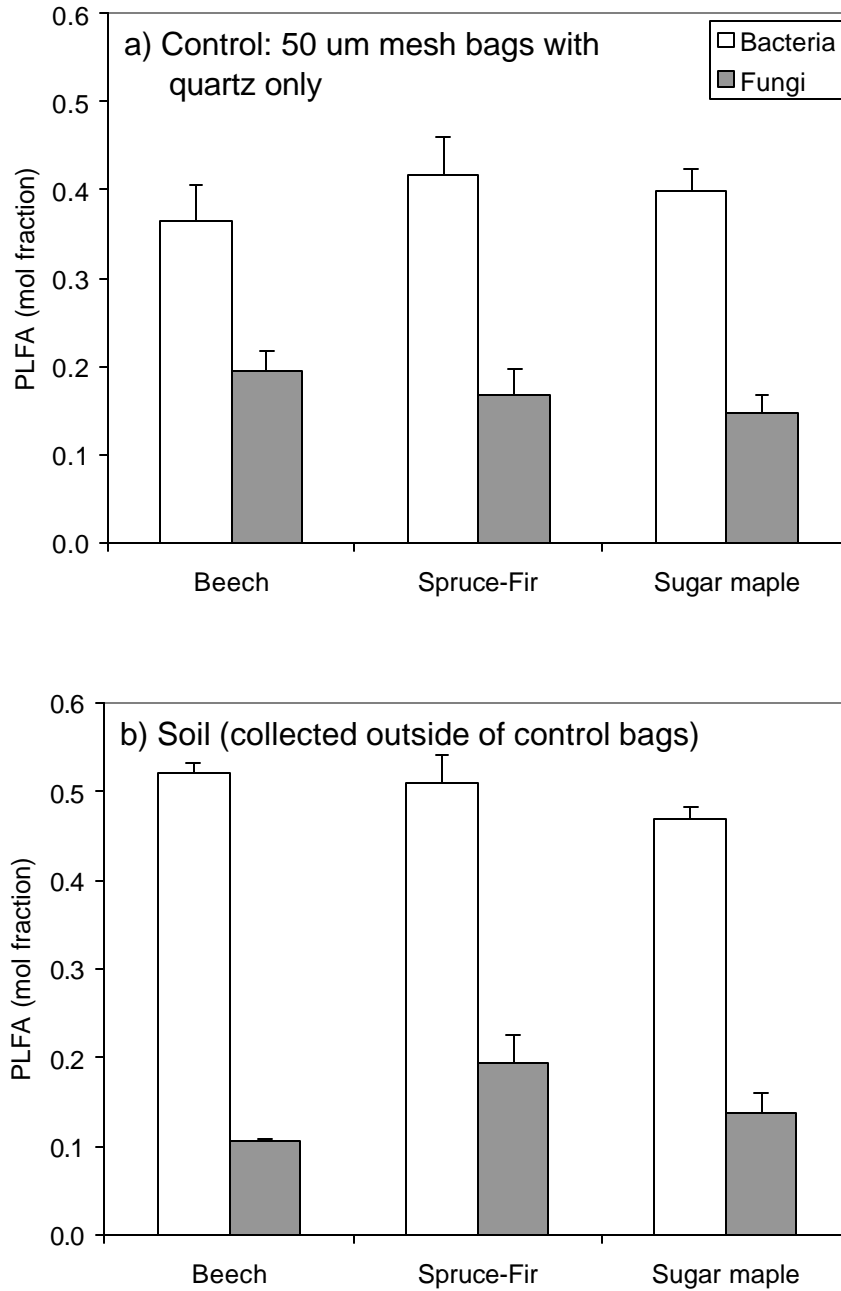seasons. Error bars are standard errors of the mean (n=3).

Figure 5-3. Fraction of bacterial and fungal PLFAs in a) control bags and b) outside of control bags in soil. Error bars are standard errors of the mean (n=3).
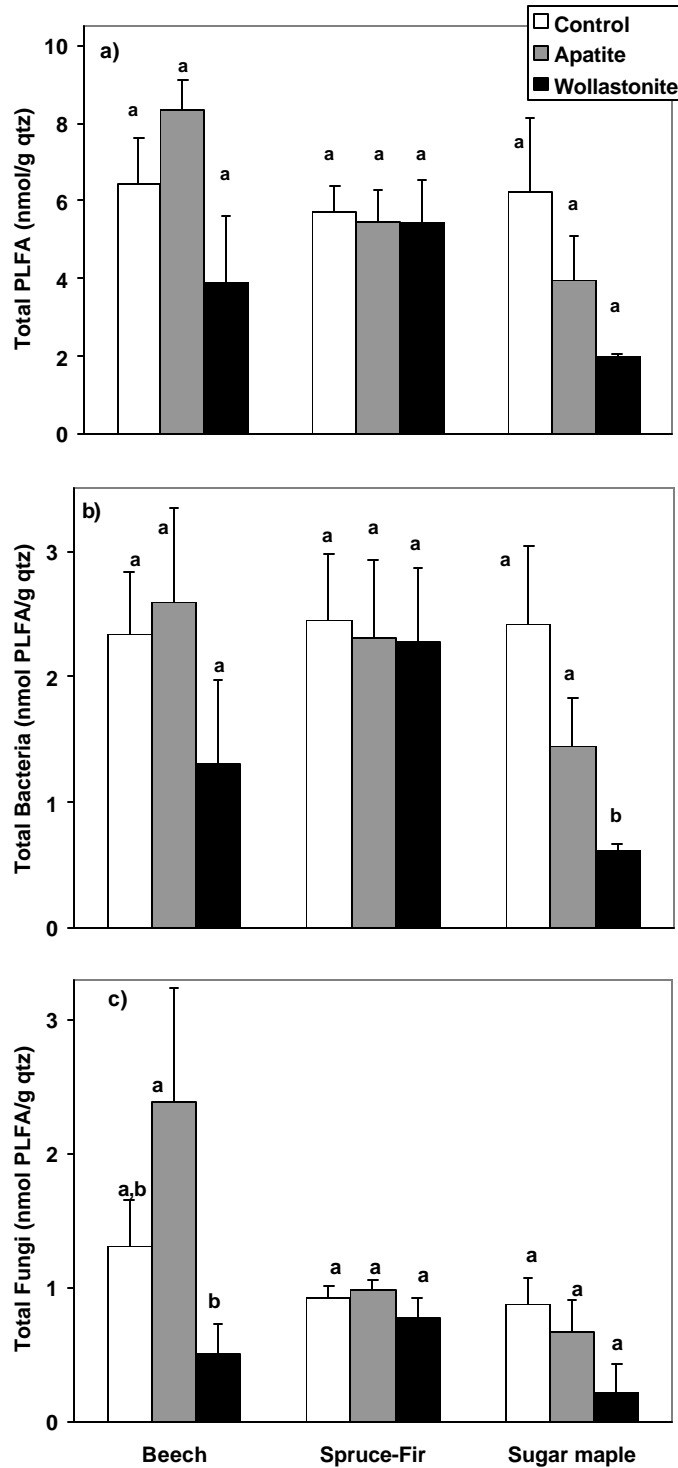
Figure 5-4. Amount of a) total PLFA, b) bacterial PLFA and c) fungal PLFA in mesh

bags after two growing seasons. Error bars are standard errors of the mean (n=3). Mean

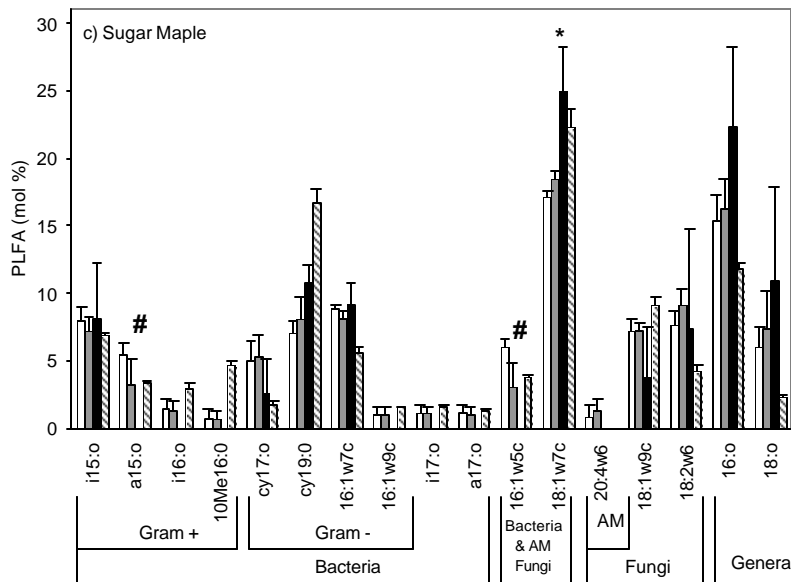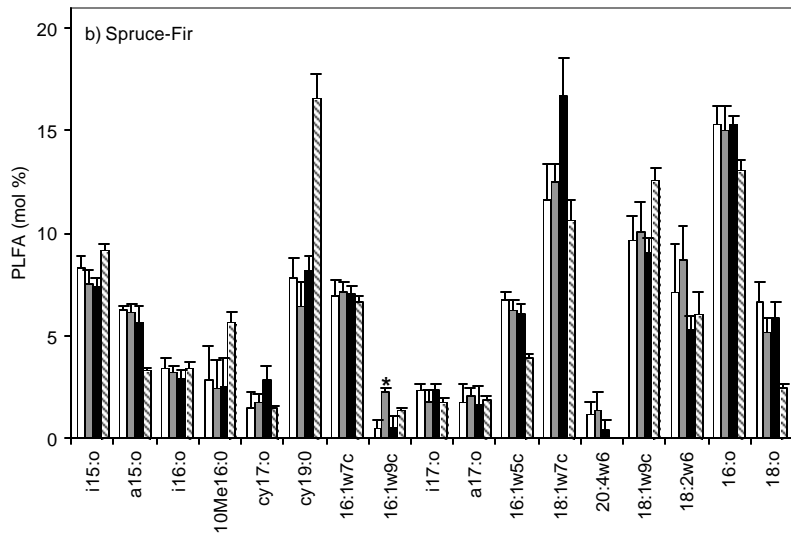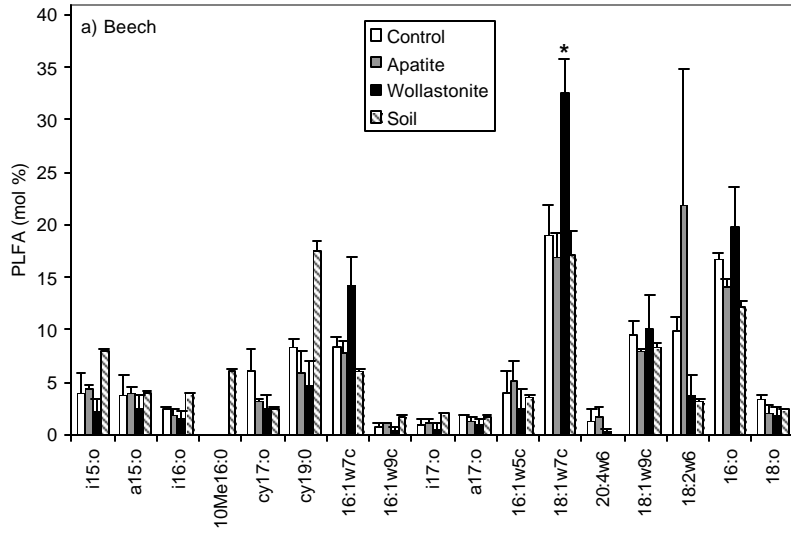values with the same letter are not significantly different.

a) Beech

b) Spruce-Fir

c) Sugar Maple

Figure 5-5. Microbial composition of 50 µm mesh bags buried under (a) beech, (b) spruce-fir, and (c) sugar maple. Error bars are standard errors of the mean (n=3). An '*' indicates that mol% PLFA in the mesh bag is significantly different than mol% PLFA in mesh bags with other mineral assemblages. A '#' indicates that mol% of the PLFA in the apatite- and wollastonite-amended bags are significantly different from each other but not different than the control.

References

Atlas, R.M., Bartha, R., 1987. Microbial Ecology: Fundamentals and Applications. Benjamin/Cummings Publishing Company, Menlo Park, 533 pp.

Bornyasz, M.A., Graham, R.C., Allen, M.F., 2005. Ectomycorrhizae in a soil-weathered granitic bedrock regolith: linking matrix resources to plants. Geoderma 126 (1-2), 141-160.

Fisk, M.C., Kessler, W.R., Goodale, A., Fahey, T.J., Groffman, P.M., Driscoll, C.T., 2006. Landscape variation in microarthropod response to calcium addition in a northern hardwood forest ecosystem. Pedobiologia 50, 69-78.

Frostegård, A., Bååth, E., 1996. The use of phospholipid fatty acid analysis to estimate bacterial and fungal biomass in soil. Biology and Fertility of Soils 22 (1-2), 59-65.

Graham, J.H., Hodge, N.C., Morton, J.B., 1995. Fatty acid methyl ester profiles for characterization of Glomalean fungi and their endomycorrhizae. Applied and Environmental Microbiology 61 (1), 58-64.

Hagerberg, D., Thelin, G., Wallander, H., 2003. The production of ectomycorrhizal mycelium in forests: Relation between forest nutrient status and local mineral sources. Plant and Soil 252 (3), 279-290.

Hoffland, E., Giesler, R., Jongmans, T., van Breemen, N., 2002. Increasing feldspar tunneling by fungi across a north Sweden podzol chronosequence. Ecosystems 5, 11-22.

Johnson, C.E., Driscoll, C.T., Siccama, T.G., Likens, G.E., 2000. Element fluxes and landscape position in a northern hardwood forest watershed ecosystem. Ecosystems 3, 159-184.

Jongmans, A.G., van Breemen, N., Lundstrom, U., van Hees, P.A.W., Finlay, R.D., Srinivasan, M., Unestam, T., Geisler, R., Melkerud, P.-A., Olsson, M., 1997. Rock-eating fungi. Nature 389, 682-683.

Juice, S.M., Fahey, T.J., Siccama, T.G., Driscoll, C.T., Denny, E.G., Eagar, C., Cleavitt, N.L., Minocha, R., Richardson, A.D., 2006. Response of sugar maple to calcium addition to northern hardwood forest. Ecology 87 (5), 1267-1280.

Klamer, M., Bååth, E., 2004. Estimation of conversion factors for fungal biomass determination in compost using ergosterol and PLFA 18:2? 6,9. Soil Biology and Biochemistry 36, 57-65.

Landeweert, R., Hoffland, E., Finlay, R.D., Kuyper, T.W., van Breemen, N., 2001. Linking plants to rocks: ecotmycorrhizal fungi mobilize nutrients from minerals. Trends in Ecology and Evolution 16, 248-253.

Larsen, J., Olsson, P.A., Jakobsen, I., 1998. The use of fatty acid signatures to study mycelial interactions between the arbuscular mycorrhizal fungus *Glomus intraradices* and the saprotrophic fungus *Fusarium culmorum* in root-free soil. Mycological Research 102 (12), 1491-1496.

Nezat, C.A., Blum, J.D., Klaue, A., Johnson, C.E., 2004. Influence of landscape position and vegetation on long-term weathering rates at the Hubbard Brook Experimental Forest, New Hampshire, USA. Geochimica et Cosmochimica Acta 68 (14), 3065-3078.

Nezat, C.A., Blum, J.D., Yanai, R.D., Hamburg, S.P., In review. A sequential extraction to selectively dissolve apatite for determination of soil nutrient pools with an application to Hubbard Brook Experimental Forest, New Hampshire, USA. Chemical Geology.

O'Leary, W.M., Wilkinson, S.G., 1988. Gram-positive bacteria. In: C. Ratledge and S.G. Wilkinson (Editors), Microbial Lipids. Academic Press, London, England, pp. 117-201.

Olsson, M.T., Melkerud, P.-A., 2000. Weathering in three podzolized pedons on glacial deposits in northern Sweden and central Finland. Geoderma 94, 149-161.

Oxburgh, R., Drever, J.I., Sun, Y.T., 1994. Mechanism of plagioclase dissolution in acid solution at 25°C. Geochimica et Cosmochimica Acta 58, 661-669.

Peters, S.C., Blum, J.D., Driscoll, C.T., Likens, G.E., 2004. Dissolution of wollastinite during the experimental manipulation of Hubbard Brook Watershed 1. Biogeochemistry 67, 309-329.

Raina, Chamola, Mukerji, 2000. Evolution of Mycorrhiza. In: Mukerji, Chamola and Singh (Editors), Mycorrhizal Biology. Kluwer Academic/Plenum Publishers, New York, pp. 1-25.

Valsami-Jones, E., Ragnarsdottir, K.V., Putnis, A., Bosbach, D., Kemp, A.J., Cressey, G., 1998. The dissolution of apatite in the presence of aqueous metal cations at pH 2-7. Chemical Geology 151, 215-233.

van Breemen, N., Finlay, R., Lundstrom, U., Jongmans, A.G., Geisler, R., Olsson, M., 2000. Mycorrhizal weathering: A true case of mineral plant nutrition? Biogeochemistry 49, 53-67.

Wallander, H., 2000. Uptake of P from apatite by *Pinus sylvestris* seedlings colonised by different ectomycorrhizal fungi. Plant and Soil 218, 249-256.

Wallander, H., Mahmood, S., Hagerberg, D., Johansson, L., Pallon, J., 2003. Elemental composition of ectomycorrhizal mycelia identified by PCR-RFLP analysis and grown in contact with apatite or wood ash in forest soil. FEMS Microbiology Ecology 44, 57-65.

Wallander, H., Nilsson, L.O., Hagerberg, D., Bååth, E., 2001. Estimation of the biomass and seasonal growth of external mycelium of ectomycorrhizal fungi in the field. New Phytologist 151, 753-760.

Weissbart, E.J., Rimstidt, J.D., 2000. Wollastonite: Incongruent dissolution and leached layer formation. Geochimica et Cosmochimica Acta 64 (23), 4007-4016.

Wilkinson, S.G., 1988. Gram-negative bacteria. In: C. Ratledge and S.G. Wilkinson (Editors), Microbial Lipids. Academic Press, London, England, pp. 299-488.

CHAPTER 6

CONCLUSIONS

Mineral dissolution provides nutrients to vegetation, neutralizes acid deposition, and controls soil water composition – functions that are vital to the growth and maintenance of forest ecosystems and stream water habitats. Understanding the controls on mineral dissolution and the method by which certain trees obtain their nutrients is important for predicting the health of forest ecosystems in response to anthropogenic disturbances such as acid deposition.

In the eastern U.S. and Europe, acid deposition from industrial sources has leached plant-essential nutrients such as calcium, magnesium and potassium from the soil. This leaching may result in calcium-related stress for vegetation and subsequently a decline in forest productivity. The northeastern U.S. may be especially sensitive to calcium limitation because the local rocks have naturally low calcium concentrations and are dominated by silicate minerals that break down very slowly, preventing a rapid release of nutrients.

In Chapter 2, long-term mineral weathering rates were calculated for soils from the Hubbard Brook Experimental Forest. Extensive soil sampling from a small watershed allowed for the study of mineral weathering as a function of landscape position and vegetation. Despite the homogeneity of the soil parent material in the watershed, long-term weathering rates are twice as high at higher elevations in the watershed where conifers are abundant and soil is thin. Using a geochemical mass balance, it was

estimated that rates of individual minerals (plagioclase, potassium feldspar and apatite) are greater in the upper part of the watershed.

The mean long-term weathering rate (35 meq m^{-2} yr^{-1}) in soils at Hubbard Brook is similar to rates in other ~10 to 15 ka old soils developed on granitic till in temperate climates. However, this weathering rate is less than the present-day loss of base cations from the watershed, which was calculated by watershed mass balance. These results support other studies that found that the pool of exchangeable base cations in HBEF soil is being diminished. Past and continued depletion of base cations, especially Ca, from soil can be detrimental to the health of terrestrial and aquatic ecosystems.

Although plagioclase contains most of the Ca in granitoid-derived soils, dissolution of apatite may be responsible for a significant amount of Ca weathered from soils. In Chapter 2, calculations are presented that suggest that up to ~20% of Ca weathered from Hubbard Brook soils over the last 14,000 years is due to apatite dissolution. This has important implications for distinguishing between Ca lost from the exchangeable pool and from mineral sources and thus modeling Ca cycling in ecosystems.

To quantify trace amounts of apatite in soil, a sequential leaching method was developed and tested (Chapter 3). Extraction of apatite from soil was optimized with 1 M HNO_3 between 0 and 20°C. A negligible amount of plagioclase was dissolved during this extract indicating that Ca-bearing minerals of differing weathering resistance could be sequentially extracted and quantified.

To understand the distribution of apatite in a region experiencing loss of calcium from the soil exchange complex, the sequential extraction procedure described in Chapter

3 was applied to soils collected from 20 different locations across the northeastern USA. Soils were developed on glacial till and derived from a range of igneous, metamorphic and sedimentary rocks. Results indicate that apatite is present in soils derived from igneous and granitoid bedrocks. Siliclastic-derived soils had negligible amounts of apatite. Although the plagioclase contained most of the Ca, the 1M HNO_3 extract removed most of the P, and the Ca fraction that is most accessible for dissolution

Chapter 5 examines the fungal and bacterial response to the presence of two Ca-bearing minerals, apatite and wollastonite, in stands of beech, spruce-fir, and sugar maple. The presence of apatite appears to stimulate the growth of ectomycorrhizal fungi associated with beech, presumably due to the dissolution of apatite by the fungi. The lack of fungal response to wollastonite suggests that the P demand is greater than that of calcium in these stands. Mixed stands of spruce and fir did not respond to either Ca-bearing mineral suggesting that the Ca- and P-nutrient requirements of the trees are being met, or that fungal response is slow relative to that in the beech stands. In the sugar maple stands, the presence of apatite appeared to suppress fungal growth. Reasons behind this are unclear. The molar fraction of one PLFA, which is found in arbuscular mycorrhizae and Gram negative bacteria, was higher in wollastonite-amended bags in all three stand types. Understanding the reasons for this change in microbial composition to wollastonite is important for evaluating the effects of a watershed-scale wollastonite addition on an ecosystem at Hubbard Brook.

APPENDICES

Appendix A. Comparison between chemical composition of sum of sequential leaches of soil versus bulk soil digest.

Appendix B. Ergosterol concentrations in soils from Hubbard Brook Experiment Forest, NH.